Design, Implementation and Control of a Self-Aligning Full Arm Exoskeleton for Physical Rehabilitation

by

Mustafa Yalçın

Submitted to the Graduate School of Sabancı University
in partial fulfillment of the requirements for the degree of
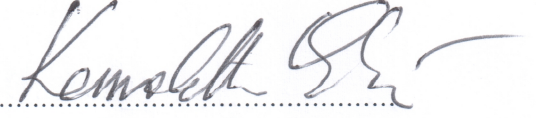Master of Science

Sabancı University

August, 2013

Design, Implementation and Control of a

Self-Aligning Full Arm Exoskeleton for
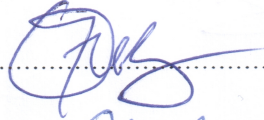
Physical Rehabilitation

APPROVED BY:

Assoc. Prof. Dr. Volkan Patoğlu
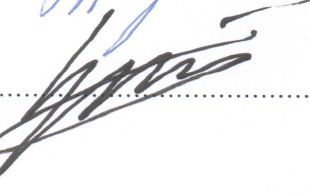(Thesis Advisor)   ....

Assoc. Prof. Dr. Kemalettin Erbatur   ....

Assoc. Prof. Dr. Güllü Kızıltaş Şendur   ....

Assist. Prof. Dr. S. Murat Yeşiloğlu   ....

Dr. Emre Özlü   ....

DATE OF APPROVAL: ....13.08.2013........

Design, Implementation and Control of a Self-Aligning Full Arm Exoskeleton for Physical Rehabilitation

Mustafa Yalçın
Mechatronics, Master of Science, 2013
Thesis Supervisor: Assoc. Prof. Dr. Volkan Patoglu

Abstract

We present kinematics, design, control, characterization and user evaluation of ASSISTON-ARM, a novel, powered, self-aligning exoskeleton for robot-assisted upper extremity rehabilitation that allows for movements of the shoulder girdle as well as shoulder rotations. ASSISTON-ARM can both actively and passively enable translational movements of the center of glenohumeral joint, while also passively compensating for the translational movements at elbow and wrist. Automatically aligning all its joint axes, ASSISTON-ARM provides an ideal match between human joint axes and the exoskeleton axes, guaranteeing ergonomy and comfort throughout the therapy, and extending the usable range of motion for upper extremity movement therapies. Furthermore, self-aligning feature of ASSISTON-ARM significantly shortens the setup time required to attach the patient to the exoskeleton. In addition to the typical shoulder rotation exercises, ASSISTON-ARM can deliver glenohumeral mobilization (scapular elevation/depression and protraction/retraction) and scapular stabilization exercises, extending the type of therapies that can be administered using the upper-arm exoskeletons. To ensure safety and gentle interactions with the patient, ASSISTON-ARM is designed to be passively backdriveable, thanks to its capstan-based multi-level transmission and spring-based passive gravity compensation mechanism. Open and closed-loop impedance controllers have been implemented to safely regulate interactions of ASSISTON-ARM with patients and performance of the device has been experimentally characterized. Ergonomy and useability of the device has also been demonstrated through human subject experiments.

iv

Üst Extremite Fiziksel Rehabilitasyonu için Kendinden Hizalamalı bir Tam Kol Dış İskeletinin Tasarımı, Uygulanması ve Kontrolü

Mustafa Yalçın

Mekatronik Mühendisliği, Yüksek Lisans Tezi, 2013

Tez Danışmanı: Doç. Dr. Volkan Patoğlu

Özetçe

Bu tezde robot destekli rehabilitasyon için omuz dönüş hareketleriyle birlikte omuz kemeri hareketlerine de izin veren, özgün, beslemeli, kendinden hizalamalı dış iskelet olan AssistOn-Arm'ın kinematiğini, dizaynını, karakterize edilmesi ve kullanıcı değerlendirmesini sunuyoruz. AssistOn-Arm glenohumeral ekleminin merkezinin öteleme hareketlerine aktif ve pasif olarak olanak sağlarken, el dirseği ve bileğinin öteleme hareketlerini de pasif olarak telafi eder. Tüm eklemlerinin kendinden hizalaması sayesinde, AssistOn-Arm insan eklemleri ile dış iskelet eksenleri arasında ideal eşleşme sağlayarak terapi süresince ergonomi ve konforu garanti etmiş ve kol ve el eklemlerinin teripilerinde kullanılan kullanılabilir hareket açıklığını genişletmiş olur. Buna ek olarak AssistOn-Arm'ın bu kendinden hizalama özelliği hastayı dış iskelete bağlamak için gereken süreyi önemli ölçüde azaltır. AssistOn-Arm glenohumeral öteleme hareketleri (kürek kemiği elevasyon/depresyon ve öne doğru uzatma/geri çekme) ve kürek kemiği dengeleme egzersizlerini, kol dış iskeletlerinin yapabildiği terapi çeşitliliğini artırarak uygulayabilmektedir. Hastayla olan etkileşiminin nazik olması ve güvenliğin sağlanması için, çok kademeli makara temelli aktarması ve yay temelli pasif yer çekimi telafi mekanizması sayesinde AssistOn-Arm pasif olarak geri sürülebilir şekilde dizayn edilmiştir. AssistOn-Arm'ın hastalarla olan etkileşimi güvenli olarak düzenlemesi için açık ve kapalı döngü empedans kontrolleri uygulanmış ve cihazın performansı deneysel olarak nitelendirilmiştir. Ayrıca cihazın ergonomisi ve kullanılabilirliği insanlı deneylerle gösterilmiştir.

Acknowledgements

It is a great pleasure to extend my gratitude to my thesis advisor Assoc. Prof. Volkan Patoğlu for his precious guidance and support. I am greatly indebted to him for his supervision and excellent advises throughout my Master study. I would gratefully thank Assoc. Prof. Kemalettin Erbatur, Assoc. Prof. Güllü Kızıltaş Şendur, Assist. Prof. S. Murat Yeşiloğlu and Dr. Emre Özlü for their feedbacks and spending their valuable time to serve as my jurors.

I am heartily thankful to Beşir Çelebi, Mine Saraç, Ahmetcan Erdoğan and Ozan Tokatlı for their support and invaluable help. Many thanks to my friends, Abdullah Kamadan, Elif Hocaoğlu, Giray Havur for making the laboratory enjoyable and memorable and other colleagues from the Department of Mechatronics supported me in my research work. Thanks to Süleyman Tutkun for his precious support throughout my research and for sharing his experience and technical knowledge.

I owe my deepest gratitude to my family for all their love and support throughout my life.

Contents

List of Figures

ix

List of Tables

Chapter I

1   Introduction

Neurological injuries, such as stroke, are one of the main reasons of permanent disability. In particular, among 15 million people that suffer from stoke, 5 million are left permanently disabled each year [1] . As a result, these disabilities place a high burden on individual welfare and national economies. Despite medical developments, number of stroke incidents continues to increase because of the ageing population in many developing countries. According to World Health Organization [1, 2], stoke is the biggest single cause of major disability in United Kingdom and average total cost of care per stroke patient during first 6 months of the incident is estimated to be about 16000 Euros in The Netherlands.

Physical rehabilitation therapy is indispensable for treating neurological disabilities. Therapies are more effective when they are

- repetitive [3],

- intense [4],

- task specific [5], and

- long term [6].

However, repetitive and high intensity therapies place physical burden on the therapist, increasing cost of treatment. With recent advancements at electro-mechanical systems, using robotic devices for rehabilitation become ubiquitous, since these devices can bear the physical burden of rehabilitation exercises, while therapists are employed as decision makers.

In this thesis, a powered exoskeleton, ASSISTON-ARM, is designed and implemented to assist physical rehabilitation of upper extremity.

The rest of this chapter is organized as follows: Robot-assisted rehabilitation devices are described in Section 1.1. Physical rehabilitation of human shoulder is detailed in Section 1.2 and upper limb exoskeleton devices developed for shoulder and arm physical rehabilitation are reviewed in Section 1.3. The contributions of this thesis are listed in Section 1.4, while the outline of thesis is presented in Section 1.5.

1.1 Robot Assisted Rehabilitation Devices

Robot assisted rehabilitation devices can be applied to patients with all levels of impairment, can quantitatively measure patient progress, allow for easy tuning of duration and intensity of therapies and make customized, interactive treatment protocols feasible. Also, robotic devices are particularly good at repetitive and intense tasks since they decrease physical burden on therapists and costs. Increase in accuracy and reliability, enhancement in effectiveness of therapy session are other advantages of rehabilitation robots. Clinical trials on robot assisted rehabilitation shows that this form of therapy is effective for motor recovery and possesses high potential for improving functional independence of patients [7–10].

Active rehabilitation devices utilized to treat upper-limb impairment can

be categorized into two main categories: end- effector type robots [11, 12] and exoskeletons [13–15].

1.1.1 End-effector Type Rehabilitation Robots

End-effector type rehabilitation robots feature a single interaction point (the end-effector) with the patient and the joint motions of these devices do not correspond to human movements. Therefore, without external restraints applied to constrain the patient, joint specific therapies cannot be delivered by such mechanisms. Moreover, compensatory movements of the patient cannot be detected when these devices are used. On the other hand, end-effector type robots are advantageous thanks to their simple kinematic structure and low cost. End-effector type of rehabilitation robots can be fixed based or mobile. Rehabilitation robots based on mobile platforms can be designed light and compact.Therefore they can be used for home based robotic therapy. While MIT-Manus [11] and Gentle/s [12] are examples of fixed based end-effector type rehabilitation devices. ASSISTON-MOBILE [16] is an example of a mobile end-effector type rehabilitation robot designed for upper limb therapy.

Figure 1.1: End-effector type upper limb rehabilitation robots: MIT-Manus, Gentle/s and ASSISTON-MOBILE, respectively.

3

1.1.2 Exoskeletons for Physical Rehabilitation

In contrast to end-effector type robots, exoskeletons are attached to the human limb at multiple interaction points and movement of these devices correspond with human joints. As a result, exoskeletons are capable of applying controlled torques to individually targeted joints and measuring movements of these specific joints decoupled from movements of the other joints. Unfortunately, exoskeletons possess more complex kinematic structure compared to end-effector type robots; hence, are more costly. Due to their high cost, exoskeletons designed specifically for rehabilitation are typically immobile devices, grounded to a fixed base and are proper for clinical use. Even though such devices are commonly employed for neurorehabilitation and clinical use, they have limitations in term of providing functional training compared to ungrounded assistive devices.

Since being able to target and measure individual joint movements of human joints is the main advantage of exoskeleton type rehabilitation robots, an imperative design criteria for their design is to ensure correspondence of human joint axes with robot axes. Misalignments can occur since (i) human joints cannot be modeled as simple revolute joints, (ii) the exact position of the human joints cannot be determined externally without using special imaging techniques, and (iii) placement of the human limb on the exoskeleton may change from one therapy session to another [17, 18].

Misalignment of joint axes is problematic as it results in parasitic forces on the patient around the attachment points and at the joints, causing discomfort or pain or even long term injury under repetitive use. Most importantly, axis misalignment may promote compensatory movements of patients which can inhibit potential recovery and decrease real life use of the limb due to

4

unfavored energetics of these movements [19].

1.2 Physical Rehabilitation of Human Shoulder

Human shoulder complex possesses two translational degrees of freedom (DoF) tightly coupled to three rotational DoFs [20, 21]. In addition to the decoupled translational movements of the center of glenohumeral (GH) joint, movements of the shoulder girdle is tightly coupled with the elevational rotation of the humerus [22]. This coupling is known as scapulohumeral (SH) rhythm. As a consequence of shoulder rotation, due to SH rhythm, tip of the humerus translates in the sagittal plane.

Stroke and upper limb paralysis may cause various impairments in the upper extremity. Inferior GH joint displacement, commonly referred to as shoulder subluxation, is one of the most common musculoskeletal problems caused by the gravitational pull on the humerus and stretching of the capsule of the shoulder joint once the shoulder muscles are weakened by paralysis [23]. Shoulder subluxation is a problem since it is one of the possible causes of shoulder pain following a stroke [24]. Moreover, it restricts passive and active RoM and can hinder recovery of upper limb function. There exists consistent evidence in literature that subluxation is correlated with poor upper limb function [25] and reflex sympathetic dystrophy [26]. As a result, prevention or counteraction of shoulder subluxation is an important aspect of upper extremity rehabilitation after stroke.

Scapular dyskinesia is another condition that refers to abnormalities in the SH rhythm. Since abnormality of SH rhythm results in secondary effects on the function of the shoulder joint, restoring a stable scapular base through scapular stabilization exercises is essential to rehabilitating shoulder

5

and returning to functional activities. Similarly, GH mobilization exercises are required for re-gaining RoM of the joint. Most stroke patient cannot perform shoulder girdle movement by themselves; hence, it is imperative that these movements are properly assisted until the patient can actively stabilize and orient his/her upper limb during ADLs.

A final aspect is related to gaining upper extremity function after stroke via recovery or compensation. Reintegration of the impaired arm into ADLs critically depends on the type of functional gains, while improvement in functional performance can be achieved through compensatory adaptations as well as from recovery of normative movement and muscle activation patterns. A recent study provides evidence that adoption of compensatory strategies early in treatment can inhibit potential recovery [19]. The study also shows that increased arm use at home is strongly predicted by increased recovery and only weakly predicted by increased function via compensation. In particular, even though patients may achieve high clinical scores using compensation strategies, they tend not to integrate these unnatural and energetically ineffective strategies in their daily lives. Hence, resorting to compensation strategies early in treatment decrease the amount of real-world limb use. On the other hand, gains that are due to recovery of normative movement and muscle activation patterns result in increased use of the limb which promotes further functional gains.

All of the above treatment guidelines suggest that to deliver effective rehabilitation therapies to shoulder, an exoskeleton should be capable of actively locating the humerus to counteract shoulder subluxation, should be able to provide assistance to patients during scapular stabilization and GH mobilization exercises such that they can restore their natural SH rhythm

and actively stabilize and orient their upper limbs during ADLs. Most importantly, an effective shoulder exoskeleton should promote recovery, not compensation. End-effector type devices and exoskeletons that do not allow natural movements of shoulder girdle necessitate compensatory movements, which can detrimentally affect further functional gains that are achievable by the upper limb.

1.3 Exoskeletons for Upper Extremity Rehabilitation

As stated at previous sections, alignment of exoskeleton axes with human joint axes is indispensable in order to deliver effective rehabilitation therapies, especially for the human shoulder. Moreover, during rehabilitation process, in order to ensure comfort and ergonomy, exoskeletons should allow for the translations elbow and wrist rotation axes, tother with the rotations of these joints. Several exoskeletons [14] feature adjustable links that enable offline adjustment of joint axes to match/approximate human joint axes; however, adjusting robot joint axes to match the human axes is a tedious process that may take up an important portion of precious therapy session.

The SH rhythm was first included into exoskeletons design in [27] as part of a passive measurement device. Later, ESA exoskeleton [28] introduced a 6 DoF passive shoulder joint for the shoulder complex. MGA exoskeleton [29] approximates transitions of the shoulder complex with a circular path and enables active adjustment to scapula rotation utilizing an extra actuated revolute joint in series with spherical rotations. Mobile exoskeleton device developed by [30] features 2 actuated DoF on shoulder excluding transitions on shoulder and 1 actuated DoF at elbow. Pneu-WREX [31] provides an additional DoF for the shoulder to enable adjustments. ARMin

II, has drastically decreased the ergonomic problems by including an extra vertical translational DoF to the shoulder joint [14]. On the other hand, the additional DoF increases the kinematic complexity of the robot. In the final version, ARMin III, the shoulder joint is simplified by eliminating passive robot elements and ergonomic movement is achieved by circular shoulder joint movement [32] similar to MGA exoskeleton. ARMin III has a simpler kinematic structure, the cost is decreased with respect to ARMin II, consequently the ergonomy of the robot is deteriorated as well. Since ARMin III can only approximate the movements of center of GH joint by a circle, it cannot fully correspond to human joints even after tedious adjustments for each patient.

In order to comply with SH rhythm, both Dampace [33] and Limpact [34] include 2 DoF self-alignment mechanisms. Despite dramatic increase in ergonomy and even though these exoskeletons allow for GH mobilization, they cannot assist/resist shoulder GH mobilization exercises. ShouldeRO [35] uses a poly-articulated structure with Bowden-cable transmission to implement an alignment-free 2 DoF exoskeleton for the shoulder. ShouldeRO cannot assist patients while performing movements of the shoulder girdle. Finally, in [36], a 6 DoF RPRPRR serial kinematic chain with 5 actuated DoF and 1 passive slider is proposed to enable complex shoulder movements. Kinematics of this exoskeleton allows for tracking and assisting all girdle movements of the human shoulder.

IntelliArm [37] utilizes PPPRRR serial kinematics with 2 passive and 1 active DoF for alignment of the center of GH joint with the exoskeleton axes. IntelliArm can assist elevation/depression movements of the shoulder girdle but not provide assistance for the protraction/retraction DoF. MEDARM [38]

8
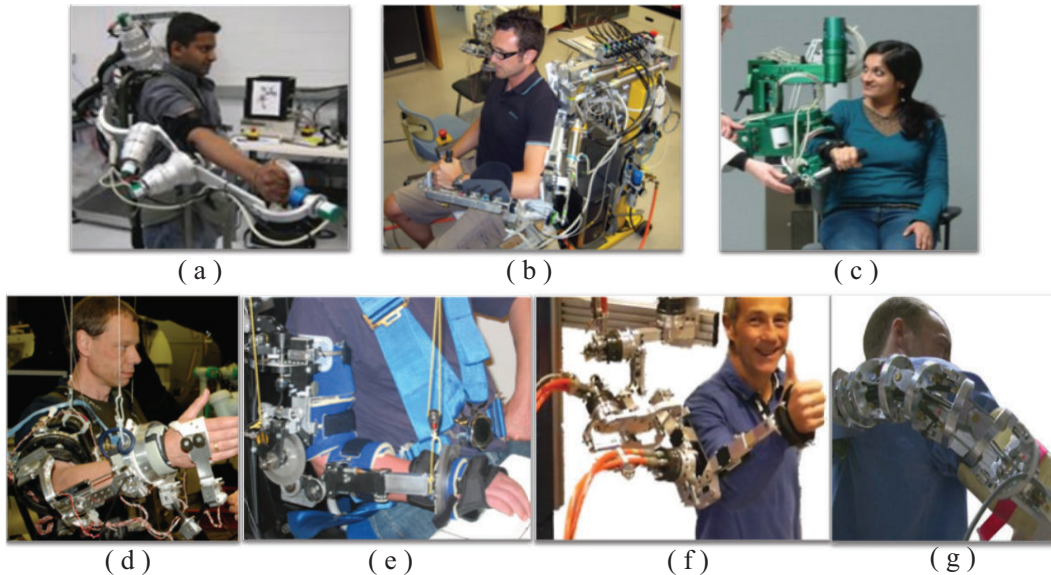
Figure 1.2: Examples of some of upper limb exoskeletons: (a) MGA-Exo [29], (b) Pneu-WREX [31], (c) ARMin III [32], (d) ESA-Exo [28], (e) Dampace [33], (f) Limpact [34], (g) ShouldeRO [35]

features <u>RRRRR</u> serial kinematics with an actuated 2 DoF shoulder girdle mechanism to assist both elevation/depression and protraction/retraction DoF. However, this design can still suffer from joint misalignment problem since the girdle mechanism is based on the approximation that the center of the GH follows a circular path at the sternoclaviular joint.

In addition to joint correspondence, minimizing the weight of the exoskeleton has been an active research topic. L-exos robot uses a cable driven actuation system to place the actuators of the robot outside the exoskeleton and decrease the weight [39]. Similar to L-exos, CADEN-7 is another cable driven exoskeleton [15]. With regard to light weight and high backdriveability, CADEN-7 is different from the L-exos with an additional joint on the wrist mechanism, correspondingly allows for a wider range of exercises. Another example of upper-extremity rehabilitation robots is the T-WREX [40].

9

(a)   (b)
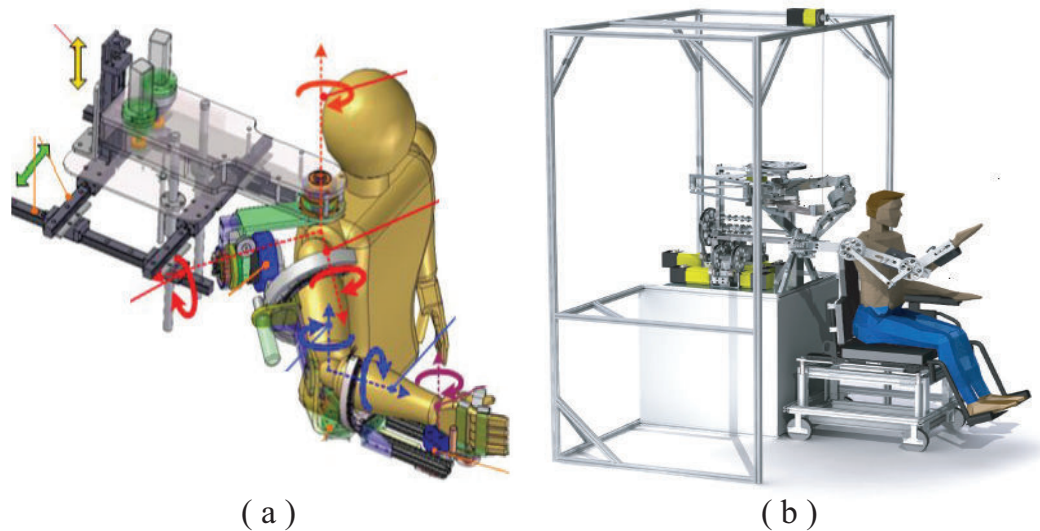
Figure 1.3: Examples of some of upper limb exoskeletons that can track GH mobilization: (a) IntelliArm [37], (b) MEDARM [38]

T-WREX robot has 2 actuators to activate the shoulder joint and a third actuator is attached serially to move the whole shoulder mechanism in a circular trajectory. In total, the shoulder joint of the robot consists of 4 DoFs, in which two of them are coupled; therefore, the robot cannot fully correspond to human shoulder kinematics for all patients. SAM exoskeleton manages mobility in addition to being light weight [41]. This robot has 7 DoFs, in which 3 DoFs are allocated for shoulder joint movements. Consequently, although SAM features mobility, it cannot preserve shoulder joint correspondence for ergonomic therapy.

Upper limb rehabilitation devices, including the ones that focus on SH rhythm of GH joint, commonly model the motion of the elbow joint motion as a 1 DoF hinge joint [28, 29, 31, 32, 34, 37]. Nevertheless, the axis of elbow rotation can be precisely described to lie on a quasi-conic frustum [42].

NEUROExos is a passive elbow exoskeleton with four (two rotational and two translational) DoFs, specifically designed to faithfully reproduce elbow rotations [43].

1.4 Contributions of the Thesis

- We designed a novel, self-aligning, powered, passively backdriveable full arm exoskeleton with 12 DoF, that allows movements of shoulder girdle with shoulder rotations and elbow and wrist transition together with their corresponding rotations.

  - Self alignment property ensures comfort and ergonomy, while guaranteeing an ideal match between exoskeleton axes and human joints axes throughout rehabilitation exercises. Shoulder module of AssistOn-Arm can both actively and passively enable coupled or decoupled shoulder transitions of glenohumeral joint along with corresponding shoulder rotations. AssistOn-Arm also allows for elbow and wrist axis transitions during rotations of these joints.

  - Self alignment of the exoskeleton significantly decreases setup time required to attach exoskeleton to the patient. In particular AssistOn-Arm can be attached to the patient within less than 20 seconds without requiring any additional adjustments.

  - AssistOn-Arm can actively deliver scapular elevation/depression, scapular protraction/retraction and scapular stabilization exercises, allowing new type of therapies administered by arm exoskeletons.

  - Passive backdriveability ensure passive alignment of joint axes and guarantees safety of the device even under power losses.

  - Thanks to the self-alignment, usable range of motions for the shoulder, elbow and wrist joints extend significantly.

- We have designed and implemented two prototypes of ASSISTON-ARM with different actuation/transmission pairs.

  - We have conducted kinematic, dynamic and workspace analysis of individual modules, as well as the entire mechanism of ASSISTON-ARM.

  - We have analytically and experimentally characterized the performance of ASSISTON-ARM.

  - We have implemented position and impedance controllers in order to impose assistive/resistive physical rehabilitation exercises to patients.

  - We have conducted ergonomy and usability studies with human subject experiments.

- We have designed and implemented a spring-based gravity compensation mechanism to counteract undesired effects of gravity on the passively backdriveable joints.

  - Gravity compensation mechanism increases comfort of patient during rehabilitation process by significantly reducing the effect of gravity on moving parts of ASSISTON-ARM.

  - Passive gravity compensator also enables us to use smaller actuators, since large motor torques are no longer necessary to counteract the gravity in an active manner.

  - Gravity compensation mechanism compensates for more than 70% of gravitational forces during the most common daily living activities.

1.5 Outline of the Thesis

The rest of the document is organized as follows. In Chapter II, kinematics of human upper extremity (shoulder, elbow, and forearm-wrist) is reviewed and kinematics and dynamics of the proposed arm exoskeleton are introduced in detail. Kinematics and statics of the passive gravity compensation mechanism is also detailed in this section. In Chapter III, actuator selection, design and implementation of each module of the arm exoskeleton are presented. In particular, details of two different prototype implementations of the system is given in Sections 3.1.1 and 3.1.2, respectively, while design and implementation of gravity compensation mechanism are given in Section 3.2. Chapter IV presents experimental characterization results, including the workspace characterization for the exoskeleton, actuation torques and system backdriveability. Control of the exoskeleton, together with feasibility studies with human volunteers are presented in Chapter V. Chapter VI concludes the thesis and provides a brief description of the planned future works.

Chapter II

2 Kinematics and Dynamics of AssistOn-Arm

In this chapter, first we review kinematics of human arm, including shoulder, elbow and forearm-wrist. Then, the design criteria for kinematic type selection are represented, in which ideal compliance with actual human kinematic is emphasized. After kinematic type selection, calculations for kinematic analysis of each module are presented. The chapter ends with kinematic and static analysis of the gravity compensation mechanism.

2.1 Kinematics of Upper Extremity

In this subsection, we review kinematics of human shoulder, elbow and forearm-wrist. A good understanding of human joint kinematics is necessary such that proper kinematic type selection can be performed for an exoskeleton to ensure ergonomy and comfort.

2.1.1 Kinematics of Human Shoulder

Human shoulder complex consists of different joints including shoulder and shoulder girdle. Shoulder complex has the ability to move both in a translational and rotational manner. The sternoclavicular (SC) and the acromioclavicular (AC) joints at the shoulder girdle each have 3 DoF, while the

scapulothoracic (ST) joint possesses 5 DoF. These joints are depicted at Figure 2.1. However, the overall movement of the shoulder girdle is constrained and the movement of these three joints causes the center of GH joint to shift [44].
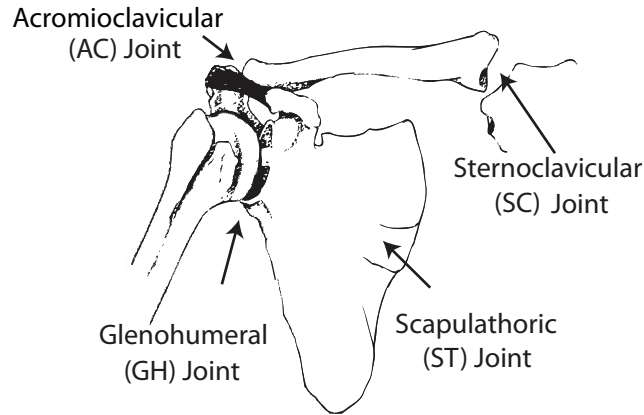
Figure 2.1: Joints at the shoulder complex

In the literature, it has been shown that shoulder girdle is mainly responsible for a 2 DoF translational movements of elevation/depression and protraction/retraction of shoulder [45]. Given the 3 rotational DoF of the shoulder socket itself, the shoulder complex can be modeled as a 5 DoF kinematic.chain [20, 21, 27], with three rotations (flexion/extension, external/internal rotation and horizontal abduction/adduction) and two translations (scapular protraction/retraction and elevation/depression) as depicted in Figure 2.2.

The center of GH joint, can be controlled independent from the shoulder rotations. Furthermore, there also exists a strong coupling between shoulder rotations and translations of the center of GH joint, called the scapulohumeral rhythm [22], as the movement of humerus causes scapular to move. It has been reported in the literature that when the human arm is fully flexed or
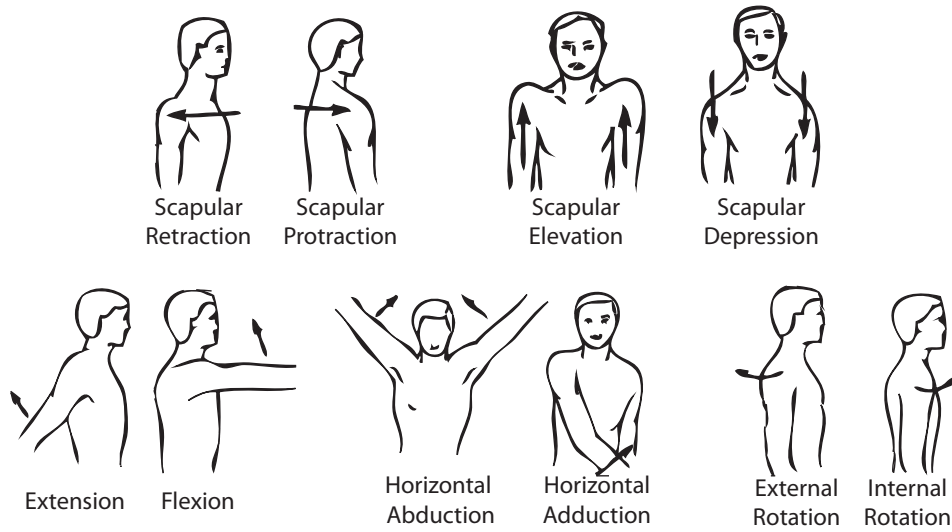
Figure 2.2: Range of movements of human shoulder

abducted (corresponding to a 180° rotation), the humerus is rotated only by an amount of 120°, while the scapular motion accounts for the remaining 60° rotation [46]. The exact motion of the humerus head shows wide variation among humans, depending on the size and orientation of shoulder bones, the shape of articulated surfaces and the constraints imposed by ligaments, capsules, and tendons.

Internal/external rotation of upper arm (not shoulder) that has similar function as pronation and supination of the elbow, can be faithfully modeled as a simple 1 DoF revolute joint, the axis of which stands on the center line of humerus [47].

2.1.2 Kinematics of Human Elbow

Human elbow possesses coupled transitions with its rotation. These translations are due to the quasi-conic double frustum of the mobile rotation axis [42], which is presented in Figure 2.3. Even though the translations
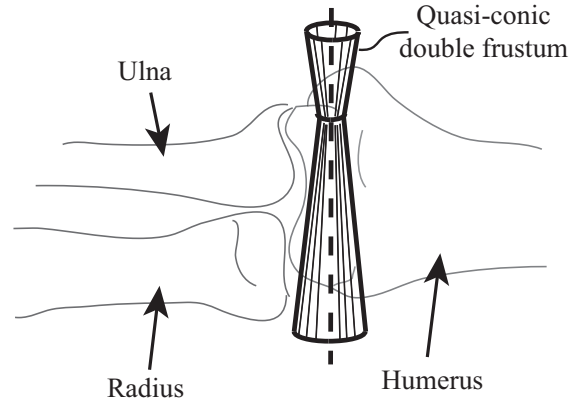
Figure 2.3: Movements of human elbow rotation axis

of the rotation axis of the elbow joint is relatively small; allowing for these translations in exoskeleton designs helps increase ergonomy, as well as adjustability of these devices to accommodate different arm sizes.

2.1.3 Kinematics of Human Forearm-Wrist

Human forearm-wrist complex can be modeled as a 3 DoF spherical kinematic chain that provides forearm supination/pronation and wrist flexion/extension and ulnar/radial deviation, if small translations of joint axes are neglected [48, 49]. As a consequence forearm and wrist rotations constitute the 3 dimensional manifold SO(3) [48].

2.2 Kinematic Type Selection for ASSISTON-ARM

In order to obtain an ideal match between axes of human and exoskeleton joints, it is imperative that exoskeleton can faithfully replicate movements of human joints. To achieve this goal, ASSISTON-ARMconsists of three modular modules, for shoulder, elbow and forearm-wrist, respectively. Each module of ASSISTON-ARM possesses self-alignment properties. Figure 2.4 presents

a schematic representation of overall integration of these modules.
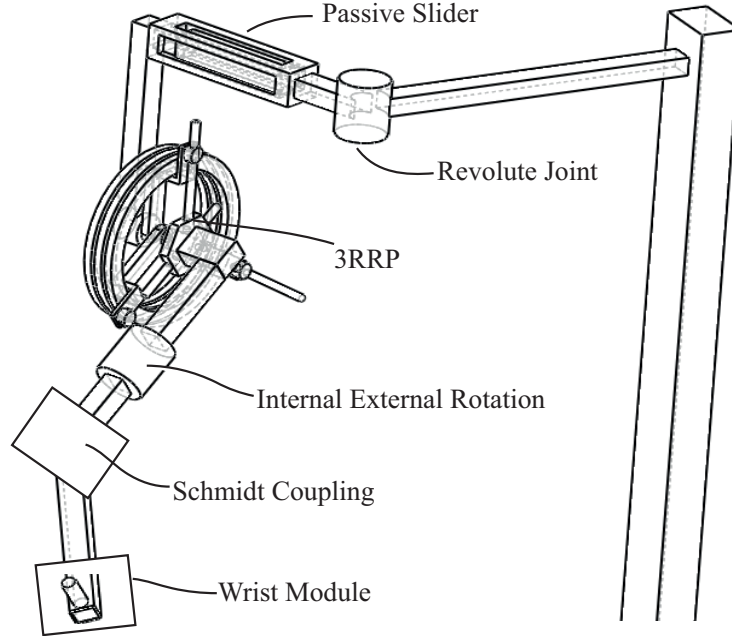
Figure 2.4: Schematic representation of the kinematics of ASSISTON-ARM

2.2.1 Shoulder Module

The shoulder module of ASSISTON-ARM is responsible for faithfully reproducing shoulder motions during rehabilitation exercises. The shoulder module possesses 6 DoF and it consists of a hybrid $\underline{R}\overline{P} - 3\underline{R}RP - \underline{R}$.[1]

First revolute joint is an actuated joint located at top of the mechanism and is responsible for shoulder abduction/adduction movements. A passive slider is located after this revolute joint forming $\underline{R}\overline{P}$ series kinematic chain for the first section of the shoulder module. The passive prismatic joint is required for ensuring ideal match of shoulder module to various human shoul-

---

[1] In this representation R refers to a revolute and P refers to a prismatic joint. Underlined joints are actuated, overlined joints are measured.

der sizes. Furthermore, this passive prismatic joint helps better alignment of joint axes during shoulder movements during which the humerus moves in the frontal plane.

The ability of ASSISTON-ARM to faithfully reproduce shoulder movements is largely due to its 3 DoF self-aligning joint, the 3$\underline{R}$RP mechanism, which is rigidly connected to passive prismatic joint. 3$\underline{R}$RP is a parallel, planar kinematic mechanism that possesses 3 DoF in plane thanks to its 3 grounded actuators. 3$\underline{R}$RP mechanism that is used in ASSISTON-ARM is depicted at Figure 2.5. The mechanism adds 2 translational and one rotational DoF in the sagittal plane of ASSISTON-ARM. These DoFs can be controlled independently or in a coupled way. Thanks to its 3 DoF kinematics, 3$\underline{R}$RP mechanism can mimic scapulohumeral rhythm, as well as allowing any other GH joint mobilization movements.

3$\underline{R}$RP mechanism has a symmetric structure and possesses large, circular, singularity free workspace. Thanks to its parallel kinematics, 3$\underline{R}$RP mechanism not only features high bandwidth and stiffness, but also serves as a mechanical summer during end-effector rotations. So, relatively small actuators can be used to impose large torques and forces at the end-effector of mechanism.

The last part of shoulder module is a half-open active revolute joint implemented using curved slides. This structure allows arm to go through the joint and can provide internal/external rotation of shoulder, faithfully tracking and reproducing RoM of healthy subjects.

End effector
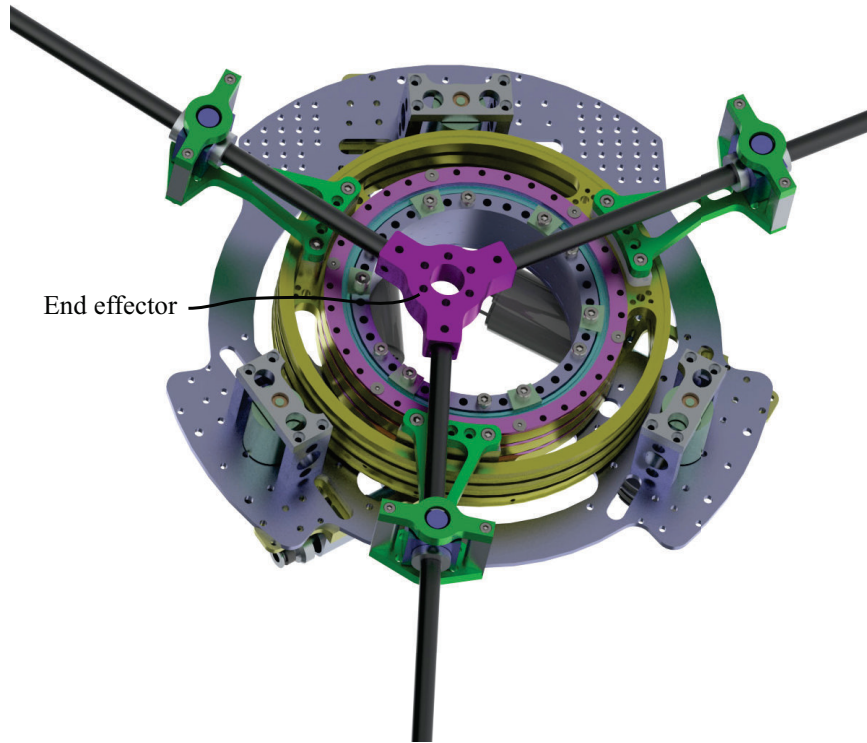
Figure 2.5: 3RRP mechanism used in AssistOn-Arm

2.2.2 Elbow Module

To accommodate for translational and rotational DoFs of human elbow, a Schmidt coupling has been utilized at the elbow joint of AssistOn-Arm as depicted in Figure 2.6. Schmidt coupling can ensure the same amount of rotation for between its input and output shafts, independent from the amount of translational non-collocation between the shafts. In particular, Schmidt coupling is a planar parallel mechanism with 2 translational and 1 rotational DoF. Actuating the rotation axis at the input shaft and instrumenting the device with optical encoders, elbow rotations can be actively controlled, while translations of rotation axis can be measured. We use the

Schmidt coupling as a underactuated mechanism, since we only actuate the input disk. We also measure the translations of its output disk.

Input component

Output component
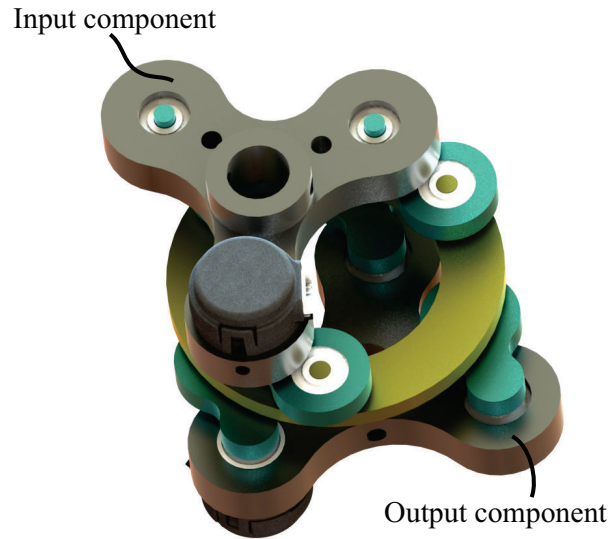
Figure 2.6: Schmidt Coupling mechanism used in AssistOn-Arm

Schmidt coupling does not have kinematic singularities within its workspace[2] and can cover a large range of rotations, that is necessary for implementation of a elbow exoskeleton with a large range of motion during flexion and extension exercises.

In the literature, Schmidt coupling has been implemented as the underlying kinematics of a knee exoskeleton [50].

---

[2]Singular configurations exist at the boundaries of ideal workspace; however, these singularities may simply be avoided by mechanically limiting the translational workspace of the mechanism to be slightly smaller than its ideal limits.

2.2.3 Forearm - Wrist Module
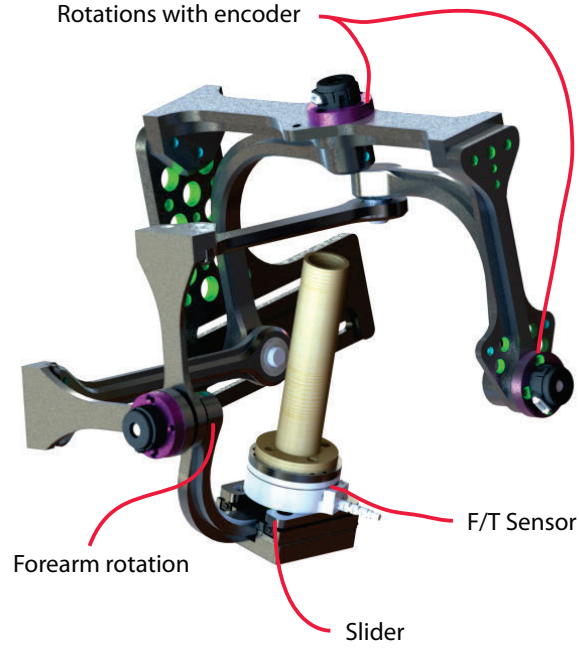
Figure 2.7: Forearm-wrist mechanism used in ASSISTON-ARM

Solid model of the forearm-wrist module at ASSISTON-ARM is depicted in Figure 2.7. Wrist module consist of a 2 DoF parallel spherical joint kinematics in series with a 1 DoF forearm rotation and a passive slider at the handle. As a result, kinematic structure of the forearm-wrist module can be given as a parallel spherical wrist $(\overline{R}RRR\overline{R})$ serially connected to a $\overline{R}P$ serial linkage. Note that currently the forearm-wrist module is not actuated and here the overlined joints represent joints with optical encoders. Passive slider at the end of the kinematic chain ensures passive alignment of human joints axes with ASSISTON-ARM wrist axes.

2.3   Kinematic Analysis of ASSISTON-ARM

ASSISTON-ARM has a hybrid kinematic chain that consists of three main modules and their series connection. The 3$\underline{R}$RP mechanism and Schmidt coupling are parallel planar mechanisms, while the wrist mechanism has spherical parallel kinematics. Overall kinematics of ASSISTON-ARM can be represented as $\underline{R}\overline{P} - 3\underline{R}RP - \underline{R} - Schmidt - \overline{R}RRR\overline{R} - \overline{R}P$ where underlined joints are actuated and overlined ones are measured. As a result ASSISTON-ARM can be modeled as a 12 DoF mechanism.

Figure 2.8 depicts a schematic representation of the kinematics of ASSISTON-ARM. ASSISTON-ARM consists of several rigid bodies connecting its modules. N represents the Newtonian reference frame attached to the ground. Point G on N is taken as the origin. Body P has gone through a simple rotation about the direction $\overrightarrow{n_1}$ with an amount of α_1. Body R translates with respect to Body P along the direction $\overrightarrow{p_2}$ with an amount of d_1. The base of 3$\underline{R}$RP parallel mechanism is rigidly attached to Body R, while its end-effector is rigidly attached to Body U. Body U translates on the $\overrightarrow{p_1} - \overrightarrow{p_3}$ plane with the configuration variables x_S and z_S and rotates about $\overrightarrow{p_2}$ with an amount of θ, with respect to Body R. Body L goes through a simple rotation with respect to Body U about the direction $\overrightarrow{u_3}$ with an amount of α_2, while the end-effector of Body H rotates with respect to Body L about $\overrightarrow{h_1}$ with an amount of α_3. At the same time due to translation of Schmidt Coupling, Body H translates between points Ξ and E on Body U about $\overrightarrow{l_2} - \overrightarrow{l_3}$ with amount of z_e and y_e. End effector of ASSISTON-ARM, that is, its handle translates on body H along $\overrightarrow{h_3}$ axis. Handle of the wrist module can rotate on 2 DoF spherical joint connected to a revolute joint thanks to its intersecting rotation axes, with Euler angles ϵ, φ and ω. As a sign con-
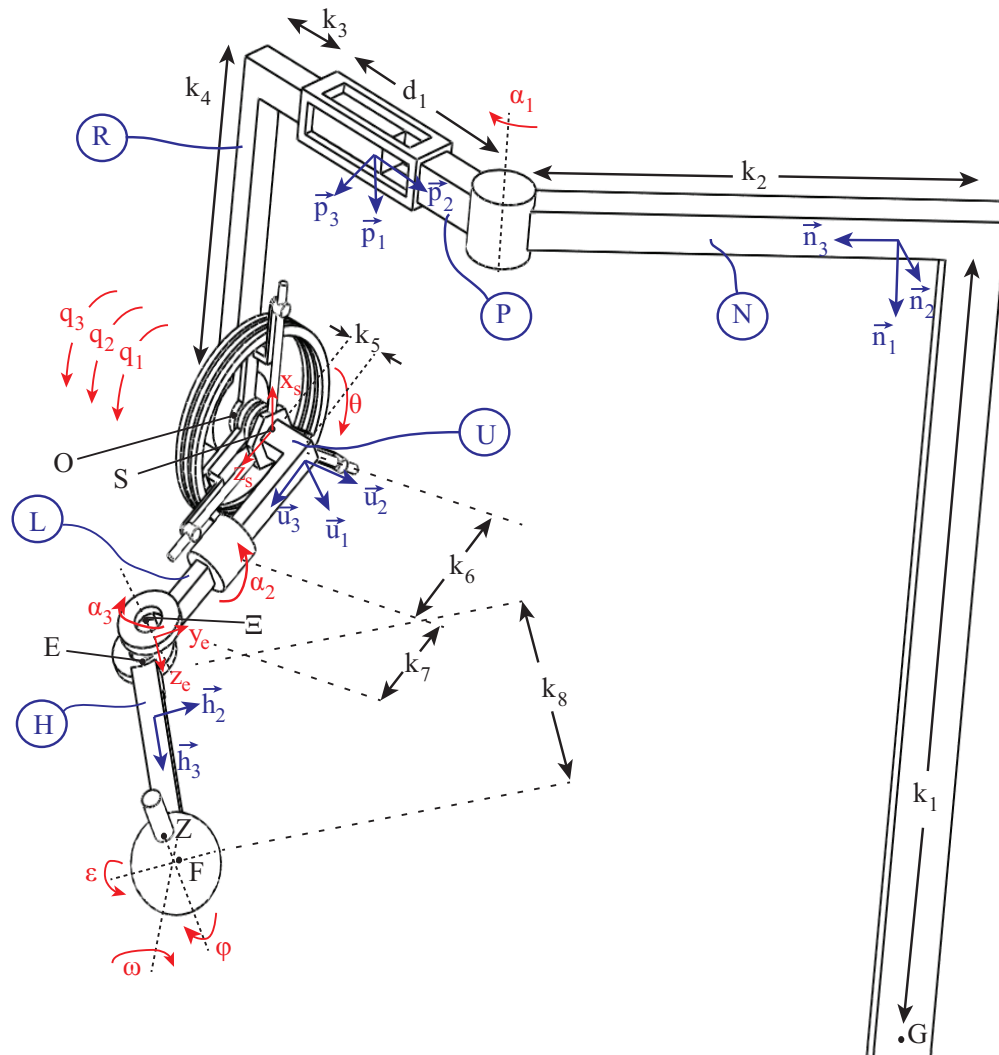
Figure 2.8: Schematic representation of the kinematics of ASSISTON-ARM

vention, all counter-clockwise angles are taken to be positive. k_i represents length of links, between specific points of the mechanism.

2.3.1 Kinematics of 3$\underline{R}$RP Planar Parallel Mechanism

Figure 2.9 depicts the kinematic schematics of 3$\underline{R}$RP planar parallel mechanism. 3$\underline{R}$RP mechanism consists of one base body, R, three body constituting the arms of the mechanism, Q, V, T and a symmetric end effector U. Arms Q, V and T have simple rotations with respect to base frame R with angles q_1, q_2 and q_3, respectively. These angles are actuated via motors that turns disks of the 3$\underline{R}$RP mechanism. Symmetric end-effector body U is connected to arm bodies from points Γ, Λ and Π via collocated linear and revolute joints. While point O is fixed on the base body R, S is the point at the middle of the end-effector body U of 3$\underline{R}$RP mechanism. End-effector body has transitions with respect to the base body about x_s at the direction of $\overrightarrow{r_1}$ and z_s at the direction of $\overrightarrow{r_3}$, also end-effector body U is rotated by θ around the axis of $\overrightarrow{r_2}$.

Fixed arm lengths of bodies between points of $O\Gamma$, $O\Pi$ and $O\Lambda$ are defined as l_1, l_2 and l_3. Variable distances between points ΓS, ΠS and ΛS are indicated as s_1, s_2 and s_3 respectively. In the kinematic calculation variable distances depicted above is assumed to be always positive as shown, while angles are positive if counter-clockwise.

At the initial configuration, homing position, when $\overrightarrow{r_1}$ vector of base frame and $\overrightarrow{u_1}$ of end-effector body are overlapping with each other, angle θ is zero. Also at the homing position, the end-effector of 3$\underline{R}$RP mechanism starts from $x_s = 0, z_s = 0$, while arm vectors $\overrightarrow{q_1}$, $\overrightarrow{v_1}$ and $\overrightarrow{t_1}$ have angles $\pi/3$, π and $5\pi/3$ from base body vector $\overrightarrow{u_1}$.
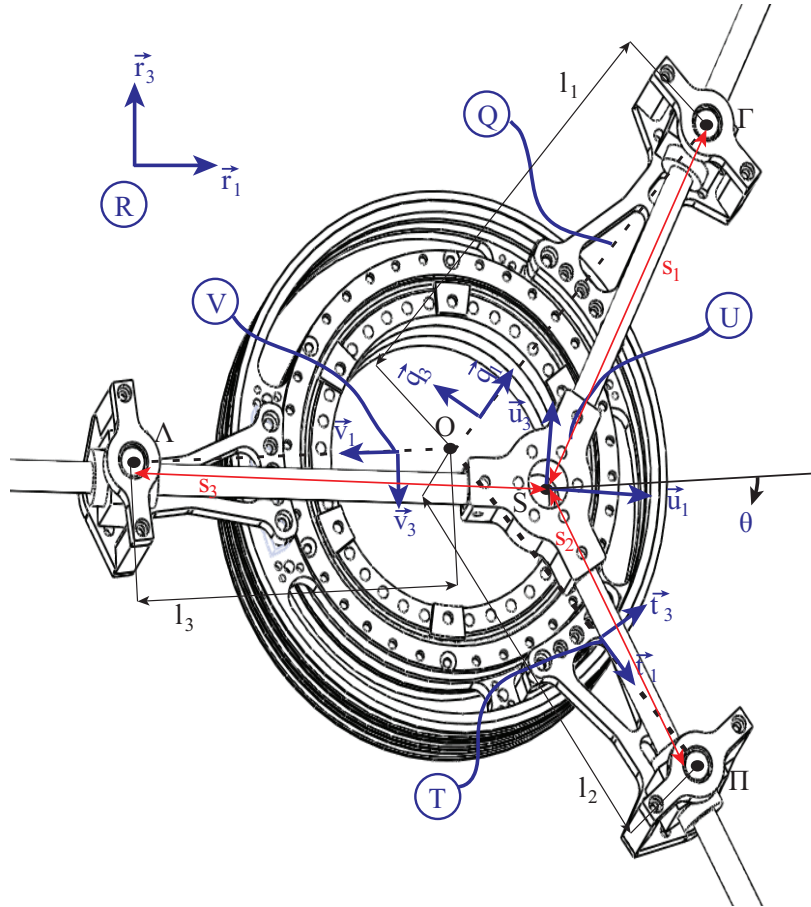
Figure 2.9: Schematic representation of the kinematics of 3RRP mechanism

Configuration and motion level kinematics of 3RRP have been presented in [51, 52] in detail. Here, we summarize these kinematic analysis results for completeness.

Configuration Level Kinematics of 3RRP Mechanism

Forward kinematics at configuration level calculates end-effector configuration given input joint angles. According to [52], given arm angles q_1, q_2 and q_3, configuration level forward kinematics (end effector variables x_s, z_s and

θ) can be analytically calculated as

$$x_s = -\frac{M}{\sqrt{3}(K^2 + L^2)} \tag{1}$$

$$z_s = c_{22} - \frac{K}{L}c_{21} - \frac{KM}{\sqrt{3}L(K^2 + L^2)} \tag{2}$$

$$\theta = atan2(K, L) \tag{3}$$

where

$$K = c_{12} + c_{32} + \sqrt{3}c_{31} - 2c_{22} - \sqrt{3}c_{11}$$

$$L = c_{11} + c_{31} + \sqrt{3}c_{12} - 2c_{21} - \sqrt{3}c_{32}$$

$$M = L(L - \sqrt{3}K)c_{12} - L(K + \sqrt{3}L)c_{11}$$
$$- (L - \sqrt{3}K)(Lc_{22} - Kc_{21})$$

$$c_{11} = l_1 \cos(q_1) \qquad c_{12} = l_1 \sin(q_1)$$

$$c_{21} = l_2 \cos(q_2) \qquad c_{22} = l_2 \sin(q_2)$$

$$c_{31} = l_3 \cos(q_3) \qquad c_{32} = l_3 \sin(q_3)$$

After results of configuration level forward kinematic obtained, intermediate variables s_1, s_2 and s_3 can be calculated analytically using trigonometric relations.

Configuration level inverse kinematics calculates arm angles given the end-effector configuration of the mechanism. In particular, actuator angles

q_1, q_2 and q_3 can be found with given x_s, z_s and θ as

$$q_1 = atan2(M_1, L_1) \tag{4}$$

$$q_2 = atan2(M_2, L_2) \tag{5}$$

$$q_3 = atan2(M_3, L_3) \tag{6}$$

where

$$K_1 = x_s \sin(\theta + \frac{\pi}{3}) - z_s \cos(\theta + \frac{\pi}{3})$$

$$K_2 = x_s \sin(\theta + \pi) - z_s \cos(\theta + \pi)$$

$$K_3 = x_s \sin(\theta - \frac{\pi}{3}) - z_s \cos(\theta - \frac{\pi}{3})$$

$$M_1 = K_1 \cos(\theta + \frac{\pi}{3}) - \sqrt{l_1^2 - K_1^2} \sin(\theta + \frac{\pi}{3})$$

$$L_1 = -K_1 \sin(\theta + \frac{\pi}{3}) - \sqrt{l_1^2 - K_1^2} \cos(\theta + \frac{\pi}{3})$$

$$M_2 = K_2 \cos(\theta + \pi) - \sqrt{(l_2^2 - K_2^2)} \sin(\theta + \pi)$$

$$L_2 = -K_2 \sin(\theta + \pi) - \sqrt{(l_2^2 - K_2^2)} \cos(\theta + \pi)$$

$$M_3 = K_3 \cos(\theta - \frac{\pi}{3}) - \sqrt{l_3^2 - K_3^2} \sin(\theta - \frac{\pi}{3})$$

$$L_3 = -K_3 \sin(\theta - \frac{\pi}{3}) - \sqrt{l_3^2 - K_3^2} \cos(\theta - \frac{\pi}{3})$$

Motion Level Kinematics of 3<u>R</u>RP Mechanism

Motion level kinematics is responsible for determining the linear relationship between actuator velocities and end-effector velocities. For the planar parallel mechanism, time derivative of configuration level kinematic equations can be utilized to solve for its motion level kinematics. In particular, the relationship

29

between end-effector velocities $\dot{x}_s$, $\dot{z}_s$ and $\dot{\theta}$ and actuator velocities $\dot{q}_1$, $\dot{q}_2$, $\dot{q}_2$, as well as velocities of intermediate variables $\dot{s}_1$, $\dot{s}_2$, $\dot{s}_2$ for 3<u>R</u>RP mechanism can be calculated as

$$\dot{X} = J_1^{-1} J_2 \dot{Q} \tag{7}$$

where

$$J_1 = \begin{bmatrix} 1 & 0 & -s_1 \sin(\theta + \frac{\pi}{3}) & \cos(\theta + \frac{\pi}{3}) & 0 & 0 \\ 0 & 1 & s_1 \cos(\theta + \frac{\pi}{3}) & \sin(\theta + \frac{\pi}{3}) & 0 & 0 \\ 1 & 0 & -s_2 \sin(\theta + \pi) & 0 & \cos(\theta + \pi) & 0 \\ 0 & 1 & s_2 \cos(\theta + \pi) & 0 & \sin(\theta + \pi) & 0 \\ 1 & 0 & -s_3 \sin(\theta - \frac{\pi}{3}) & 0 & 0 & \cos(\theta - \frac{\pi}{3}) \\ 0 & 1 & s_3 \cos(\theta - \frac{\pi}{3}) & 0 & 0 & \sin(\theta - \frac{\pi}{3}) \end{bmatrix} \tag{8}$$

and

$$J_2 = \begin{bmatrix} -l_1 \dot{q}_1 \sin(q_1) & -l_2 \dot{q}_2 \sin(q_2) & -l_3 \dot{q}_3 \sin(q_3) \\ l_1 \dot{q}_1 \cos(q_1) & l_2 \dot{q}_2 \cos(q_2) & l_3 \dot{q}_3 \cos(q_3) \end{bmatrix} \tag{9}$$

while

$$\dot{X} = \begin{bmatrix} \dot{x}_s & \dot{z}_s & \dot{\theta} & \dot{s}_1 & \dot{s}_2 & \dot{s}_3 \end{bmatrix}^T \text{ and } \dot{Q} = \begin{bmatrix} \dot{q}_1 & \dot{q}_2 & \dot{q}_3 \end{bmatrix}^T \tag{10}$$

The kinematic Jacobian is the matrix that maps joint velocities to end-effector velocities and frequently used for characterizing system and used in control algorithms. The kinematic Jacobian of 3<u>R</u>RP mechanism can be

30

found as

$$J_{3\underline{R}RP} = J_1^{-1} J_2 \tag{11}$$

At motion level inverse kinematics with given end-effector velocities, actuator velocities can be found. Motion level inverse kinematics is simple linear inverse of motion level forward kinematics; hence, it can be formulated as

$$\dot{Q} = J_{3\underline{R}RP}^{-1} \dot{X} \tag{12}$$

2.3.2   Kinematics of Schmidt Coupling Mechanism

Schmidt coupling is a parallel planar mechanism that has 3 DoF [53]. Kinematic chain of Schmidt coupling allows 2 DoF translations, and 1 DoF rotation about the axis perpendicular to its working plane. Due to its kinematics, end effector of Schmidt coupling rotates with same amount as its input body. Kinematic of Schmidt coupling has been studied in [50].

A schematic representation of Schmidt coupling is given in Figure 2.10. Input and output bodies of Schmidt coupling are indicated with I and H, respectively. The mechanism has seven more rigid bodies connecting input Body I and output Body H. For simplification only Bodies A are B are represented in the schematics, since arms of Schmidt coupling are parallel to each other. Point Ξ is fixed on the input Body I, Point Ψ is fixed on the intermediate disk and Point E is fixed on the output body H. Points Σ, Ω, also Ψ represent revolute joints at the connection points of bodies. Note that, Body I rotates with respect to Body L about $\overrightarrow{l_1}$ direction with an amount of α_3. Body A goes trough a simple rotation with respect to body I about $\overrightarrow{i_3}$

31
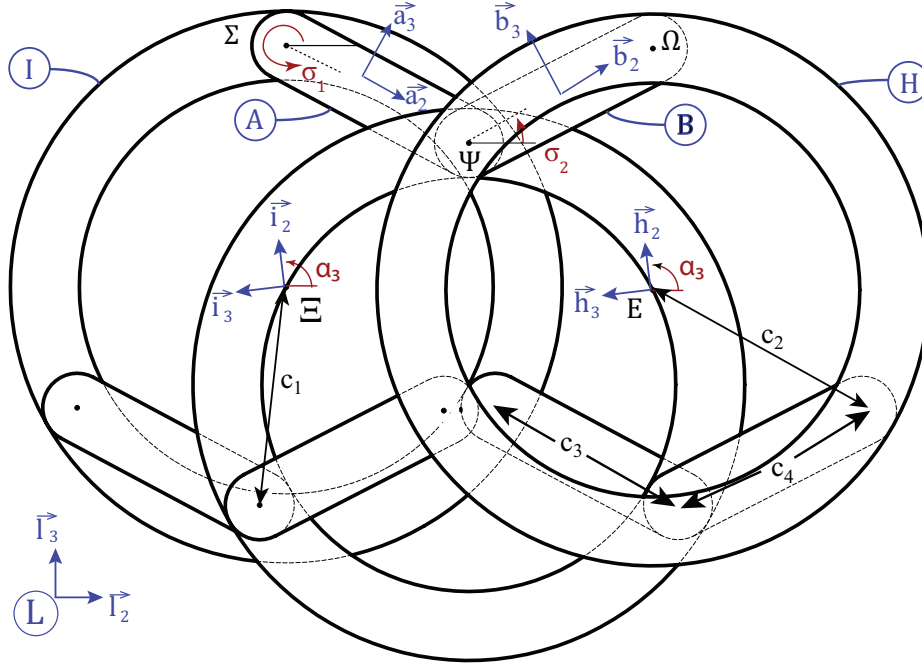
Figure 2.10: Schematic representation of the kinematics of Schmidt coupling

direction with amount of σ_1. Body B rotates with respect to body I about $\overrightarrow{i_3}$ with amount of σ_2. Since Schmidt coupling directly transmits the amount of rotation of Body I to Body H without changing its direction or amplitude, Body H also rotates about $\overrightarrow{l_1}$ direction with an amount of α_3. Also Body H translates on Body I along $\overrightarrow{l_2}$-$\overrightarrow{l_3}$ with amounts of y_e-z_e, respectively.

Configuration Level Kinematics

Kinematics of Schmidt coupling can be derived analytically at the configuration level, using the vector loop equation

$$c_1 \overrightarrow{i_2} + c_3 \overrightarrow{a_2} + c_4 \overrightarrow{b_2} - c_2 \overrightarrow{h_2} - y_e \overrightarrow{l_2} - z_e \overrightarrow{l_3} = 0 \tag{13}$$

if angles σ_1 and σ_2 are known. Expressing the loop equation on Body L,

following result can be derived

$$y_e = c_3 \cos \sigma_1 + c_4 \cos \sigma_2 \tag{14}$$

$$z_e = c_3 \sin \sigma_1 + c_4 \sin \sigma_2 \tag{15}$$

Motion Level Kinematics

Motion level kinematic equations can be obtained simply by taking time derivative of equations (14) and (15). Angle α_3 has not been included in the configuration level kinematic calculation of Schmidt coupling for simplicity, but since Schmidt coupling has 3 DoF, it is included in the Jacobian. Motion level forward kinematics of Schmidt coupling is given as

$$\dot{X}_{sc} = J_{sc}\dot{Q}_{sc} \tag{16}$$

where
$$\dot{X}_{sc} = [\dot{y}_e \ \dot{z}_e \ \dot{\alpha}_3]^T \tag{17}$$

$$\dot{Q}_{sc} = [\dot{\sigma}_1 \ \dot{\sigma}_2 \ \dot{\alpha}_3]^T \tag{18}$$

and J_{sc} is the Jacobian of Schmidt coupling

$$J = \begin{bmatrix} -c_1 sin(\sigma_1) & -c_2 sin(\sigma_2) & 0 \\ c_1 cos(\sigma_1) & c_2 cos(\sigma_2) & 0 \\ 0 & 0 & 1 \end{bmatrix} \tag{19}$$

2.3.3 Kinematics of Spherical Forearm-Wrist Module

Figure 2.11 depicts a schematic representation to study kinematic of the forearm-wrist mechanism. Kinematics of wrist module consists of a 2 DoF spherical parallel mechanism. This mechanism is connected to $\overline{R}P$ forearm linkage in series. Kinematic structure of forearm-wrist mechanism can be represented as $\overline{R}RRR\overline{R} - \overline{R}P$. Because palm of the hand is naturally offset from the rotation axes, handle of the wrist mechanism is designed to feature a passive slider for alignment. However, the axes of all rotations of the forearm-wrist module intersect at the same point, resulting in simplified kinematic solutions for the forearm-wrist module.

All links of the forearm-wrist module undergo simple rotations with respect to the link they are connected to. Body H indicates the base frame of the module, that is rigidly attached to the lower arm link of the exoskeleton. Bodies Ra, Rb, Rc, Ta, Tb and J represent other links of the module. Point Pr is a fixed point on the base frame H and points Pr, Ps, W, Qr and Qs mark revolute joints at connection points of links. Point Z is fixed at the end effector Body J. Body Ra undergoes simple rotation with respect to Body H about $\overrightarrow{h_1}$ direction with an amount of γ_1 and Body Ta rotates with respect to Body H about $\overrightarrow{h_1}$ direction with an amount of γ_2. Similarly, Body Rb rotates with respect to Body Ra about $\overrightarrow{Ra_2}$ direction with an amount of γ_2 and Body Tb rotates with respect to Body Ta about $\overrightarrow{Ra_2}$ direction with an amount of γ_1. Body Rc performs a simple rotation with respect to Body Rb about $\overrightarrow{Rb_3}$ direction with an amount of γ_3. Also, due to the slider attached to handle, Body J translates along the direction $\overrightarrow{Rc_3}$ with an amount of d_2. All rotation axes of wrist module intersect with each other at a single point. The configuration of the end effector Body J is represented by three Euler angles

ϵ, ω and φ and the translation amount d_2 with respect to the coordinate system fixed on Body H. Symbols k_i (i=9..13) indicate link lengths.
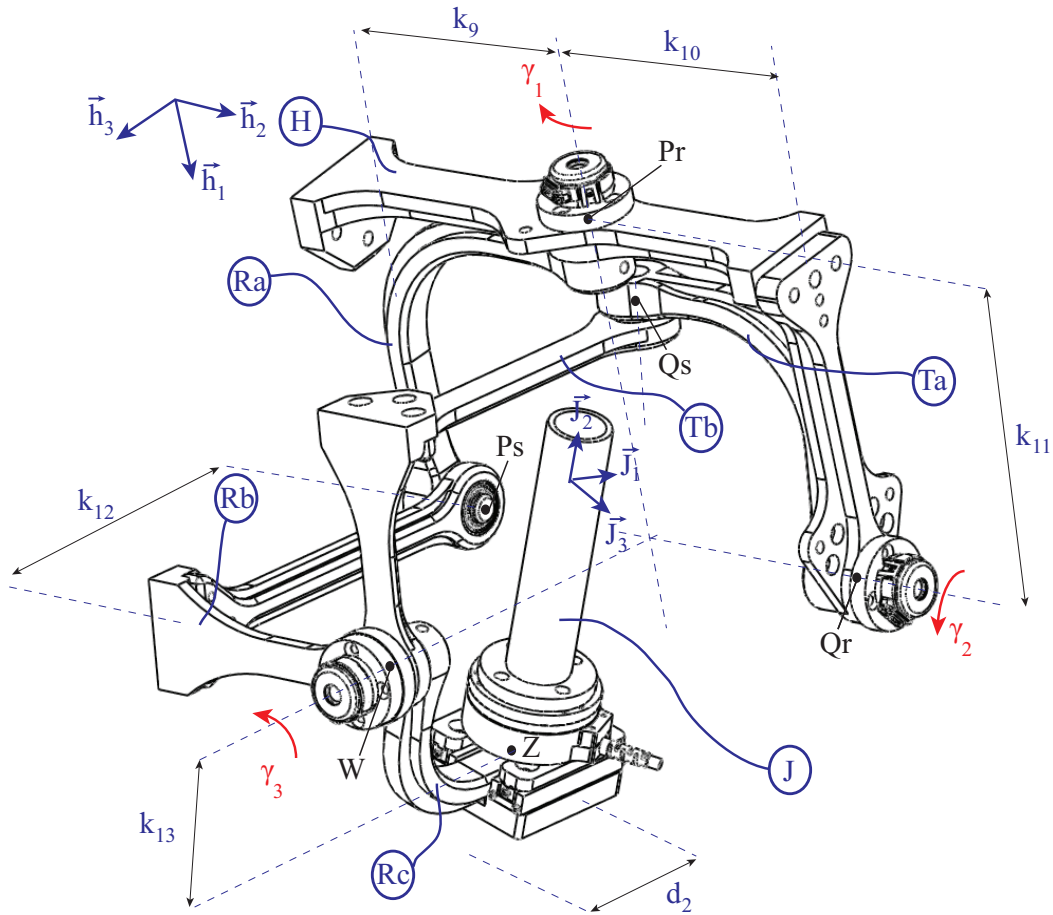
Figure 2.11: Schematic representation of the forearm-wrist module

Given the above description, the rotation matrices that correspond to rotations of relevant bodies of the forearm-wrist module can be represented as follows:

$$
{}^{H}R^{Ra} =
\begin{bmatrix}
1 & 0 & 0 \\
0 & \cos\gamma_1 & -\sin\gamma_1 \\
0 & \sin\gamma_1 & \cos\gamma_1
\end{bmatrix}
\tag{20}
$$

$$
{}^{H}R^{Ta} =
\begin{bmatrix}
\cos\gamma_2 & 0 & \sin\gamma_2 \\
0 & 1 & 0 \\
-\sin\gamma_2 & 0 & \cos\gamma_2
\end{bmatrix}
\tag{21}
$$

$$
{}^{Ta}R^{Tb} =
\begin{bmatrix}
1 & 0 & 0 \\
0 & \cos\left(\gamma_1 - \pi/2\right) & -\sin\left(\gamma_1 - \pi/2\right) \\
0 & \sin\left(\gamma_1 - \pi/2\right) & \cos\left(\gamma_1 - \pi/2\right)
\end{bmatrix}
\tag{22}
$$

$$
{}^{Ra}R^{Rb} =
\begin{bmatrix}
\cos\left(\gamma_2 + \pi/2\right) & 0 & \sin\left(\gamma_2 + \pi/2\right) \\
0 & 1 & 0 \\
-\sin\left(\gamma_2 + \pi/2\right) & 0 & \cos\left(\gamma_2 + \pi/2\right)
\end{bmatrix}
\tag{23}
$$

$$
{}^{Rb}R^{J} =
\begin{bmatrix}
1 & 0 & 0 \\
0 & \cos\gamma_3 & -\sin\gamma_3 \\
0 & \sin\gamma_3 & \cos\gamma_3
\end{bmatrix}
\tag{24}
$$

$$
{}^{H}R^{J} =
\begin{bmatrix}
\sin\epsilon\sin\omega & \sin\epsilon\sin\varphi\cos\omega - \sin\omega\cos\varphi & \sin\omega\sin\varphi + \sin\omega\cos\epsilon\cos\varphi \\
\sin\omega\cos\epsilon & \cos\omega\cos\varphi + \sin\epsilon\sin\omega\cos\varphi & \sin\epsilon\sin\omega\cos\varphi - \sin\varphi\cos\omega \\
-\sin\epsilon & \sin\varphi\cos\epsilon & \cos\epsilon\cos\varphi
\end{bmatrix}
\tag{25}
$$

36

Configuration Level Kinematics

The forearm-wrist module is a serial combination of a 2 DoF spherical mechanism connected to a $\overline{R}P$ 2 DoF serial kinematic chain. The prismatic joint is used for assuring ideal aligning of the device axes with human arm. The linear translation at this joint is currently is not of interest, hence not measured. Omitting the contribution of this prismatic joint, configuration level kinematics (orientation) of 3 DoF spherical kinematic chain of wrist module can be calculated as

$$^{H}R^{Ra}._{\cdot}{}^{Ra}R^{Rb}._{\cdot}{}^{Rb}R^{J} = {}^{H}R^{J} \tag{26}$$

Given the rotation relationship, the end effector rotation variables, that is the Euler angles used to represent the orientation of forearm-wrist module, can be solved analytically from the following set of nonlinear equations

$$\begin{aligned}
\cos\gamma_2 &= -\sin\epsilon \\
\sin\gamma_1\sin\gamma_2 &= \sin\varphi\cos\epsilon \\
\sin\gamma_2\cos\gamma_3 &= -\sin\omega\cos\epsilon
\end{aligned} \tag{27}$$

Motion Level Kinematics

Motion level kinematics and the kinematic Jacobian matrix that maps the joint velocities to end-effector (angular) velocities of the forearm-wrist module can be determined with differentiating Equations (27) and considering the nonlinear relationship between the time derivatives of Euler angles and

angular velocities of the end-effector.

2.3.4 Kinematics of the Full Arm Exoskeleton

Given the analytic kinematic solutions to 3$\underline{R}$RP, Schmidt coupling and forearm-wrist modules, the hybrid kinematics of whole exoskeleton can be calculated by properly connecting these modules in series. In particular, kinematic representation of AssistOn-Arm is a serial connection of $\underline{R}\overline{P}, 3\underline{R}RP, \underline{R}$, Schmidt coupling and forearm-wrist modules. Neglecting unmeasured offset of forearm-wrist module, position of the end-effector of AssistOn-Arm can be expressed as

$$\overrightarrow{r}^{GO} + \overrightarrow{r}^{OS} + \overrightarrow{r}^{S\Xi} + \overrightarrow{r}^{\Xi E} + \overrightarrow{r}^{EF} = x_w\overrightarrow{n_1} + y_w\overrightarrow{n_2} + z_w\overrightarrow{n_3} \qquad (28)$$

where x_w, y_w and z_w are end-effector coordinates of AssistOn-Arm at the same time handle of the forearm-wrist module, with respect to Newtonian ground frame. Note that, when forward kinematics solutions of 3$\underline{R}$RP, Schmidt coupling and forearm-wrist module are known, some of the vectors in Equation (28) can be expressed as

$$\overrightarrow{r}^{SO} = -x_s\overrightarrow{r_1} + z_s\overrightarrow{r_3} \qquad (29)$$
$$\overrightarrow{r}^{\Xi E} = y_e\overrightarrow{l_2} + z_e\overrightarrow{l_3} \qquad (30)$$

while x_s and z_s indicate the end-effector positions of 3$\underline{R}$RP in the sagittal plane, while y_e and z_e are end-effector position variables of the Schmidt coupling.

Configuration Level Kinematics

Configuration of the end-effector of ASSISTON-ARM the handle of forearm-wrist module, can be represented using 6 generalized coordinates: x_w, y_w, z_w for end-effector position and Euler angles ϵ_w, ω_w, φ_w for its orientation. Among these six generalized coordinates, end-effector positions can be solved using the position vector Equation (28). In particular, the end effector position can be calculated as

$$x_w = k_4 - k_1 - x_s - k_6 \sin\theta - \sin\theta(k_7 + z_e)$$
$$-y_e \sin\alpha_2 \cos\theta - k_8(\sin\theta \cos\alpha_3 - \sin\alpha_2 \sin\alpha_3 \cos\theta) \tag{31}$$

$$y_w = k_5 \sin\alpha_1 + z_s \cos\alpha_1 + k_6 \cos\alpha_1 \cos\theta + \cos\alpha_1 \cos\theta(k_7 + z_e)$$
$$+y_e(\sin\alpha_1 \cos\alpha_2 - \sin\alpha_2 \sin\theta \cos\alpha_1) - \sin\alpha_1(k_3 + d_1)$$
$$-k_8(\sin\alpha_1 \sin\alpha_3 \cos\alpha_2 - \cos\alpha_1(\cos\alpha_3 \cos\theta + \sin\alpha_2 \sin\alpha_3 \sin\theta)) \tag{32}$$

$$z_w = k_2 + z_s \sin\alpha_1 + \cos\alpha_1(k_3 + d_1) + k_6 \sin\alpha_1 \cos\theta$$
$$+ \sin\alpha_1 \cos\theta(k_7 + z_e) + k_8(\sin\alpha_3 \cos\alpha_1 \cos\alpha_2 + \sin\alpha_1(\cos\alpha_3 \cos\theta$$
$$+ \sin\alpha_2 \sin alpha_3 \sin\theta)) - k_5 \cos\alpha_1 - y_e(\cos\alpha_1 \cos\alpha_2 + \sin\alpha_1 \sin\alpha_2 \sin\theta) \tag{33}$$

where k_i (i=1,...,13) are the link lengths. The end-effector position of Schmidt coupling y_e, z_e and the end-effector position x_s, z_s and orientation θ of 3<u>R</u>RP can be utilized to express configuration level forward kinematics of ASSISTON-ARM in terms of actuated joint angles and other measured joint

variables.

End effector orientation of ASSISTON-ARM with respect to Newtonian frame can be shown to be

$$^{N}R^{J} = {}^{N}R^{P} \cdot {}^{P}R^{R} \cdot {}^{R}R^{U} \cdot {}^{U}R^{L} \cdot {}^{L}R^{H} \cdot {}^{H}R^{J} \tag{34}$$

where rotations between bodies can be extracted analytically using kinematic solutions of relevant modules. In particular, the analytical solution of configuration level orientation can be found as

$$^{N}R^{J} = \begin{bmatrix} {}^{N}R^{J}_{(1,1)} & {}^{N}R^{J}_{(1,2)} & {}^{N}R^{J}_{(1,3)} \\ {}^{N}R^{J}_{(2,1)} & {}^{N}R^{J}_{(2,2)} & {}^{N}R^{J}_{(2,3)} \\ {}^{N}R^{J}_{(3,1)} & {}^{N}R^{J}_{(3,2)} & {}^{N}R^{J}_{(3,3)} \end{bmatrix} \tag{35}$$

where

$$^{N}R^{J}_{(1,1)} = \cos\alpha_2 \cos\epsilon \cos\omega \cos\theta + \sin\epsilon(\sin\theta \cos\alpha_3$$
$$- \sin\alpha_2 \sin\alpha_3 \cos\theta) - \sin\omega \cos\epsilon(\sin\alpha_3 \sin\theta + \sin\alpha_2 \cos\alpha_3 \cos\theta) \tag{36}$$

$$^{N}R^{J}_{(1,2)} = -\sin\varpi \cos\epsilon(\sin\theta \cos\alpha_3 - \sin\alpha_2 \sin\alpha_3 \cos\theta)$$
$$- \cos\alpha_2 \cos\theta(\sin\omega \cos\varphi - \sin\epsilon \sin\varphi \cos\omega) - (\sin\alpha_3 \sin\theta$$
$$+ \sin\alpha_2 \cos\alpha_3 \cos\theta)(\cos\omega \cos\varphi + \sin\epsilon \sin\omega \sin\varphi) \tag{37}$$

$$^{N}R^{J}_{(1,3)} = \cos\alpha_2 \cos\theta(\sin\omega \sin\varphi + \sin\epsilon \cos\omega \cos\varphi) + (\sin\alpha_3 \sin\theta$$
$$+ \sin\alpha_2 \cos\alpha_3 \cos\theta)(\sin\varpi \cos\omega - \sin\epsilon \sin\omega \cos\varphi)$$
$$- \cos\epsilon \cos\varphi(\sin\theta \cos\alpha_3 - \sin\alpha_2 \sin\alpha_3 \cos\theta) \tag{38}$$

40

$$
{}^{N}R^{J}_{(2,1)} = \cos\epsilon\cos\omega(\sin\alpha_1\sin\alpha_2 + \sin\theta\cos\alpha_1\cos\alpha_2)
$$

$$
+ \sin\omega\cos\epsilon(\sin\alpha 3\cos\alpha 1\cos\theta + \cos\alpha_3(\sin\alpha_1\cos\alpha_2
$$

$$
- \sin\alpha_2\sin\theta\cos\alpha_1)) - \sin\epsilon(\cos\alpha_1\cos\alpha_3\cos\theta - \sin\alpha_3(\sin\alpha_1\cos\alpha_2
$$

$$
- \sin\alpha_2\sin\theta\cos\alpha_1)) \quad (39)
$$

$$
{}^{N}R^{J}_{(2,2)} = \sin\varphi\cos\epsilon(\cos\alpha_1\cos\alpha_3\cos\theta - \sin\alpha_3(\sin\alpha_1\cos\alpha_2
$$

$$
- \sin\alpha_2\sin\theta\cos\alpha_1)) + (\cos\omega\cos\varphi + \sin\epsilon\sin\omega\sin\varphi)(\sin\alpha_3\cos\alpha_1\cos\theta
$$

$$
+ \cos\alpha_3(\sin\alpha_1\cos\alpha_2 - \sin\alpha_2\sin\theta\cos\alpha_1)) - (\sin\alpha_1\sin\alpha_2
$$

$$
+ \sin\theta\cos\alpha_1\cos\alpha_2)(\sin\omega\cos\varpi - \sin\epsilon\sin\varphi\cos\omega)
$$

$$
(40)
$$

$$
{}^{N}R^{J}_{(2,3)} = (\sin\alpha_1\sin\alpha_2 + \sin\theta\cos\alpha_1\cos\alpha_2)(\sin\omega\sin\varphi + \sin\epsilon\cos\omega\cos\varphi)
$$

$$
+ \cos\epsilon\cos\varphi(\cos\alpha_1\cos\alpha_3\cos\theta - \sin\alpha_3(\sin\alpha_1\cos\alpha_2 - \sin\alpha_2\sin\theta\cos\alpha_1))
$$

$$
- (\sin\varphi\cos\omega - \sin\epsilon\sin\omega\cos\varphi)(\sin\alpha_3\cos\alpha_1\cos\theta
$$

$$
+ \cos\alpha_3(\sin\alpha_1\cos\alpha_2 - \sin\alpha_2\sin\theta\cos\alpha_1))
$$

$$
(41)
$$

$$
{}^{N}R^{J}_{(3,1)} = \sin\omega\cos\epsilon(\sin\alpha_1\sin\alpha_3\cos\theta - \cos\alpha_3(\cos\alpha_1\cos\alpha_2
$$

$$
+ \sin\alpha_1\sin\alpha_2\sin\theta)) - \cos\epsilon\cos\omega(\sin\alpha_2\cos\alpha_1 - \sin\alpha_1\sin\theta\cos\alpha_2)
$$

$$
- \sin\epsilon(\sin\alpha_1\cos\alpha_3\cos\theta + \sin\alpha_3(\cos\alpha_1\cos\alpha_2 + \sin\alpha_1\sin\alpha_2\sin\theta)) \quad (42)
$$

$$^N R^J_{(3,2)} = (\sin \alpha_2 \cos \alpha_1 - \sin \alpha_1 \sin \theta \cos \alpha_2)(\sin \omega \cos \varphi - \sin \epsilon \sin \varphi \cos \omega)$$

$$+ \sin \varphi \cos \epsilon (\sin \alpha_1 \cos \alpha_3 \cos \theta + \sin \alpha_3 (\cos \alpha_1 \cos \alpha_2 + \sin \alpha_1 \sin \alpha_2 \sin \theta))$$

$$+ (\cos \omega \cos \varphi + \sin \epsilon \sin \omega \sin \varphi)(\sin \alpha_1 \sin \alpha_3 \cos \theta$$

$$- \cos \alpha_3 (\cos \alpha_1 \cos \alpha_2 + \sin \alpha_1 \sin \alpha_2 \sin \theta))$$

$$(43)$$

$$^N R^J_{(3,3)} = \cos \epsilon \cos \varphi (\sin \alpha_1 \cos \alpha_3 \cos \theta + \sin \alpha_3 (\cos \alpha_1 \cos \alpha_2$$

$$+ \sin \alpha_1 \sin \alpha_2 \sin \theta)) - (\sin \omega \sin \varphi + \sin \epsilon \cos \omega \cos \varphi)(\sin \alpha_2 \cos \alpha_1$$

$$- \sin \alpha_1 \sin \theta \cos \alpha_2) - (\sin \varphi \cos \omega - \sin \epsilon \sin \omega \cos \varphi)(\sin \alpha_1 \sin \alpha_3 \cos \theta$$

$$- \cos \alpha_3 (\cos \alpha_1 \cos \alpha_2 + \sin \alpha_1 \sin \alpha_2 \sin \theta)) \quad (44)$$

The configuration level inverse kinematics of ASSISTON-ARM does not assume an analytical solution; however, the equations characterizing the inverse kinematics can be decoupled and simplified, assuming that the location of the passive slider d_1 is specified or omitted from calculations. Then, an efficient numerical solution can be found by implementing an iterative algorithm.

Motion Level Kinematics

Motion level kinematics and the kinematic Jacobian matrix which maps the joint velocities to end-effector velocities of whole exoskeleton can be determined by differentiating Equations (28) and (35) and considering the relationship between Euler angle derivatives and angular velocities. Neglecting passive prismatic joint position variable d_1, 6 end-effector (angular) veloci-

ties can be obtained with using 11 motion variables at the joints, including the end-effector velocities of 3<u>R</u>RP mechanism, Schmidt coupling and the forearm-wrist module. As a consequence, the kinematic Jacobian of full arm exoskeleton is not a square matrix but has dimensions of 6x11. Kinematic Jacobian matrix J_{exo} of AssistOn-Arm is given in the Appendix.

2.4 Dynamics of AssistOn-Arm

After configuration and motion level kinematics of individual modules and the exoskeleton as a whole have been derived, dynamic calculations of AssistOn-Arm are performed using Kane's method [54]. Realization of Kane's method is carried out utilizing Autolev, an advance symbol manipulation program designed to analyze dynamics of mechanical systems. To implement Kane's method, first acceleration level kinematic calculations are calculated via derivation of velocity level kinematics with respect to time. Mass properties consisting of center of gravity and inertial properties of components are extracted from solid models of components using a CAD program after assigning appropriate material choices. External forces F_x, F_y, F_z and torques T_x, T_y, T_z are considered at multiple interaction points of exoskeleton with the human user. Also motor torques T_i that drive joints are also added to the calculations. Equations of motions derived symbolically using Kane's method.

Due to their very large size, dynamic equations cannot be included in the thesis.

2.5 Kinematics and Statics of the Gravity Compensation Mechanism

In order to increase efficiency and safety, gravity compensation has been introduced to many robotic rehabilitation devices. When a mechanism is gravity balanced, gravity effects on components eliminated and mechanism always stays in equilibrium.

There are two main ways to compensate for the gravity: (i) Derive dynamics of the system and actively balance gravity utilizing actuators, and (ii) passively balance the mechanism by adding auxiliary spring and inertias.

One of the first passive equilibrators has been introduced by [55] with one spring attached to 1 DoF arm. Then, [56] showed that passive balancing for gravity can be done using many different techniques, including counterweight method, linkage and cam mechanism method and spring suspension method. Since realizing counterweight method adds additional inertia to the system and design of the linkage and cam mechanisms are relatively more complex, spring based passive gravity mechanisms have gained popularity. Especially in [57–62] extensive studies on gravity compensation mechanisms with zero-length springs have been introduced. Many kinematic design options for gravity compensation are given in [63]. In [59], it is showed that with zero-length springs, less number of springs can be used in the compensation mechanisms. Gravity compensation mechanisms have also been used for rehabilitation of human limbs by assisting patients through elimination of arm weight [59].

AssistOn-Arm is a 12 DoF mechanism whose center of mass constantly moves in 3 dimensional space when its joints move. On the other hand, if the gravity compensation mechanism can be fixed on the base of the 3RRP

mechanism, then center of gravity of translates only in the sagittal plane of the mechanism. Internal/external rotation and elbow rotation adds another DoF to the movement of center of gravity, but this movement is relatively small.

The gravity balancing of an n DoF manipulator can be obtained by using at least n zero-length springs [64] or $2(n-1)$ conventional springs and $4(n-1)$ links [65]. Since full compensation of gravity for ASSISTON-ARM requires a very complex design due to 3 DoF movements of the center of gravity of the exoskeleton, we have decided to partially compensate for the gravity by tracking movement of center of mass only on the sagittal plane. Remaining effects of gravity can easily be compensated actively using actuators of the device. For instance, double motored actuation of internal/external rotation enables active compensation of gravity at this joint, while non-backdriveable Bowden cable based actuation on elbow joint prevent movements of this joint under the influence of gravity.

According to [61, 62], constant gravity balancing can be obtained with either facilitating fixed inertia during motion or constant potential energy of system including the compensation mechanism. Keeping potential energy constant can be realized using springs and parallelogram mechanisms to locate center of mass of the system [66]. Let V_g be the potential energy of the system, where θ_i is the joint angle of ith DoF of the system. Also let V_s represent the potential energy stored at the gravity compensation mechanism. Total potential energy V_t can be calculated as

$$V_t = V_g + V_s \tag{45}$$

For static balancing

$$\frac{\partial V_t}{\partial \theta} = 0 \qquad (46)$$

where θ represents joint angles of gravity compensator.

In order to obtain constant potential energy, design of compensation mechanism and selection of springs should be realized in an interactive way. Also, for the case of ASSISTON-ARM compensation mechanism must cover workspace of movement of the gravity center and this within workspace collisions between the exoskeleton and gravity compensation mechanism should be avoided.

For ASSISTON-ARM we have considered three gravity compensator mechanisms shown in Figure 2.12. The first gravity compensator [56] (Figure 2.12(a)) can not be used to keep the potential energy of the system constant since excessive loads are not compatible with this design and there exists a singular position inside the workspace of the mechanism. The second gravity compensator [62] has limited workspace as shown in Figure 2.12(b). If this workspace is extended, then gravity compensation mechanism does not fit into the exoskeleton and starts colliding with the other structural elements of the robot. We designed a gravity compensator based on [65]. This compensator can both cover workspace of the center of mass of ASSISTON-ARM and keep potential energy of the system constant. A schematic representation of this gravity compensation mechanism is depicted in Figure 2.12(c). In Figure 2.12, zero-length springs, links of the gravity compensation mechanism and joints are also indicated. Gravitational acceleration signifies the compensated weight.

Schematics of gravity compensation mechanism is depicted in Figure 2.13. A, O, P, R, S, Q and Z are revolute joint points of the compensator. Springs
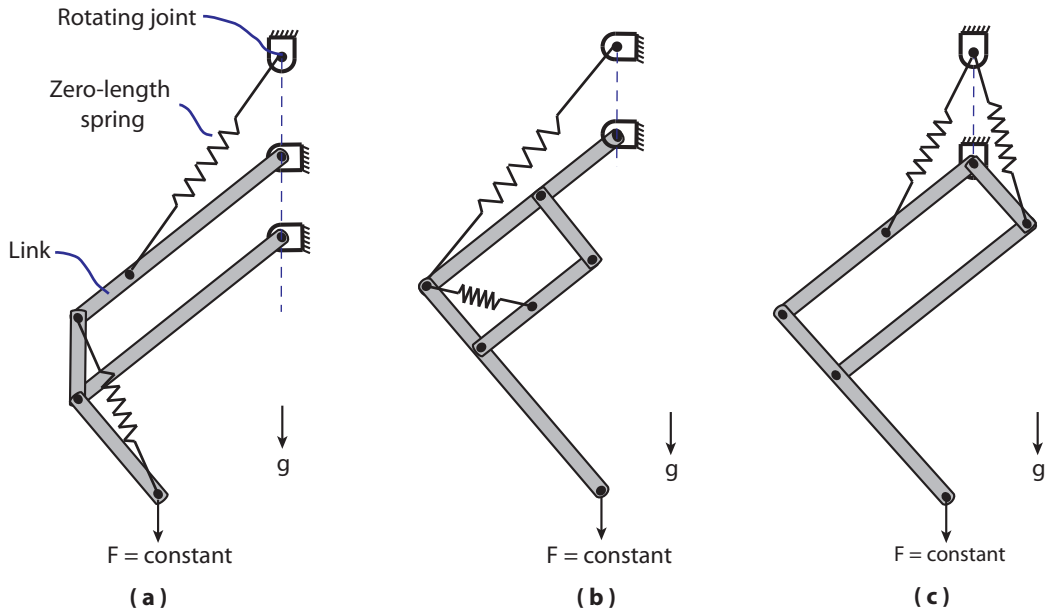
Figure 2.12: Several gravity compensation mechanisms

are attached between Points A, Q and Points A, P. O is on the frame link of the gravity compensator. O, P, R, S compose an auxiliary parallelogram and ASSISTON-ARM is attached to this mechanism from point Z, where the gravity center of moving parts of ASSISTON-ARM lies. c_i and l_i represent distance of gravity center of links from O and length of links, respectively. b_i are the distance of attachment points of spring to links from point O. In the figure, masses of the compensator links and exoskeleton are approximated as point masses. While m_i represents mass of links, m_e represents mass of the exoskeleton. Symbol h is the distance between points O and A. Both A and O represent joints on the frame link.

In Figure 2.13, zero-length springs' deflections and spring constants are represented by x_i and k_i, respectively. β is the angle between link OR and horizontal axis, while θ emphasizes angle between link OP and the vertical
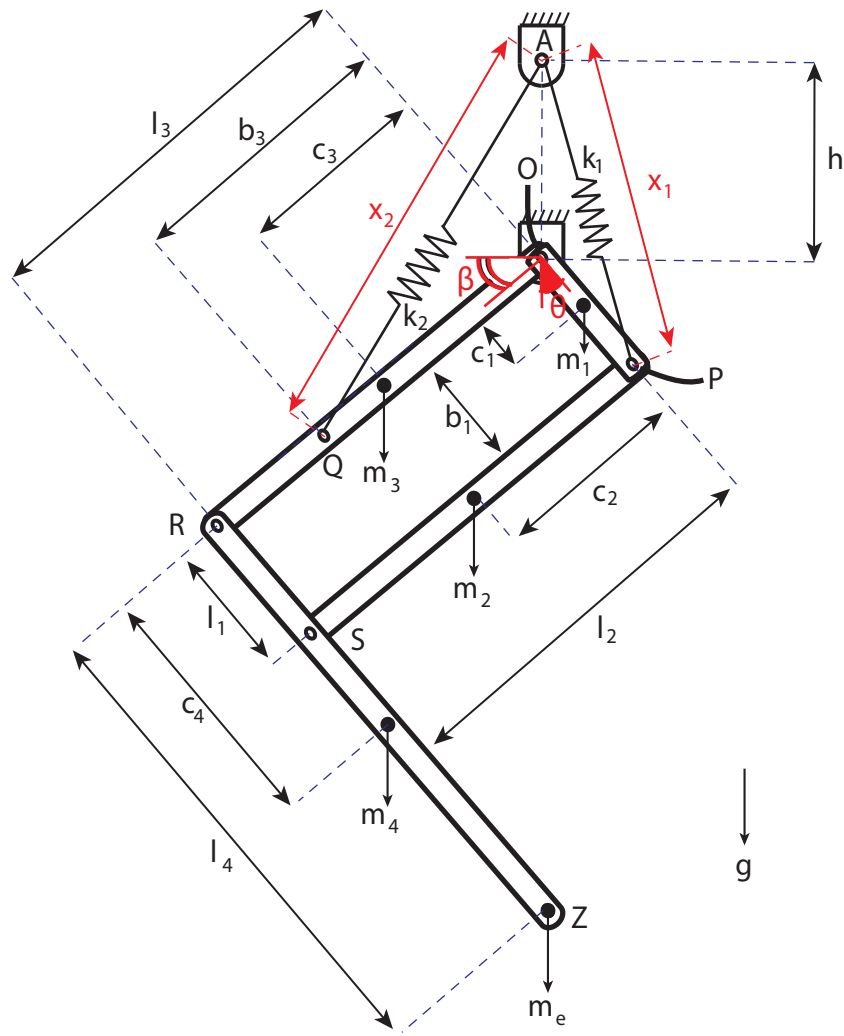
Figure 2.13: Schematics of gravity compensator used with ASSISTON-ARM

axis. Due to kinematics of the parallelogram, links OR and PS are parallel to each other, while links OP and RZ are also parallel to each other.

Gravity Balancing

Gravity balancing is possible by assuring constant potential energy of overall system including gravity compensator. After omitting mass of springs, potential energy resulting from gravitational pull on mechanisms can be found as:

$$V_g = -m_1 g c_1 \cos\theta - m_2 g(l_1 \cos\theta + c_2 \sin\beta) - m_3 g c_3 \sin\beta$$
$$-m_4 g(l_1 \sin\beta + c_4 \cos\theta) - m_e g(l_1 \sin\beta + l_4 \cos\theta) \tag{47}$$

where g represents the gravitational acceleration. Potential energy stored in springs can be formulated as:

$$V_s = \frac{1}{2}k_1 x_1^2 + \frac{1}{2}k_2 x_2^2 \tag{48}$$

where

$$x_1^2 = (b_1 \sin\theta)^2 + (b_1 \cos\theta + h)^2$$
$$x_2^2 = (b_3 \cos\beta)^2 + (b_3 \sin\beta + h)^2$$

Then, the total potential energy in the system is

$$V_t = V_g + V_s = -m_1 g c_1 \cos\theta - m_2 g(l_1 \cos\theta + c_2 \sin\beta) - m_3 g c_3 \sin\beta$$

$$-m_4 g(l_1 \sin\beta + c_4 \cos\theta) - m_e g(l_1 \sin\beta + l_4 \cos\theta) + \tfrac{1}{2}k_1(h^2 + b_1^2 + 2b_1 h \cos\theta)$$

$$+\tfrac{1}{2}k_2(h^2 + b_3^2 + 2b_3 h \sin\beta) \tag{49}$$

After partial derivatives of potential energy $\frac{\partial V_t}{\partial \beta} = 0$ and $\frac{\partial V_t}{\partial \theta} = 0$ are set to zero, necessary spring constants for constant potential energy, while locating centrum inside workspace are determined as:

$$k_1 = \frac{m_1 g c_1 + m_2 g l_1 + m_4 g c_4 + m_e g l_4}{b_1 h}$$

$$k_2 = \frac{m_2 g c_2 + m_3 g c_3 + m_4 g l_2 + m_e g l_2}{b_3 h} \tag{50}$$

Note that, these spring constants are independent from location of gravity center and joint angle variables.

Chapter III

3 Implementation of AssistOn-Arm

This chapter presents design and implementation details for two prototypes of AssistOn-Arm full arm rehabilitation exoskeleton. Both prototypes have been designed and implemented for comparison of different actuation types in terms of their performance. After detailing design, implementation, actuator and transmission selection of exoskeleton for both prototypes, the design of gravity compensation mechanism is discussed.

3.1 Actuator and Transmission Selection for AssistOn-Arm

AssistOn-Arm have three main joint modules including shoulder module, elbow module and forearm-wrist module, each of which aligns human joints with exoskeleton ones.

In Figure 3.1 all of these joints and modules explained in a detailed way. While shoulder module is responsible for all shoulder DoFs, elbow module ensures patients comfort and axis alignment while actuating elbow rotation. Forearm-wrist module is responsible for tracking forearm-wrist rotations while ensuring full self-aligning property of AssistOn-Arm.

AssistOn-Arm can be configured for use with both right and left arm of patients, by rotating first revolute joint by 180°, and manually reconfiguring

3<u>R</u>RP mechanism and the handle at the end-effector to their mirror imaged positions.

Thanks to its self-aligning kinematics, different users can be connected to ASSISTON-ARM without any adjustments.

In addition to its actuation modules, ASSISTON-ARM features Bowden cable based actuation for its elbow joint, a passive gravity compensation mechanism, an electric board and a holonomic moving cart for mobility of the device. Holonomic cart is designed as a stable platform that holds all of modules. In order to obtain stability and keep center of mass close to the ground, heavy steel plates are attached to 4 caster wheels. Wheels can freely turn toward the steering direction and can be locked to not drive. Structure of the cart is designed with aluminum profiles and houses the electric board, a desktop computer. The cart also serves as a table for the therapist.

The exoskeleton is attached to the cart utilizing a commercial telescopic pillar. Telescopic pillar allows for different chair elevations and different human body sizes ensuring comfort and ergonomy.

3.1.1 First Prototype of ASSISTON-ARM

Shoulder module consists of <u>R</u>P-3<u>R</u>RP-<u>R</u> hybrid kinematic chain. Here, the first revolute joint is responsible for abduction/adduction of shoulder joint. To actuate this joint a capstan mechanism with 1:24 reduction ratio is employed. Capstan is a cable based actuation method that uses surface friction between cable and disks in order to transmit forces/torques. A grounded 250 W direct-drive brushed DC motor equipped with 2000 count optical encoders (under quadrature decoding) provides nominal joint torque of 17.5 Nm after reduction, while simultaneously ensuring passive back-driveability

First revolute joint

Bowden cable tensioner

Passive slider

Elbow actuator

Gravity compensation mechansim

Bowden cable

Telescopic pillar

Moving cart

Elbow module

Electric board

Wrist module

Horizontal abduction/adduction

Shoulder Flexion/Extension
Scapular Elevation/Depression
Scapular Adduction/Abduction

Internal/External Rotation

Elbow Rotation

Elbow Yaw/Pitch/Roll

Figure 3.1: Solid Model of ASSISTON-ARM

53

of this joint.

The passive slider attached to first revolute joint is implemented using a low-friction custom made linear stage with linear encoder of 2000 counts per inch resolution attached to it. L-shaped aluminum beam rigidly connects 3$\underline{R}$RP to the moving end of the passive slider.

Design of 3$\underline{R}$RP mechanism realized with custom made rings attached to slim bearings with a concentric way. Rings enable to use of cable based actuation as capstan and Bowden cable. Then, custom made aluminum brackets attached to every disks. End of the bracket collocated revolute and linear bearings which drive symmetric end-effector. Descriptive figure of 3$\underline{R}$RP design is given in Figure 3.2.

Figure 3.2: Solid Model of 3$\underline{R}$RP mechanism

To actuate this mechanism, a two-layered transmission is utilized. At the first level of transmission is implemented using timing belts with 2 mm pitch and provides 1:5 reduction ratio. Furthermore, orthogonal orientation of the actuator shaft with respect to the mechanism is achieved with this belt

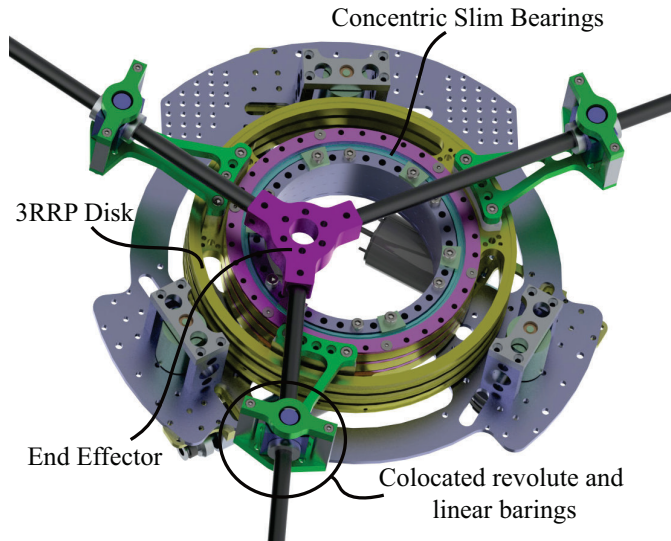transmission through use of two idle pulleys. Tension of the belt can be adjusted by moving the motors and connected pulley mechanisms on the slots provided at the base of the mechanism. The second layer of the transmission utilizes capstan with a 1:7 reduction ratio. The capstan ring is connected to driven pulley of the belt driven first level transmission. As a result, the two-layer design provides an overall 1:35 transmission ratio, in a very compact package. Moreover, thanks to utilization of capstan drive overall friction at the transmission can be kept rather low. To actuate the 3R̲RP mechanism, 150 W direct-drive brushed DC motors equipped with 2000 count optical encoders under quadrature decoding are employed. Note that, these motors can be attached to the L-shaped link; hence, passive gravity compensation is not required to counteract their weights. This prototype of 3R̲RP mechanism possesses a circular workspace with 240 mm diameter for translational movements and can rotate up to 300°. Actuation of first prototype of 3R̲RP module is pictured in Figure 3.3.
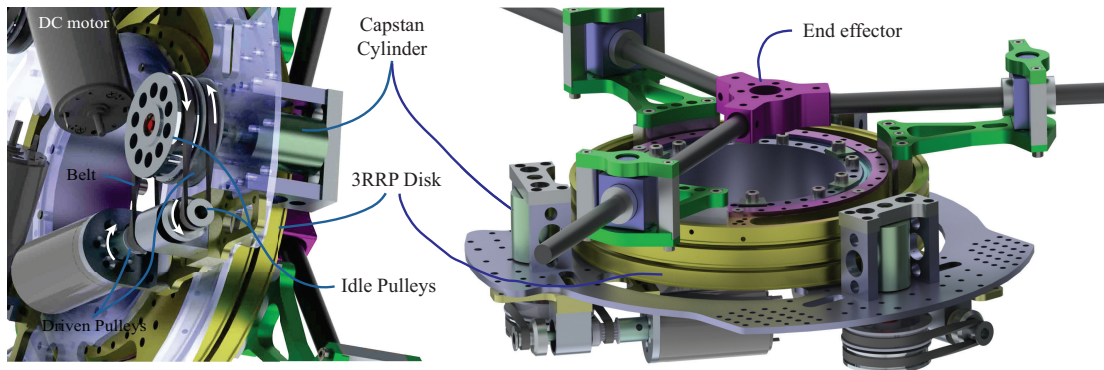

Figure 3.3: Solid Model of 3R̲RP with Two Layered Transmission Design

The end effector of 3R̲RP mechanism is attached to a curved curved slider with a 210° open ring shape, that is designed to driven with Bowden Cables

(for the first prototype of shoulder module) to actuate internal/external rotations of the upper arm. Bowden cables of internal external rotation are planned to be actuated by 200 W DC motor equipped with 2000 count optical encoders and harmonic drives of which have 1:50 ratio. Bowden cable actuated internal/external rotation is capable of delivering 21 Nm nominal torque to the joint. In addition to the 3RRP mechanism that can align its joint axes according to with human counterparts, custom made link component connects end-effector of 3RRP mechanism and curved slider, can be manually adjusted to extend range of upper arm length.

To ensure passive alignment of joint axis, elbow joint features a Schmidt coupling. Schmidt coupling possesses a translational workspace covering a 48 mm diameter circle and is instrumented with three 1440 count optical encoders for measuring translational movement elbow joint. Similar to the internal/external rotation, elbow rotation is also actuated using an identical Bowden cable based transmission and can deliver 21 Nm nominal torque to the elbow joint. Schmidt coupling design is inspired from [50].

The friction in Bowden cables and harmonic drives has a negative impact on passive backdriveability of the internal/external rotation and the elbow joint. On the other hand, this friction is useful to counteract the gravity induced movements due to weight of internal/external rotation, elbow and handle modules. Active back-driveability of internal/external rotation and the elbow joint are achieved by introducing two 6 DoF force/torque sensors. One such sensor is placed at the end-effector of the 3-RRP mechanism, while the other is attached to the handle where the patient holds the device. In this early prototype, a counter-weight based passive gravity compensation mechanism is employed in the system to ensure safety of the patients. Integration

of a more sophisticated passive gravity compensation mechanism has been realized for the second prototype. This first prototype of AssistOn-Arm is depicted in Figure 3.4 together with details of its underlying modules. In Figure 3.4(a), the first revolute joint actuated with capstan mechanism and passive slider, Figure 3.4(b) actuated 3$\underline{R}$RP mechanism, Figure 3.4(c) actuation module of internal/external rotation with Bowden cable, Figure 3.4(d) belt transmission system from two layered transmission, Figure 3.4(e) internal/external joint (C shaped curved slider), Figure 3.4(f) Schmidt Coupling are presented in detail.

AssistOn-Arm is completely self-adjustable at the shoulder complex and elbow joint; hence, no manual adjustable links are necessary for these joints. On the other hand in order to increase compatibility of exoskeleton with all variations of human limb lengths, components are also designed to permit manual adjustment.

(a) Capstan

Passive slider

(c) Harmonic drive

Bowden cable

Capstan disk

(e) Internal/External rotation joint

Passive gravity compensation cable

Sabancı Universites

Force/Torque sensors

Curved slide

(b) 3RRP

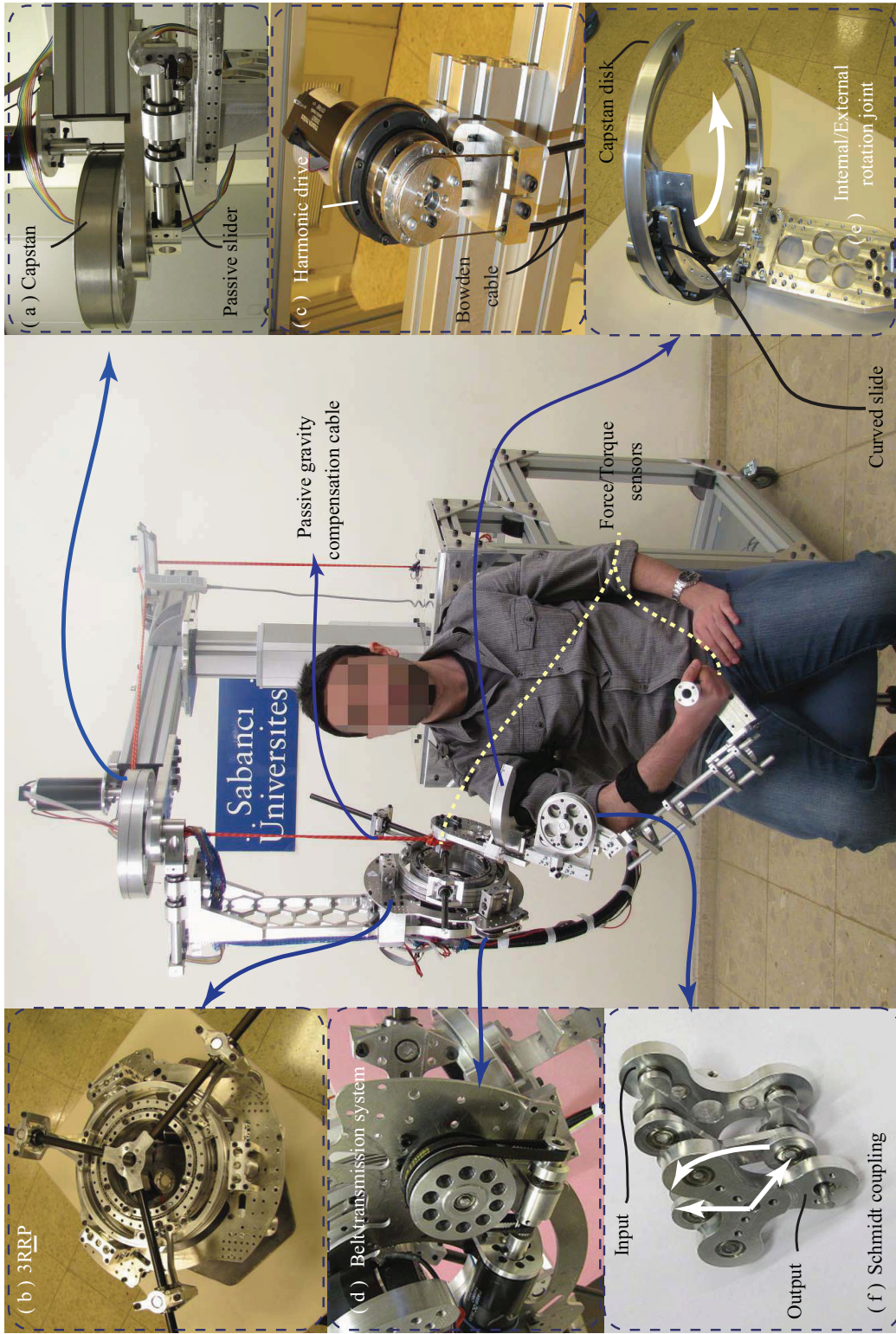(d) Belt transmission system

Input

Output

(f) Schmidt coupling

Figure 3.4: ASSISTON-ARM I with close-ups of its underlying modules

58

During design of AssistOn-Arm each component is designed to overcome more force/torque than maximum force/torque they are expected to encounter during use. Stronger components have bigger wall thickness and have more weight. On the other hand, an exoskeleton need to be light, especially parts which moves and close to end-effector due to safety during interaction with humans. In order to arrange tradeoff between weight of mechanism and resistance to external forces, minimum factor of safety for the design of each component is set as 2.5. After solid design, mechanical analysis of parts implemented via Cosmos finite element analysis (FEA) program embedded in SolidWorks CAD program.

Among the whole design of AssistOn-Arm we analyzed critical modules that encounter highest forces and torques. One of the these critical modules is the 3RRP mechanism. Mechanical stress analysis of current design of 3RRP with Cosmos FEA program is depicted in Figure 3.5. Many parts of 3RRP module are produced using aluminum alloys with 60 MPa yield strength, but critical parts under heavy load are designed with stronger aluminum alloys with 95 MPa yield strength. End-effector of 3RRP encounters separate three forces in three perpendicular directions and a torque applied at the out-plane axis of end-effector. Maximum torques and forces applied at the end-effector of 3RRP are conservatively determined as a summation of the maximum forces/torque that 3RRP can produce and forces/torques that healthy human shoulder can produce. Weight of moving parts of exoskeleton is omitted, due to implementation of gravity compensation mechanism. While element size of 4 point jacobian mesh of bigger parts are selected as 2.5 mm, mesh size of intricate and small parts selected as 0.3 mm. Rotations due to bearings and frictions of contact bodies are included in the analysis. As a consequence

of analysis minimum factor of safety of 3RRP is found as 2.6. In the figure deflection of parts are exaggerated by choice.
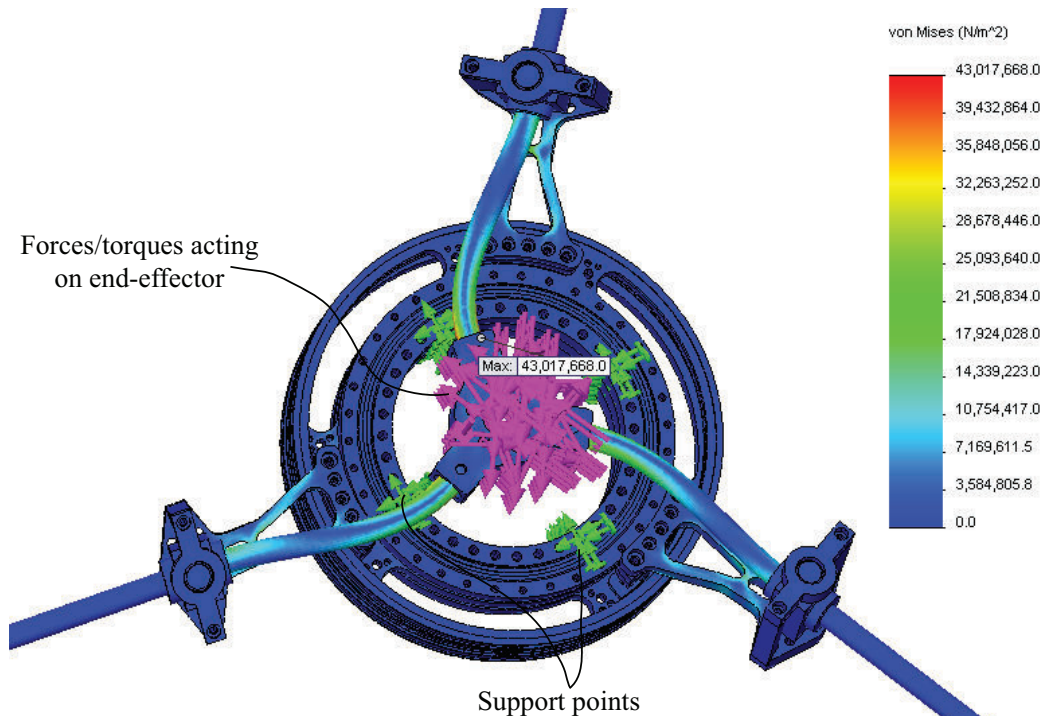
Figure 3.5: Finite element stress analysis of 3RRP mechanism

Also, mechanical stress analysis of L shaped support component, which holds 3RRP mechanism as well as other modules of exoskeleton, with passive slider mechanism is presented in Figure 3.6. Same parameters of FEA and method are pursued at the mechanical stress analysis of the assembly. Furthermore, L shaped custom made part is under effect of forces/torques that human produce during interaction, forces produced by tension in gravity compensation mechanism and force created by weight of all modules. When all forces are included, maximum deflection and factor of safety of assembly are calculated as 3.3 mm and 4.6, respectively.

60

Figure 3.6: Finite element stress analysis of L-shaped assembly

61

3.1.2 Second Prototype of AssistOn-Arm

For the second prototype of AssistOn-Arm a 3<u>R</u>RP mechanism with two layered capstan based transmission, double motor d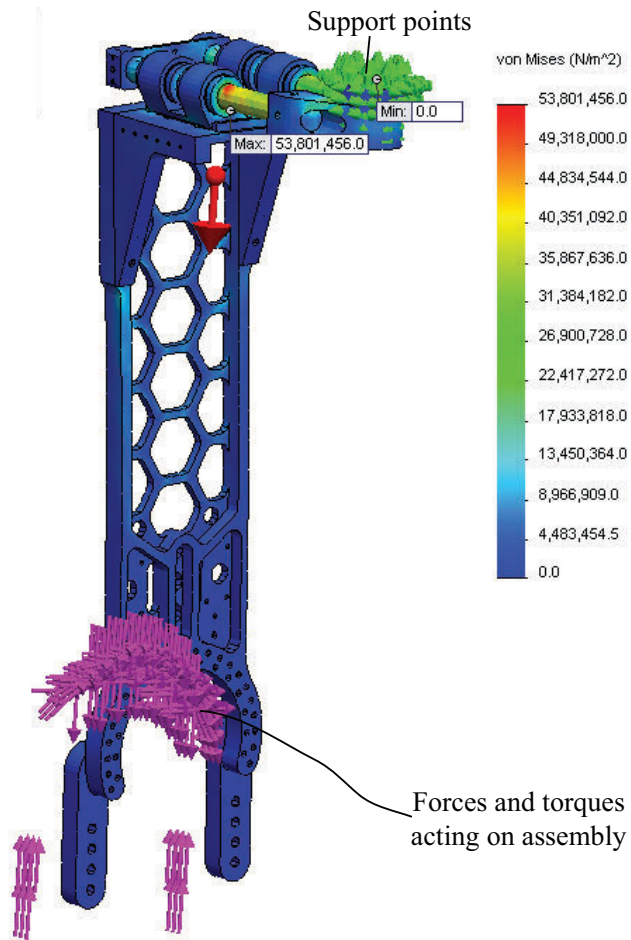riven capstan transmitted internal/external rotation and the forearm-wrist mechanism are implemented. Other modules of AssistOn-Arm are kept the same as the first prototype. Introducing only capstan based transmission on 3<u>R</u>RP mechanism and internal external rotation increases passive backdriveability of the system, but also the need of gravity compensation. So, gravity compensation that is described in the next section is also implemented as a part of the second prototype of AssistOn-Arm.

Actuation of second prototype of 3<u>R</u>RP module is pictured in Figure 3.7. Second prototype of 3<u>R</u>RP has the same circular workspace and can cover up to 300° rotational and 240 mm translational movements. To actuate second prototype of AssistOn-Arm a two-layered capstan transmission is utilized. The first level capstan of transmission provides 1:5 reduction ratio. First capstan transmission employed at the back side of mechanism so moving arms of AssistOn-Arm are not hindered. The second layer of the transmission utilizes capstan with a 1:5.5 reduction ratio. The small capstan ring at second level transmission is connected big capstan ring at first level transmission. As a result, the two-layer design provides an overall 1:27.5 transmission ratio. Apart from first prototype, due to implementation of capstan to obtain whole transmission, friction losses are minimized and passive backdriveability of 3<u>R</u>RP mechanism is significantly increased. To actuate the 3<u>R</u>RP mechanism, 48 V 200 W direct-drive brushed DC motors equipped with 2000 count optical encoders under quadrature decoding are employed. With stronger motor selection, second prototype can deliver up

to 135 N force on its translational DoFs and 36 Nm torque on its rotational DoF. Similar to the first prototype of 3$\underline{\text{R}}$RP mechanism, these motors are directly attached to the L-shaped link; hence, passive gravity compensation is not required to counteract their weight.
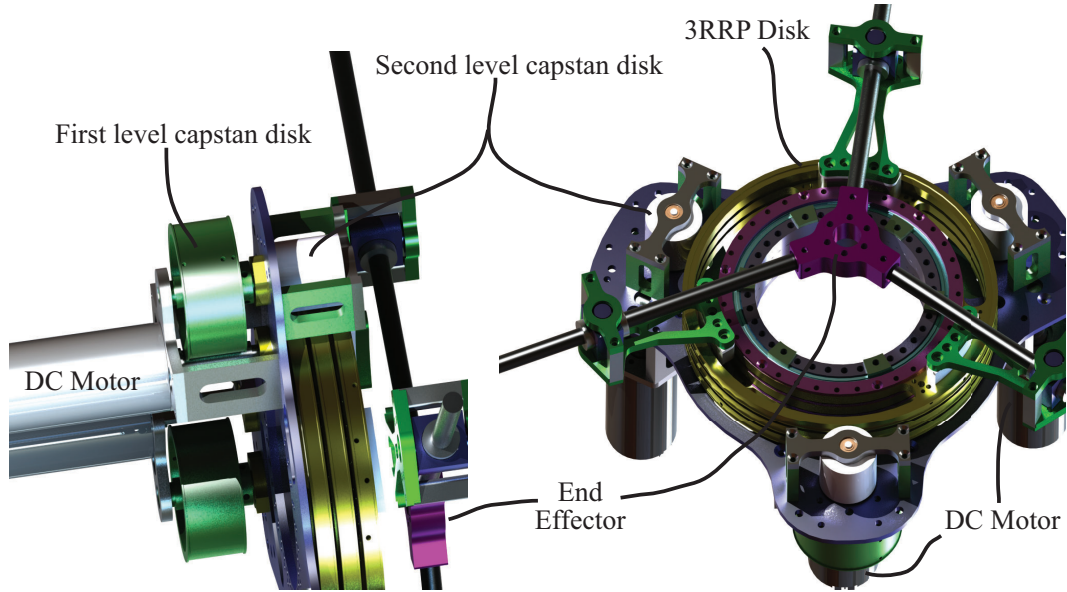
Figure 3.7: Solid model of 3$\underline{\text{R}}$RP with two layered capstan transmission

Also at second prototype of ASSISTON-ARM, in order to increase back-driveability of internal/external rotation, actuation type of this joint has been changed from harmonic driven Bowden cable transmission to direct driven capstan transmission. Using Bowden cables is advantageous since motors can be remotely located and are not attached on moving parts of exoskeleton, but high friction in Bowden cables and harmonic drives hinders passive back-driveability. In order to minimize friction forces during power transmission and sustain high torques at this joint, a double motor actuated capstan transmission is implemented in the second prototype of internal/external rotation as depicted in Figure 3.8. In order to implement a capstan transmission

63

with high ratio capstan disks, height of disks are increased in the second prototype and motors are attached next to the driven disk as seen at the figure. Force/torque sensor attached between the end-effector of 3$\underline{R}$RP and upper arm body is responsible for determining forces on shoulder module, so it also enables torque sensing on internal/external rotation disk. New internal/external rotation joint is detailed in Figure 3.8.
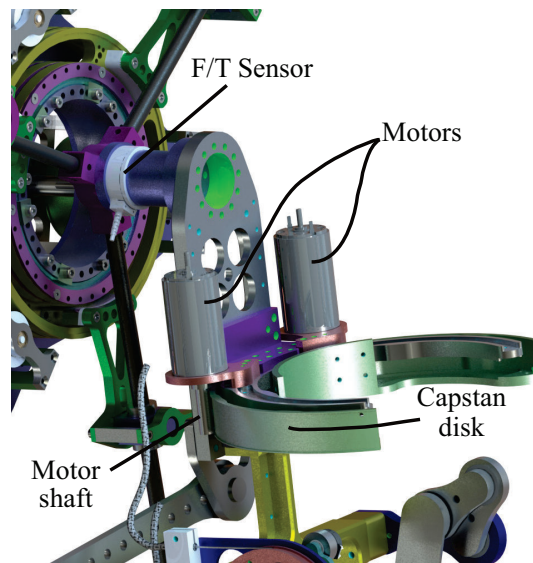
Figure 3.8: Solid model of internal/external joint with two motored capstan transmission

Forearm-wrist module consists of a hybrid $\overline{R}R R R \overline{R} - \overline{R}P$ kinematic chain and effectively constitutes 4 DoF including translation and orientation at handle. Design of wrist module is realized in such a way that grasping of handle can be achieved without interfering with the custom made components while reaching the handle. Also, a translational offset on the direction of forearm axis is implemented in order to simulate offset of human wrist joint and palm during grasping. Current forearm-wrist module is not actuated, on the other hand overlined revolute joints in kinematic chain are equipped

with 1440 counts per turn optical encoders for measurement of forearm-wrist rotations. Rotations observed from encoders used to calculate orientation and position of handle of the forearm-wrist module. Low friction precision sliders are attached between handle and end-effector of wrist module to meet small deviations during forearm and wrist movements. Also, sliders fulfill self-aligning characteristics of the exoskeleton and contribute to the comfort during operation. With sliders attached to handle, ASSISTON-ARM ensures self-alignment for the whole arm complex. A 6 DoF force/torque sensor with $0.1N$ force and $0.00265Nm$ torque precision is attached between the slider and handle. Force/torque sensor is proposed to be used for detecting intention of movements of human arm/hand during therapies. Overall design of forearm-wrist module is realized with custom made aluminum parts.

Second prototype of ASSISTON-ARM is presented in Figure 3.9. Due to delay in manufacturing of Schmidt coupling and forearm-wrist module, these modules are not yet assembled to the prototype. Implementation of 3RRP mechanism in the second prototype is realized with two layered capstan transmission which increases backdriveability of shoulder module. A 6 axis force/torque sensor is also attached to end effector of 3RRP mechanism. Force/torque sensor is not only detects movement intention of human shoulder, but also can be used to help with gravity compensation in active manner. High backdriveability of shoulder module is supported with passive gravity compensation mechanism detailed in the next section. High tensile cables used for gravity compensation mechanism are routed with custom made idle pulleys. Zero-length springs which conserves potential energy of the system, are placed back side of the L shaped link. Zero-length springs are anchored to ground via catenary wire tensioners, so pretension of springs can

be easily adjusted. Internal/external rotation of shoulder is actuated with two small motors with capstan transmission and motors are grounded to the end effector of 3RRP mechanism. For actuation of elbow joint, Bowden cable actuation disks are placed on top of the telescopic pillar.

Mechanism details of second prototype of ASSISTON-ARM is depicted at Figure 3.10. In this figure modules of the exoskeleton and actuation details can be seen. At upper row of pictures second prototype of 3RRP with two layered capstan transmission is represented. A torque/force sensor is attached between end-effector of 3RRP mechanism and upper arm part of exoskeleton. With the lower row of images shoulder internal/external rotation and elbow joints are visualized. As seen at the figure shoulder internal/external rotation is realized with capstan transmission mechanism with two small DC motors. Elbow joint is actuated via Bowden cables. End-effector of gravity compensation mechanism is strictly attached to upper arm part of the exoskeleton.

At the Figure 3.11, ASSISTON-ARM is depicted while human subjects with different arm lengths and gender attached to the exoskeleton. Users can be connected to the ASSISTON-ARM with attachment parts located at upper arm and lower arm. Due to self-aligning nature of the exoskeleton, setup time required to attach exoskeleton to human subjects is less then 20 seconds. But due to the different size of forearm of human subjects position of handle is manually adjusted, on the other hand after implementation of wrist module and Schmidt coupling there will be no need of manual adjustment.

Springs

Wire tensioners

Back view

Cable routing

3R<u>R</u>P with
force/torque
sensor

Bowden cable
actuation

Gravity compensation
mechanism

Internal/external
rotation

Elbow

End-effector

Front view

Figure 3.9: Second prototype of AssistOn-Arm

67

First level capstan

Second level capstan

End effector of 3RRP mechansim

3RRP mechansim

T/F sensor

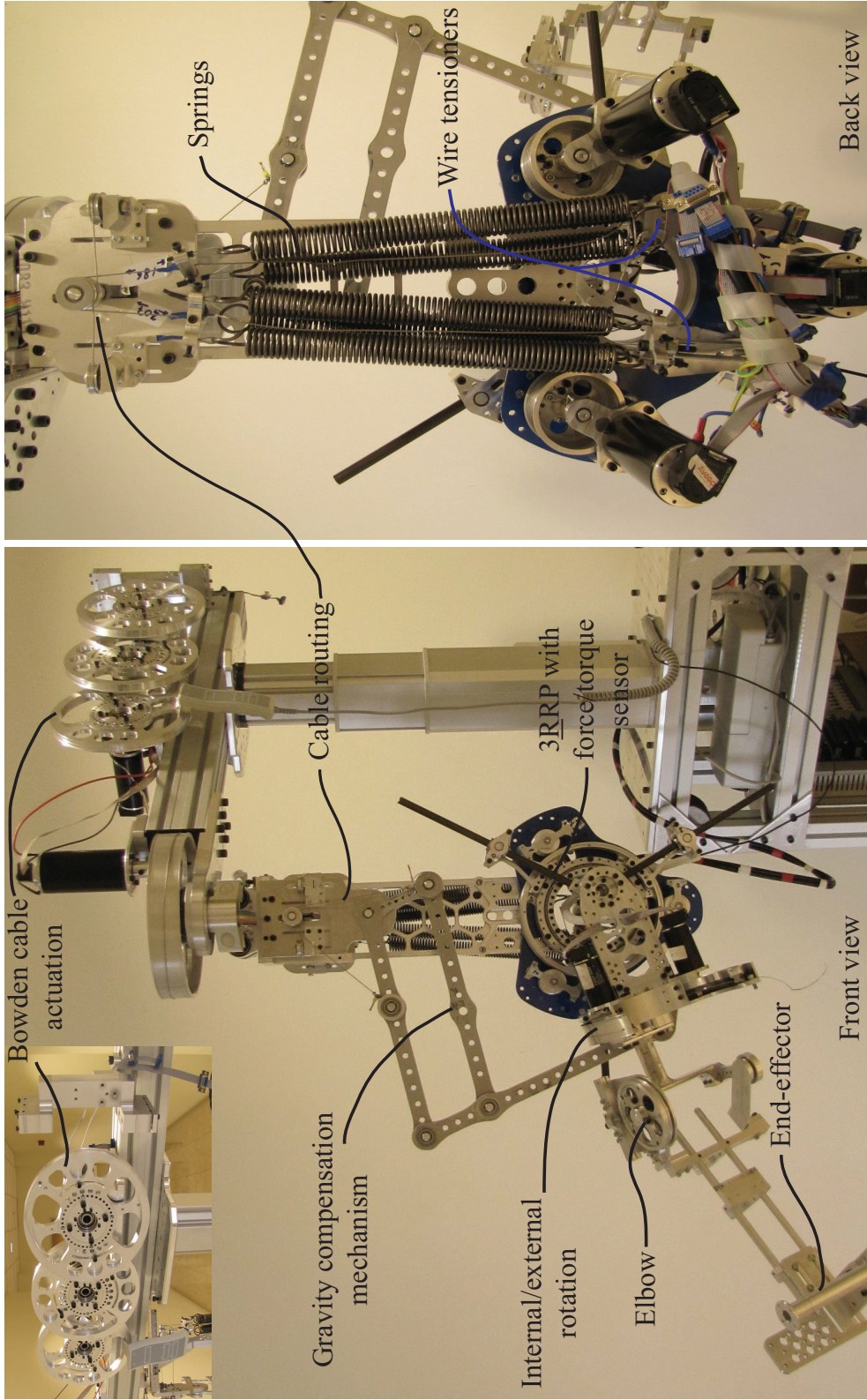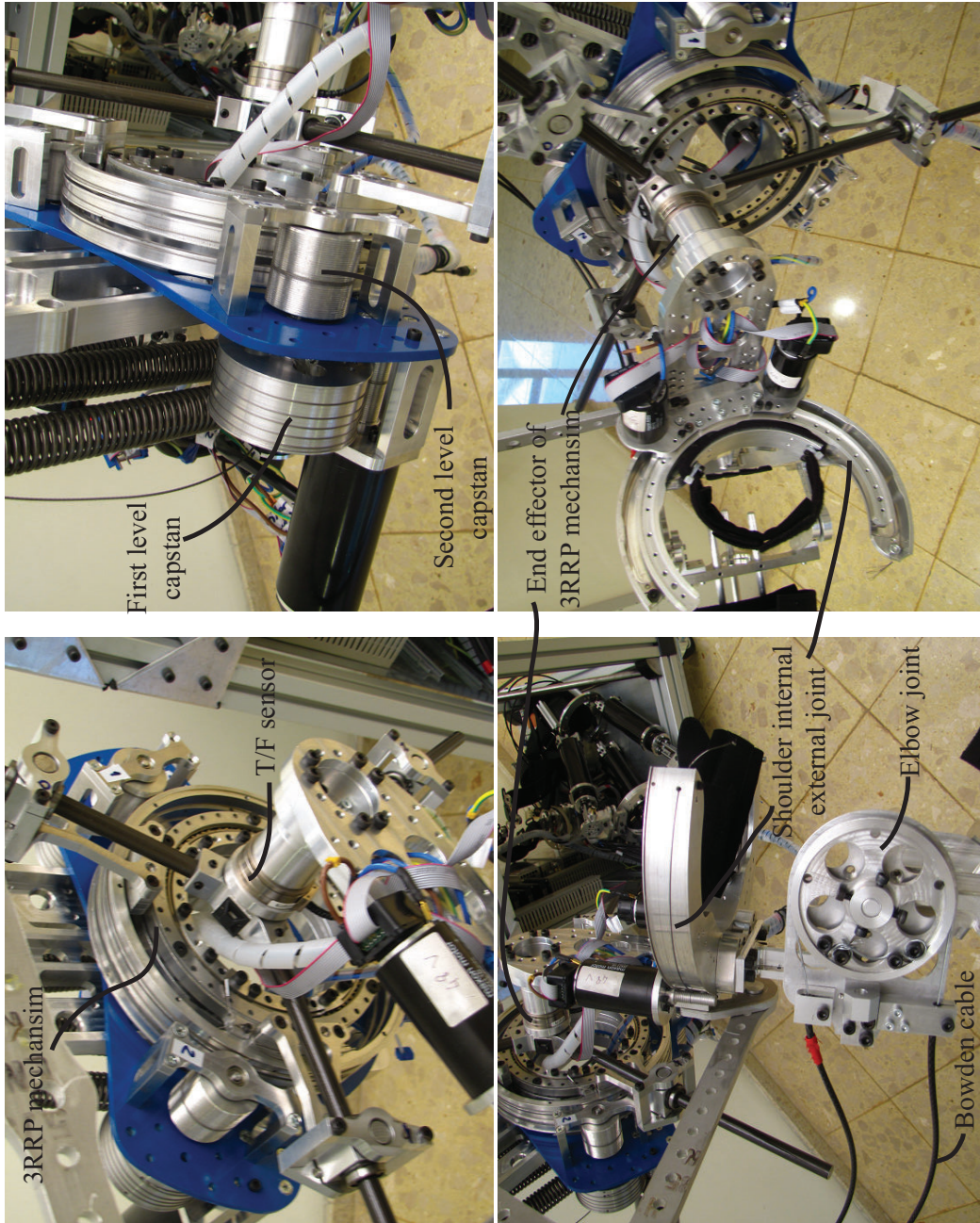Shoulder internal external joint

Elbow joint

Bowden cable

Figure 3.10: Details of Second prototype of AssistON-Arm
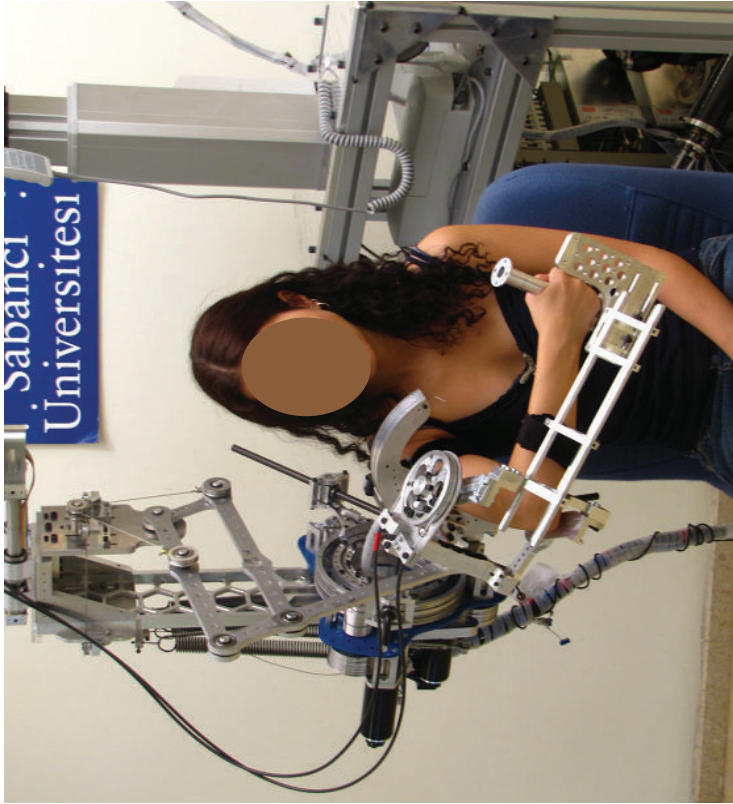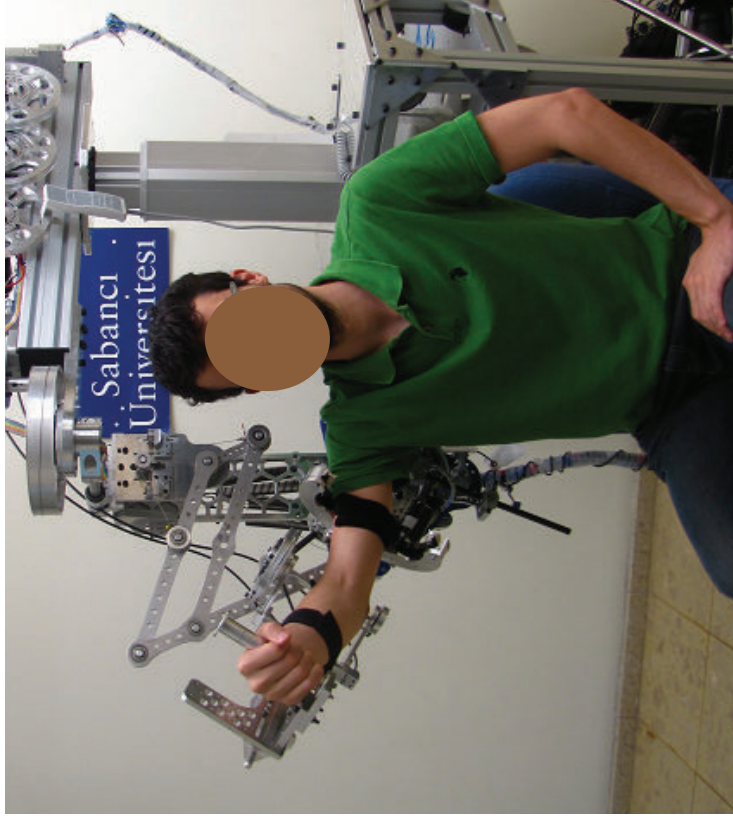
Figure 3.11: Second prototype of AssistOn-Arm attached to different human arm sizes
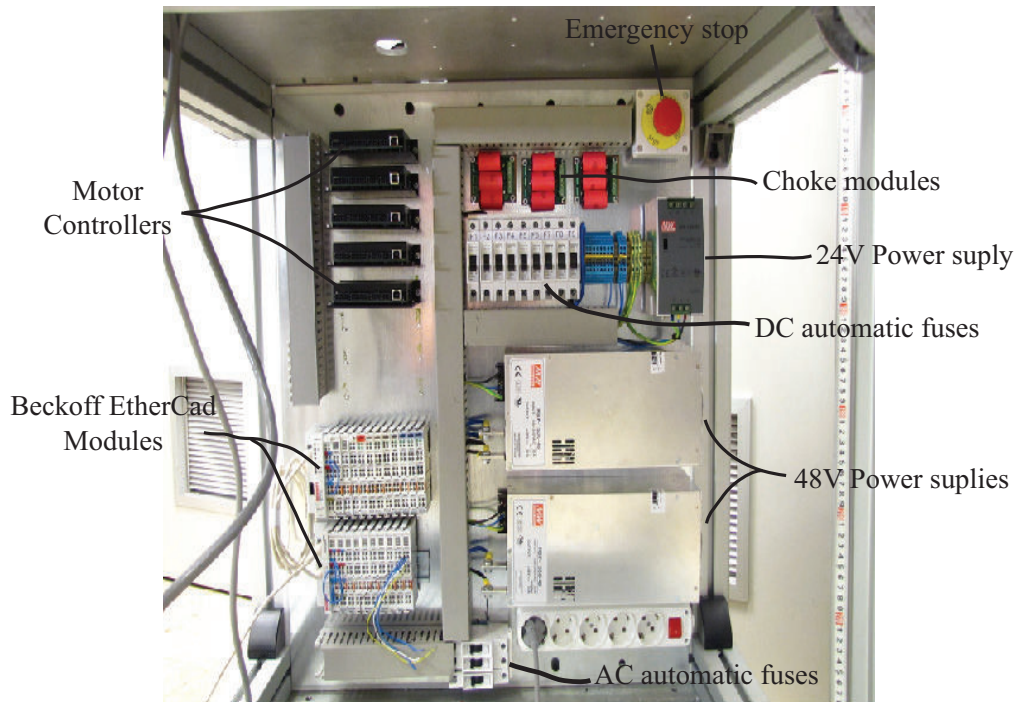
Figure 3.12: Electric board attached to holonomic cart

Electric board which is depicted at Figure 3.12 has also been implemented with the second prototype of ASSISTON-ARM. Electric board contains EPOS 2 motor controllers for up to 9 actuated joints, 3000 W-48 V and 150 W-24 V power supplies, emergency stops, automatic fuses for AC and DC circuits, choke modules for 9 actuators and Beckoff EtherCAT terminals and input/output modules. EtherCAT is a fieldbus communication system that enables very low cycle time even with high number of joints. EtherCAT also eliminates need to real time control board to be attached to the computer, enable real-time control of the system with above 1 kHz sampling rates.

3.2 Design and Implementation of the Gravity Compensation Mechanism

There are two main design criteria for gravity compensation mechanism for ASSISTON-ARM. First, end-effector of gravity compensator should track gravity center of ASSISTON-ARM during all movements of ASSISTON-ARM. So, link lengths of compensator need to be selected in a way such that compensator covers all workspace of the gravity center. Secondly, limitations in the selection of spring constant and stroke determine connection points of springs to gravity compensator.

In Figure 3.13, CAD design of the gravity compensation mechanism of ASSISTON-ARM is given together with its link lengths. Links are manufactured as custom made aluminum parts and joints are supported with ball bearings. Link lengths are selected in a such way that workspace of gravity compensator covers nearly all possible points that gravity center reaches in the sagittal plane. Workspace of gravity compensator and gravity center of ASSISTON-ARM are depicted in Figure 3.14, where red points represent all possible gravity center positions for ASSISTON-ARM and black stars represents points that the compensation mechanism can reach.

Components of gravity compensator weights about 400 grams and moving parts of the exoskeleton (from end-effector of 3RRP mechanism to the handle) have 5980 grams of mass. According to [67] and [68], average male human arm weights about 3500 grams. As a consequence for proper compensation of all these weights due to exoskeleton, gravity compensator and human arm, with given link lengths of compensator, the spring constants are determined as $k_1 = 3$ N/mm and $k_2 = 2$ N/mm. In order to implement these spring constants, springs that have 1 N/mm stiffness and 225 mm stroke are
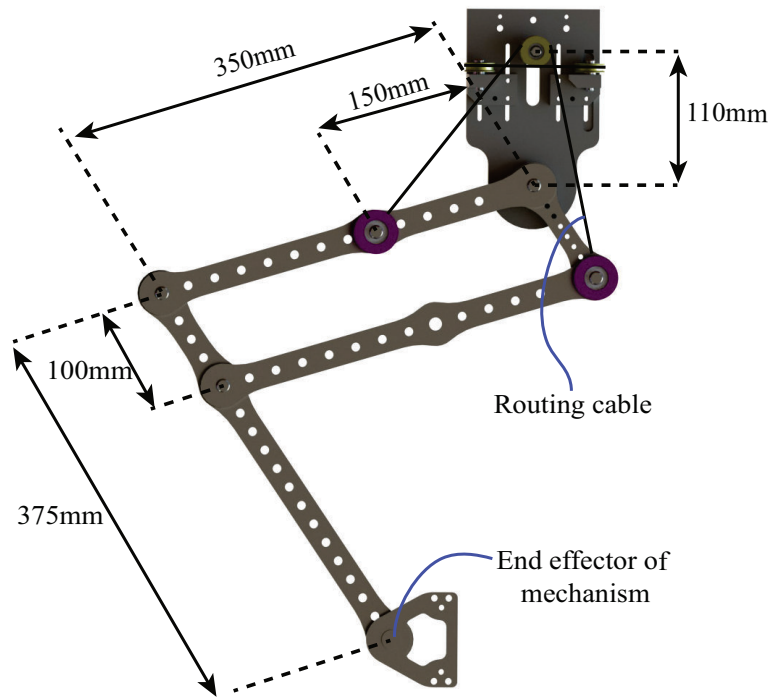
Figure 3.13: Solid model of the gravity compensation mechanism
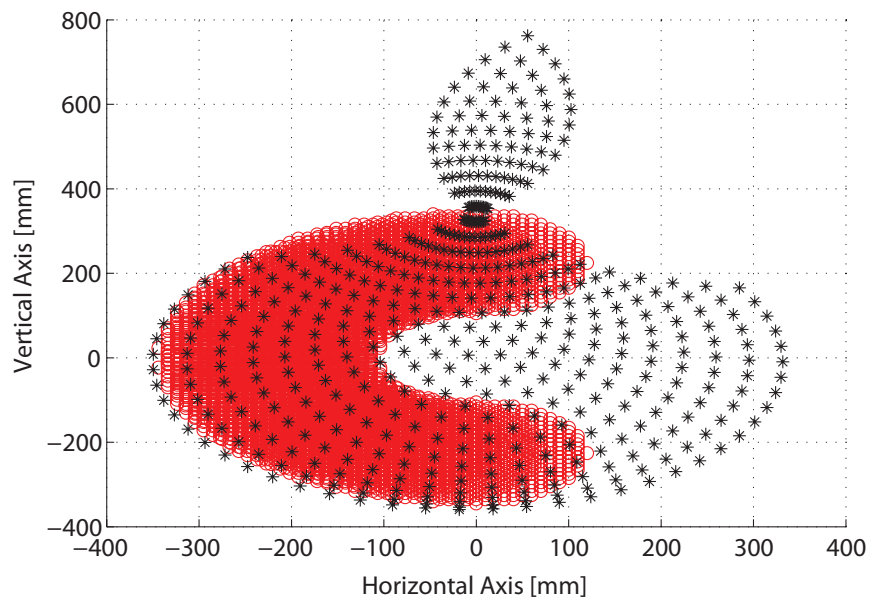
Figure 3.14: Workspace of the gravity compensation mechanism and center of mass of ASSISTON-ARM

connected each other in a parallel manner.
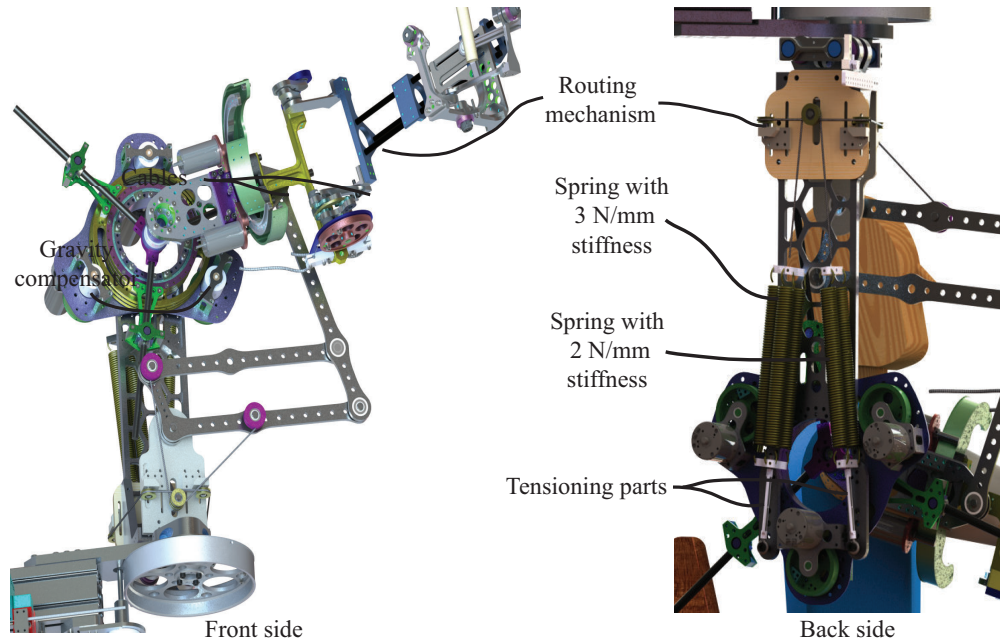
Figure 3.15: Gravity compensation mechanism of ASSISTON-ARM

Within the workspace of the gravity compensator, springs need to reach 225 mm stroke. In order to permit this stroke with the design, springs are fixed to the back side of frame of the 3$\underline{R}$RP mechanism and forces/deflections of springs are conveyed with cables. As shown in Figure 3.15, cables are routed with idle pulleys from the gravity compensator to the springs. Even though, it is not possible to assign a constant gravity center to ASSISTON-ARM due to elbow and shoulder internal/external rotations, the end effector of gravity compensator is attached to ASSISTON-ARM at the point where gravity center is when the elbow is fully flexed. This gravity center point determined using solid model of the device. Springs tension and preload can be adjusted with tensioning components.

In order to observe performance of gravity compensation mechanism, we

73
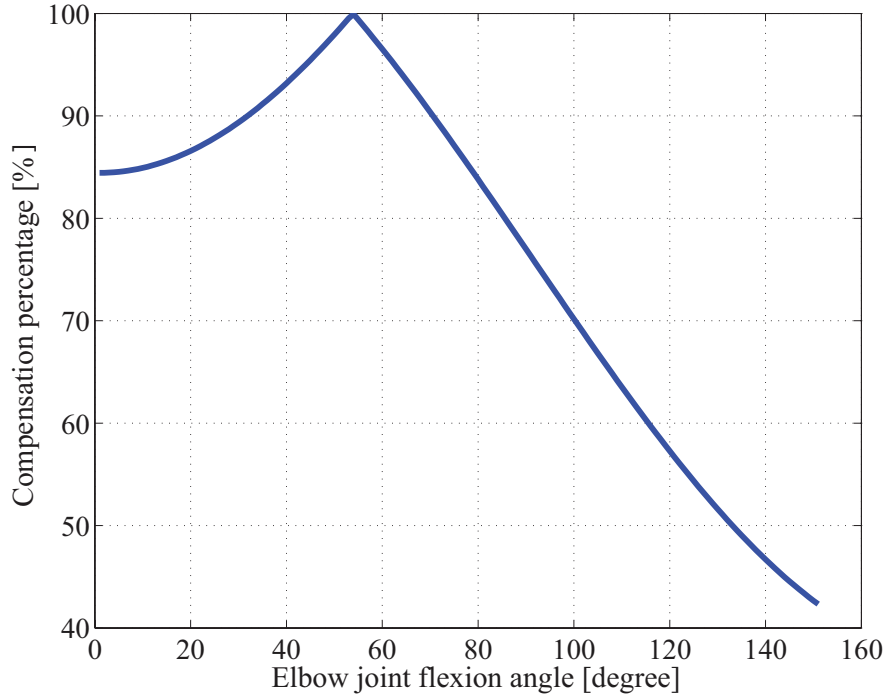
Figure 3.16: Performance characteristics of gravity compensation mechanism with respect to elbow joint motions

have analyzed compensation percentage metric with respect to different joint angles. During analysis we have calculated the potential energy stored at gravity compensation mechanism and compared with gravitational potential energy of the system for different joint positions. We have observed that motion of 3RRP and rotational motion of shoulder internal/external joint do not change the position of gravity center which is projected on sagittal plane with respect to end-effector of gravity compensation mechanism. So, performance of the compensator do not change with movements of these joints. Only joint that effects performance metric of gravity compensation mechanism is elbow joint. At Figure 3.15, for different elbow flexion angles, cancelation rate of gravitational potential energy with gravity compensation mechanism is depicted. Average arm weight of human subject is selected as 3500 grams

as indicated at [67] and [68]. According to [69], daily living activities elbow joint requires minimum 27 and maximum 149 degrees flexion. For majority number of daily living tasks with elbow joint, gravity compensation mechanism can compensate more than 70% gravitational effects including subject arm and system weight.

Chapter IV

4 Experimental Characterization

In this chapter, experimental and analytic characterization of AssistOn-Arm is presented. In the first section, workspace of AssistOn-Arm is analyzed. In the second section, manipulability of 3RRP mechanism is presented. Third section covers force/torque, resolution, backdriveability and inertia characteristics of each module.

4.1 Workspace of AssistOn-Arm

Human arm joints have wide range of transitions and rotations. Rotations and transitions of individual joints of the exoskeleton are designed to cover RoM of human joints. Table 4.1 presents RoM for the translations and rotations of a healthy human shoulder complex [70], as well as RoM of AssistOn-Arm for the corresponding movements. Apart from some structural limitations due to self-collisions of the device, AssistOn-Arm can cover the whole RoM of human shoulder complex. Note that, in addition to allowing GH mobilization during the rotations of the shoulder complex, AssistOn-Arm also allows for scapular elevation/depression and protraction/retraction decoupled from these rotations. Also in Table 4.2, RoM for the elbow, forearm and wrist joint movements of a healthy human is presented [71, 72] together with RoM of AssistOn-Arm for the corresponding movements. Human wrist

joint possesses two active DoFs including extension/flexion and ulnar/Radial deviations. As seen from tables, ASSISTON-ARM covers almost whole RoM of a healthy human.

Table 4.1: RoM of the Human Shoulder vs ASSISTON-ARM

Joint Plane	Frontal		Sagittal		Horizontal		Scapular	
Movement	Abduction	Adduction	Flexion	Extension	Abduction	Adduction	Elevation/Depression	Protraction/Retraction
Human Amplitude	180°	30°	180°	50°	30°	140°	30/50mm	25/25mm
Range	210°		230°		170°		80 mm	50 mm
Movement	Abduction	Adduction	Flexion	Extension	Abduction	Adduction	Elevation/Depression	Protraction/Retraction
Exo Amplitude	170°	30°	170°	50°	30°	140°	120/120 mm	120/120mm
Range	200°		220°		170°		240 mm	240 mm

Table 4.2: RoM of the Human Elbow, Forearm and Wrist vs ASSISTON-ARM

Joint	Elbow		Forearm		Wrist		Wrist	
Movement	Extension	Flexion	Pronation	Supination	Extension	Flexion	Ulnar Deviation	Radial Deviation
Human Amplitude	0°	146°	80°	90°	60°	54°	40°	17°
Range	146°		170°		114°		57°	
Movement	Extension	Flexion	Pronation	Supination	Extension	Flexion	Ulnar Deviation	Radial Deviation
Exo Amplitude	0°	170°	60°	60°	60°	60°	60°	60°
Range	170°		120°		120°		120°	

Figure 4.1(a) depicts the translational workspace of ASSISTON-ARM at the shoulder complex, calculated using the forward kinematics of the first two sub-linkages (RP-3RRP hybrid kinematics) of the exoskeleton. Figure 4.1(a) demonstrates that ASSISTON-ARM can effectively locate its rotation axes at a relatively large volume around the shoulder complex; hence, can faithfully track and assist the movements of the humerus head even during GH mobilization exercises.

Figure 4.1(b) presents the translational workspace of ASSISTON-ARM at its end-effector. In order to obtain the boundary of the workspace presented in Figure 4.1, forward kinematics of the exoskeleton is calculated at a large number of joints configurations using a brute force method. The resulting 1.2 million points for the end-effector location forms a point cloud. The points that constitutes outer boundary of this point cloud is extracted and smooth mesh surface is fitted on these points to represent the boundary. Inspecting the resulting workspace, one can verify that ASSISTON-ARM can cover almost whole of workspace of human arm.

Also, the self-aligning kinematics of ASSISTON-ARM is not only useful for alignment of joint axes with device axes, but can also compensate for variations in the arm lengths of different patients. As a result, since no manual adjustment of link lengths is required for 90% of patients, ASSISTON-ARM significantly shortens the setup time required to attach a patient to the exoskeleton. Furthermore, thanks to its self-aligning kinematics, manipulator can cover reachable workspace of human shoulder.

In addition, ASSISTON-ARM allows for additional manual adjustments to better accommodate different user groups. Table 4.1 presents statistical data on human arm lengths and the range of arm lengths that can be covered by
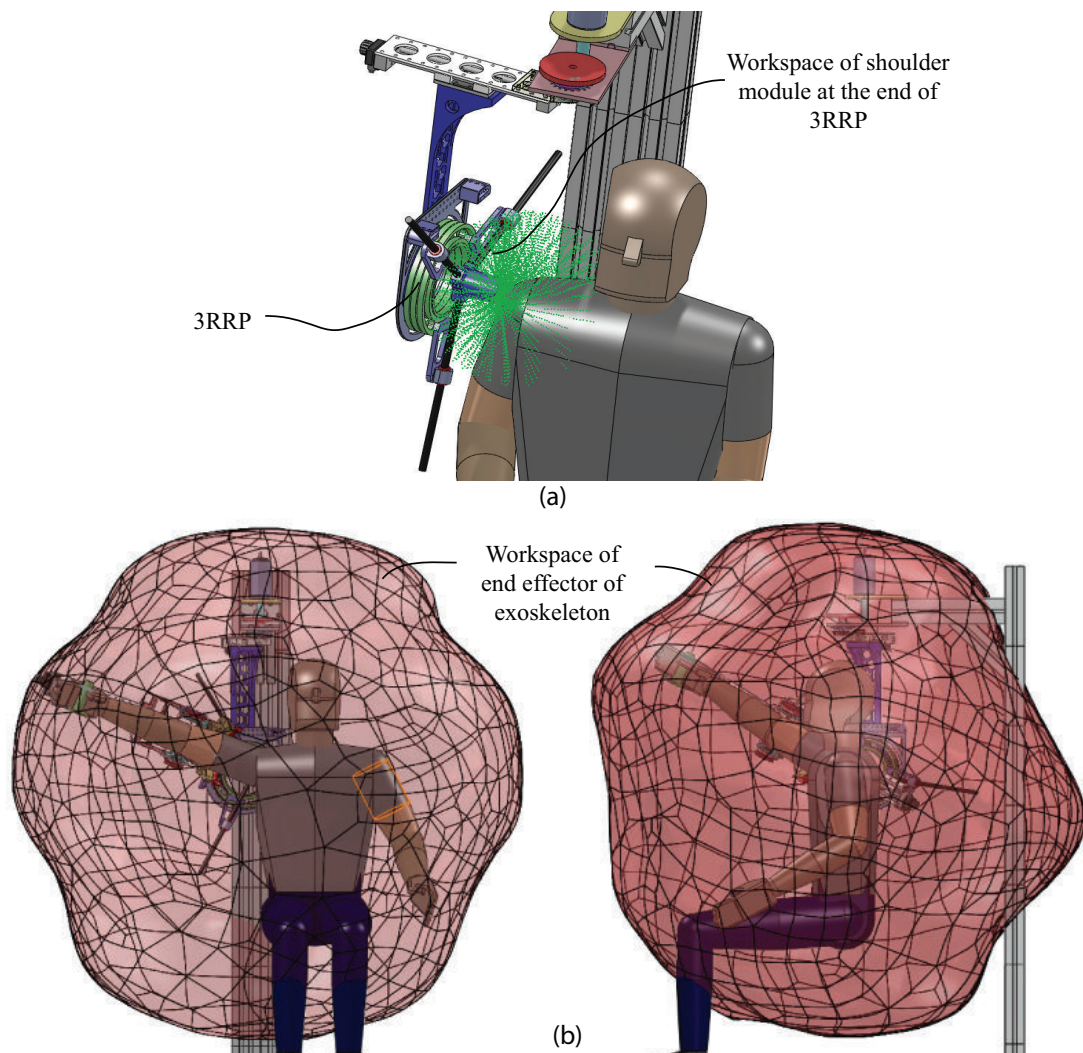
Figure 4.1: Translational workspace of ASSISTON-ARM at the shoulder complex and at its end-effector

ASSISTON-ARM with passive self-alignment and manual adjustment together with self-alignment, respectively.

Table 4.3: Human Arm Size [68] and Corresponding ASSISTON-ARM Link Lengths [mm]

	Bone/Links	Humerus		Ulna	
	Gender	Male	Female	Male	Female
Human	Bone Lengths	330 ± 17.9	304.3 ± 17.3	262.2 ± 14.0	239.9 ± 13.7
	Link Lengths	Maximum	Minimum	Maximum	Minimum
Exo	Passive Alignment	430	190	280	230
	Manual Adjustment + Alignment	465	155	310	200

4.2 Manipulability of 3R̲RP Mechanism

Manipulability measure is a physical interpretation of the scaling factors that represent task-space and joint-space performance of a manipulator [73]. Manipulability equals to product of singular values of normalized Jacobian matrix of manipulator at a specific task or joint space configuration. So, manipulability of a mechanism differs for every point within the workspace. While very low manipulability measure indicates presence of a singularity, high manipulability value represents absence of singularity and high performance of the manipulator. Isotropy of the mechanism is a measure of how homogenous the manipulator measure is distributed over the workspace of the mechanism. In this section we analyze manipulability of the most critical mechanism of system, 3R̲RP mechanism, in order to evaluate the isotropy of the mechanism within its workspace, and to study its distance from singularities.

Manipulability measure, calculated using the Jacobian of the mechanisms, is dimensionless. On the other hand, Jacobian of manipulators, which contains different type of joints (prismatic, rotational, spherical) and DoFs, con-

81

tains mixed physical units. So in order to obtain Jacobian that has comparable physical units, a normalization technique has been proposed in [73]. Normalized Jacobian matrix can be derived as

$$\hat{J} = S_J J^T S_T \tag{51}$$

where J is the Jacobian of the manipulator, S_J is the maximum torque/force capabilities of actuators and S_T contains maximum desired torques/forces of manipulator at its end effector along DoFs of mechanism.

After the normalized Jacobian matrix is obtained, manipulability measure of system can be revealed via using methods that gives product of singular values of normalized Jacobian matrix. Let u represent the manipulability measure, then manipulability measure can be derived using Singular Value Decomposition (SVD) of the normalized Jacobian through the equation

$$u = \sqrt{\left[\hat{J}\hat{J}^T\right]} \tag{52}$$

Manipulability of the 3$\underline{R}$RP mechanism is plotted in Figure 4.2 when the end-effector rotation kept at $\theta = 0°$. Since the Jacobian matrix of 3-$\underline{R}$RP mechanism involve both translational and rotational components, it is normalized using task-dependent design matrix normalization technique [73] and product of three singular values of the normalized Jacobian matrix is selected as the manipulability metric. Note that for every task space point, Jacobian of manipulator changes. Figure 4.2 indicates all manipulability measures in a contour plot among whole workspace of 3$\underline{R}$RP. For presentation in figures, resulting manipulability values are normalized by dividing with the

82

largest manipulability within the whole translational workspace, so that the range is between 0 and 1. Figure 4.2 shows that manipulability measure is bounded away from singularities and its variation stays within 25% of its maximum value with the workspace, indicating a highly uniform behavior of 3-$\underline{R}$RP mechanism.
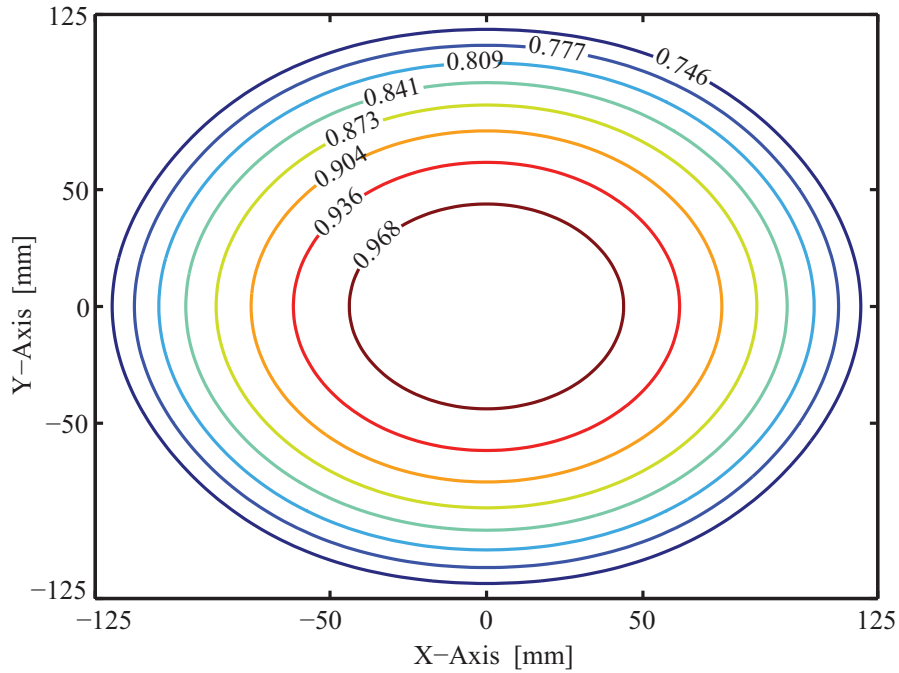

Figure 4.2: Manipulability measure of 3$\underline{R}$RP mechanism at $\theta = 0°$

Figure 4.2 depicts manipulability contour plots for the translational workspace. 3$\underline{R}$RP mechanism has an additional DoF, the end effector rotation. Figure 4.3 presents the manipulability of the mechanisms when the end-effector is rotated from $\theta = 0°$ to $\theta = 120°$ with 30° intervals. Note that rotations above $\theta = 120°$ need not be plotted due to the symmetric construction of the mechanism. As seen in Figure 4.3, 3-$\underline{R}$RP mechanism displays very similar characteristics with Figure 4.3; hence, the mechanism preserves its isotropic

nature even under rotations of its end-effector.
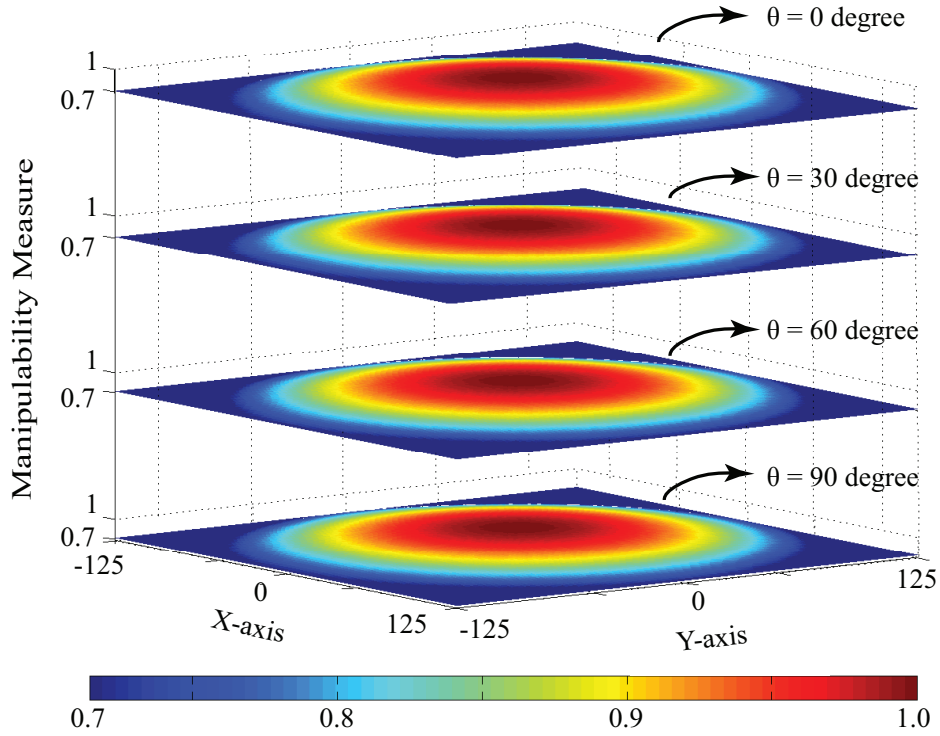
Figure 4.3: Manipulability of 3R̲RP mechanism for at various orientations of its end-effector

4.3 Performance Characterization of ASSISTON-ARM

Transmission ratios and actuators of ASSISTON-ARM are determined by considering human force/torque limits and utilizing the Jacobian of the device.

In the first design, a direct drive 250 W 24 V motor with a capstan transmission is utilized for first revolute joint. 1:24 capstan ratio gives ability for this joint to deliver 11.64 Nm continuous torque. With two layered belt-capstan transmission of 1:35 ratio 3R̲RP mechanism can produce 70 N forces and 17.85 Nm torque at its translational and rotational DoFs, respectively.

Internal/external rotation of shoulder and elbow joints are actuated by 200 W 24 V 1:50 ratio harmonic driven motor and Bowden cable transmission in the first prototype. These joints can generate up to 20.25 Nm continuous torques. Table 4.4 provides a comparison between the force/torque capabilities of a healthy human [74,75] and the first prototype of AssistOn-Arm. The table includes all shoulder DoFs, shoulder abduction/adduction, flexion/extension, elevation/depression and scapular adduction/adduction.

Table 4.4: Actuation Characteristics of the First Prototype of AssistOn-Arm

	Exoskeleton Continous	Exoskeleton Peak	Human	Exoskeleton Actuator	Transmission Type and Ratio
Abduction/Adduction Rotation	11.7Nm	338Nm	-	250W DC	Capstan 1:24
Shoulder Flex./Exten. Scapular Ele./Dep. Scapular Add./Abd.	17.9Nm 70N 70N	271.5Nm 1000N 1000N	27Nm 115N 134N	3RRP 3 units of 150W DC	Two Layered Bowden and Capstan 1:35
Internal/External Shoulder Rotation	20.3Nm	676.4Nm	30Nm	200W DC	Bowden/Harmonic Drive 1:50
Elbow Rotation	20.3Nm	676.4Nm	72.5Nm	200W DC	Bowden/Harmonic Drive 1:50

Table 4.5 presents the experimental characterization of the first prototype of 3-RRP mechanism that serves as the core of the self-aligning kinematics of AssistOn-Arm. Maximum instantaneous and continuous forces applied at horizontal and vertical directions of 3-RRP mechanism and maximum instantaneous and continuous torque applied by the end effector of 3-RRP mechanism are listed in Table 4.5. These values are determined as the minimum values within the given workspace of 3-RRP mechanism. Moreover, resolutions of the end-effector motions of 3-RRP mechanism along translational directions and about its rotation axis are calculated and presented in Table 4.5. Back-driveability analysis of this mechanism indicates that end-effector of 3-RRP mechanism can be moved with 4.7 N to 6 N force along the

translational directions, while 1.3 N-m torque is required for rotation under passive gravity compensation.

The apparent inertia of ASSISTON-ARM up to its internal/external rotation module is 0.1 kg-m^2 for shoulder extension/flexion rotations and 2 kg for all shoulder translations. With the addition of internal/external rotation, elbow and wrist modules, maximum task space inertia at vertical and horizontal directions of sagittal plane and rotation at the end effector reach to 6.5 kg, 4.8 kg and 1.3 kg-m^2, respectively. As a result, passive gravity compensation is designed to ensure safety and comfort of patients and back-driveability of the device.

Table 4.5: Experimental Characterization Results for the First Prototype of 3RRP Mechanism

Criteria	x	y	θ
Instantaneous Peak Force/Torque	1000 [N]	1000 [N]	260 [Nm]
Maximum Continuous Force/Torque	70 [N]	70 [N]	18 [Nm]
End-Effector Resolution	0.017 [mm]	0.03 [mm]	0.000087 [rad]
Back-driveability	4.7 [N]	6 [N]	1.3 [Nm]
Task Space Inertia	2 [kg]	1.8 [kg]	0.1 [kg m^2]

At second prototype actuators and transmission of 3RRP mechanism has been changed in order to obtain higher forces/torques with better backdriveability. Two layered capstan transmission enables 1:27.5 transmission ratio. Second prototype of 3RRP mechanism can deliver up to 135 N forces and 36.4 Nm torque on its translational and rotational DoFs, respectively. While actuation of elbow rotation stays same, internal/external rotation of shoulder joint of the exoskeleton is actuated with two direct driven motors which have 1:25 capstan ratio with 9.15 Nm continuous torque. In the second prototype, internal/external rotation can deliver less torque than first prototype, on the other hand backdriveability of overall exoskeleton has been significantly in-

creased and passive gravity compensation minimizes effect of gravity on the joint. Table 4.6 provides the force/torque capabilities of the second prototype of ASSISTON-ARM.

Table 4.6: Actuation Characteristics of the Second Prototype of ASSISTON-ARM

	Exoskeleton Continous	Exoskeleton Peak	Exoskeleton Actuator	Transmission Type and Ratio
Abduction/Adduction Rotation	11.7Nm	338Nm	250W DC	Capstan 1:24
Shoulder Flex./Exten. Scapular Ele./Dep. Scapular Add./Abd.	36.4Nm 135N 135N	638Nm 2300N 2300N	3RRP 3 units of 200W DC	Two Layered Capstan 1:27.5
Internal/External Shoulder Rotation	9.2Nm	100Nm	150W DC 2 units	Capstan 1:25
Elbow Rotation	20.3Nm	676.4Nm	200W DC	Bowden/Harmonic Drive 1:50

Table 4.7 presents the experimental characterization of the second prototype of 3-RRP mechanism. Values at the table are determined with same method as used for Table 4.7. Task space inertia values do not changes between prototypes. Back-driveability analysis of this mechanism indicates that end-effector of 3-RRP mechanism can be moved with 3.39 N to 4.3 N force along the translational directions, while 0.923 N-m torque is required for rotation when mechanism is not attached to ASSISTON-ARM.

Table 4.7: Experimental Characterization Results for the Second Prototype of 3RRP Mechanism

Criteria	x	y	θ
Instantaneous Peak Force/Torque	2300 [N]	2300 [N]	638 [Nm]
Maximum Continuous Force/Torque	135 [N]	135 [N]	36.4 [Nm]
End-Effector Resolution	0.0216 [mm]	0.0382 [mm]	0.0001107 [rad]
Back-driveability	4.3 [N]	3.4 [N]	0.923 [Nm]

Table 4.8 presents the experimental back-driveability characterization of assembly of ASSISTON-ARM. In this experimental analysis all modules in-

Table 4.8: Experimental Back-Driveability Characterization Results of Realized Assembly

Criteria	Back-driveability
Horizontal shoulder rotation joint	5.58 [Nm]
Horizontal DoF of 3RRP	10.67 [N]
Vertical DoF of 3RRP	10.02 [N]
Rotational DoF of 3RRP	2.56 [Nm]
Shoulder internal/external joint	0.43 [Nm]
Elbow joint	3.32 [Nm]

cluding gravity compensation mechanism is realized and assembled. So, back-driveability information at the table reflects actual forces-torques that human subject need to implement to the system in order to drive system passively. Back-driveability analysis of this mechanism indicates that first revolute joint can be moved with 5.58 N-m torque. Horizontal shoulder rotation joint realized with lubrication free polymer bearing so back-driveability torque of this joint is expected to be high. Experimental analysis shows that end-effector of 3-RRP mechanism can be moved with 10.02 N to 10.67 N force along the translational directions, while 2.56 N-m torque is required for rotation under passive gravity compensation and all modules are assembled. Also, analysis indicates that shoulder internal/external rotation can be moved with 0.43 N-m torque. Bowden cable actuated elbow joint can be passively moved with 3.32 N-m torque.

Chapter V

5 Control and Useability Studies of ASSISTON-ARM

5.1 Control Performance

In order to test control performance of ASSISTON-ARM we implemented joint and task space impedance control on every individual joint of exoskeleton.
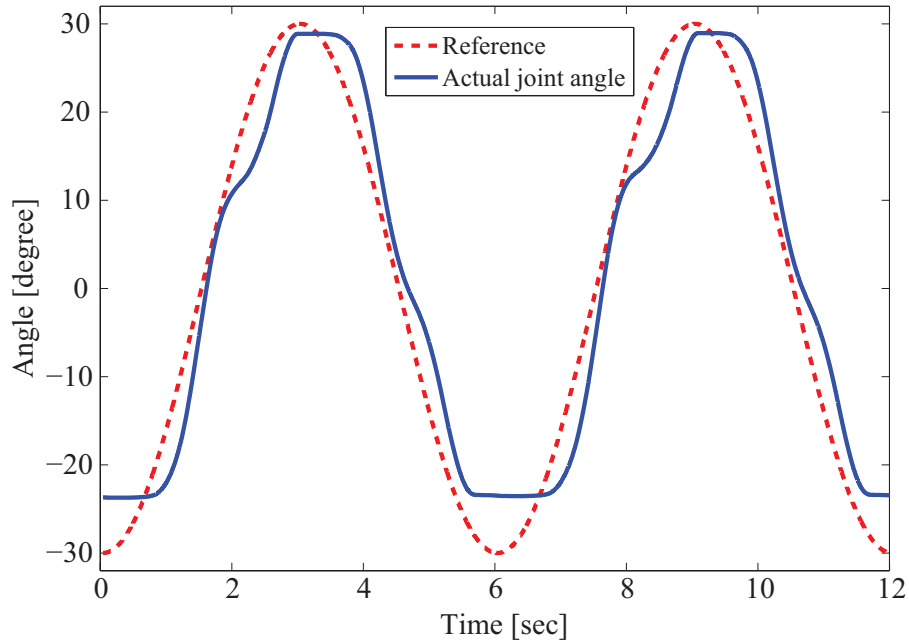

Figure 5.1: Reference and actual trajectories of joint space impedance control of first revolute joint

Figure 5.1 represents joint space impedance control results of first joint of ASSISTON-ARM which is responsible for shoulder abduction/adduction movement. For the joint control, a sinusoidal reference trajectory with 60° amplitude and 1/6 Hz frequency is imposed to joint. Controller stiffness of the joint space impedance control determined as 50 Nm/rad. Due to sticking-slipping friction of polymer slewing ring bearing located at this joint, RMS error of the joint control calculated as 5.18°.
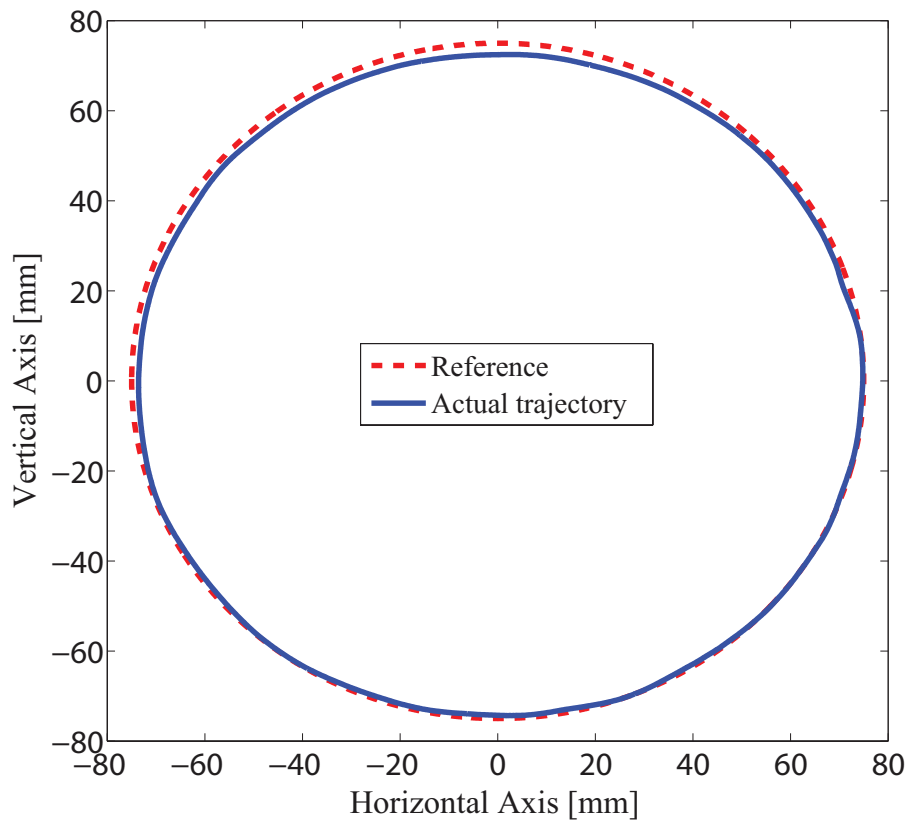

Figure 5.2: Reference and actual trajectories of task space impedance control of 3RRP

Figure 5.2 depicts task space impedance control result of 3RRP mechanism when all of modules-mechanisms are connected to ASSISTON-ARM. Different from joint space space control at task space control end effector

position of mechanism is controlled. In this case we controlled end effector of 3RRP, which is responsible for horizontal shoulder motions at the exoskeleton with using impedance control. For the task control, a circular task reference trajectory with 75mm radii is imposed to end effector of 3RRP. Frequency of the circular movement is determined as 0.5Hz. Controller stiffness of the task space impedance control determined as 33 N/mm at the translational DoFs. RMS error of the task space impedance control control for 150mm diameter circular trajectory calculated as 2.1mm. During this control experiment, a constant trajectory to rotational DoF of 3RRP is given with 50 Nm/rad rotational stiffness imposed by impedance control.
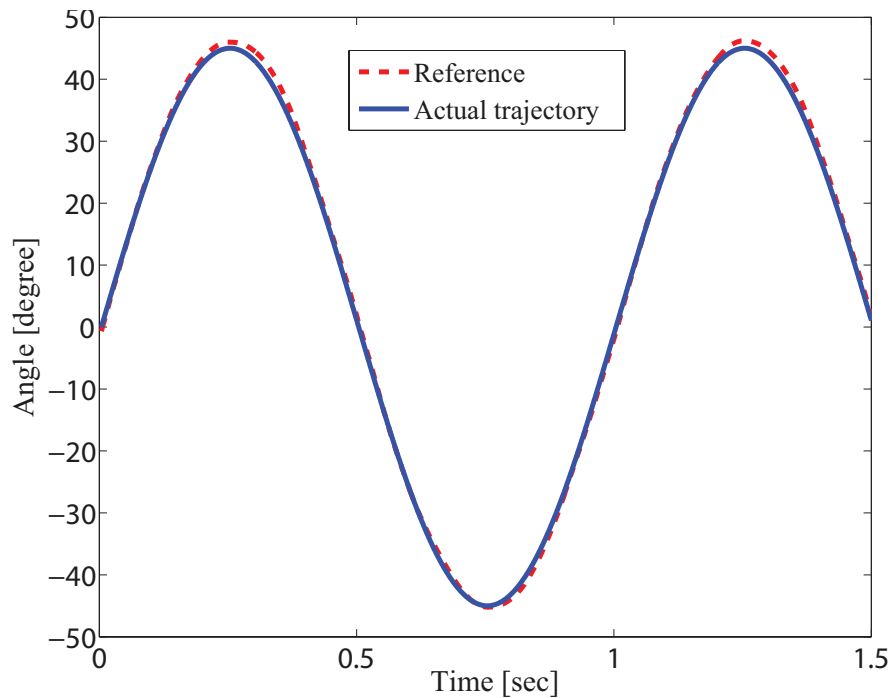

Figure 5.3: Reference and actual trajectories of joint space impedance control of internal/external rotation joint

Figure 5.3 represents joint space impedance control results of shoulder internal/external rotation joint of ASSISTON-ARM. For the joint control, a

sinusoidal reference trajectory with 90° amplitude and 1.33 Hz frequency is imposed to joint. Controller stiffness of the joint space impedance control determined as 100 Nm/rad. Note that this joint is actuated by two motors. RMS error of the joint control calculated as 0.85°.
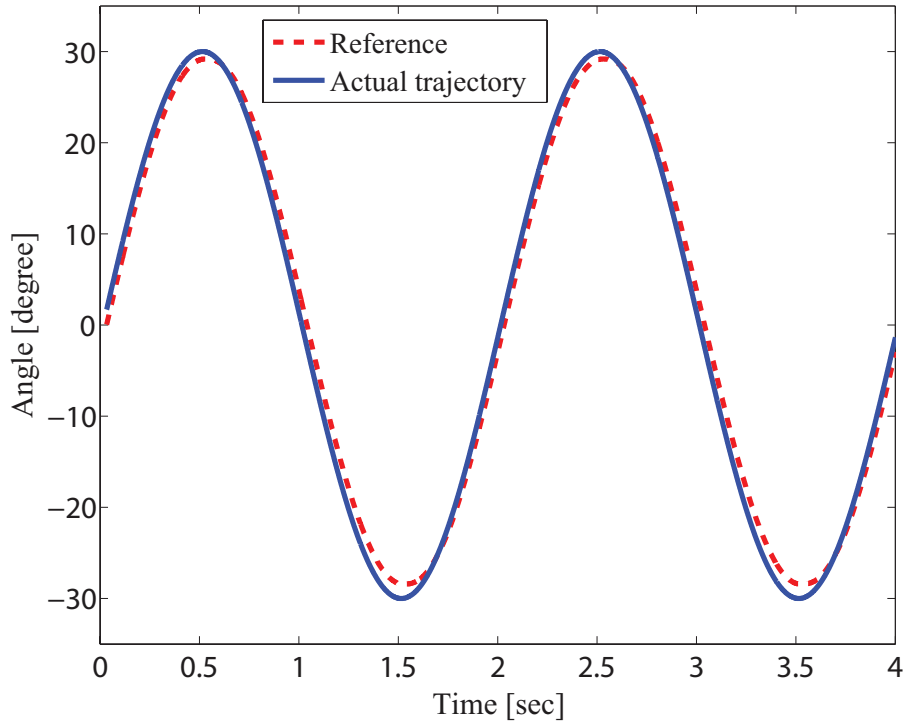

Figure 5.4: Reference and actual trajectories of joint space impedance control of elbow joint

Figure 5.4 represents joint space impedance control results of elbow joint of ASSISTON-ARM. For the joint control, a sinusoidal reference trajectory with 60° amplitude and 0.5 Hz frequency is imposed to joint. Controller stiffness of the joint space impedance control determined as 85 Nm/rad. Due to backlash of Bowden cable transmission method, RMS error of the joint control observed as 1.62°.
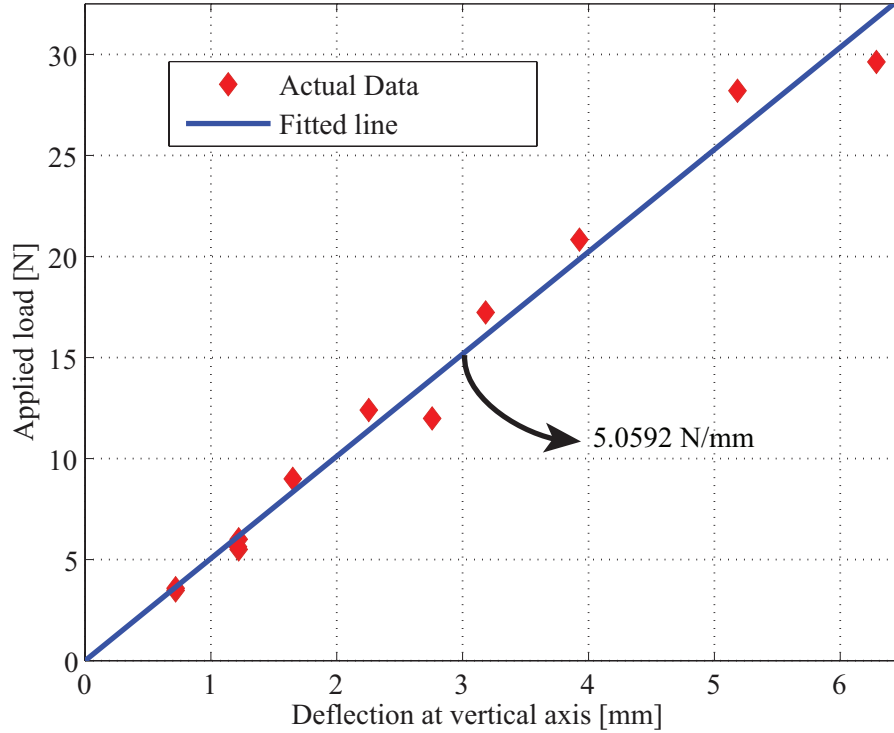
Stiffness Rendering

Figure 5.5: Stiffness rendering results of 3R̲RP device under impedance control and 5N/mm control stiffness

In order to observe impedance control performance of the system, especially 3R̲RP mechanism located at the shoulder, apart from trajectory tracking experiments we also implemented stiffness rendering experiments with 3R̲RP mechanism when its attached to exoskeleton as a module and all other modules and gravity compensation mechanism are realized. In order to realize stiffness rendering experiment, we have hang various loads weights from 425grams to 5000grams at the end-effector of 3R̲RP device. During this experiment we set stiffness of translational DoFs of 3R̲RP as 5 N/mm. While weights of the loads had verified and measured with force/torque sen-

sor attached to end-effector of 3RRP device, deflection of end-effector with respect to each load had measured using encoders attached to motors and forward kinematics of 3RRP device. Figure 5.5 depicts the stiffness rendering experiment under impedance control with 5 N/mm virtual control stiffness. At the figure while rhombuses represents actual data collected from experiments, blue line is the least square fitted line of these data. Slope of the fitted line represents fitted stiffness of the control experiment which is 5.05 N/mm.

5.2 Impedance Control

To test feasibility and useability of ASSISTON-ARM to assist shoulder movements, we have tested flexion/extension movements of healthy volunteers under close-loop control of the robot.

High backdriveability and low inertia and friction of actuators at the shoulder module alleviates need of force/torque sensor and facilitates use of open-loop impedance control at shoulder module. On the other hand, non-backdriveable joints including internal/external rotations of the shoulder and the elbow rotations are fixed for the control experiments of first prototype of ASSISTON-ARM. Also gravity compensation based on counter weight had been implemented during open-loop impedance control experiments.

Impedance control is a highly preferred control method used for interaction with environment. In Figure 5.6 open-loop impedance control architecture is depicted. In the figure while q and $\dot{q}$ represent joint position and velocities, x and $\dot{x}$ indicate task space position and velocities of the robot. Mapping from joint space velocities $\dot{q}$ to task space velocities $\dot{x}$ is realized with the Jacobian matrix J. Also Jacobian can be used to obtain the mapping between joint space torques from task space forces via the equation $T = J^{-T}F$.

In Figure 5.6, F_d represents desired forces on task space of robot. T_d and T are the desired and actual torques at joints, respectively. Symbol d is used for signifying external disturbances acting on system, while M is the robot inertia matrix, C is centrifugal and Coriolis matrices and N indicates gravity forces. Impedance control realized with the desired impedance Z_d for the robot.
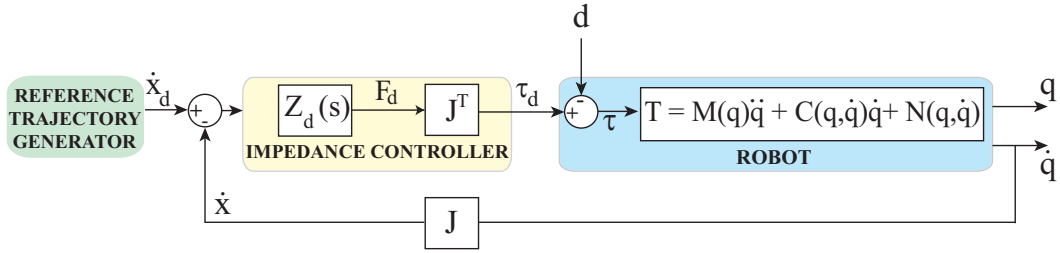

Figure 5.6: Block diagram for open loop impedance control

During the experiments, we have fixed the first revolute joint responsible for shoulder abduction/adduction by setting a high stiffness value of 50 Nm/rad. To impose flexion/extension movements to volunteers, we have used a stiffness value of 50 Nm/rad for task space rotations of 3-RRP mechanism, while setting very low stiffness values (12.5 N/m) for its translations with open loop impedance control. With this section of impedances, rotational part of flexion/extension movement can be imposed to the subject, while translations due to SH rhythm are left to the subject.

A 0.25 Hz sinusoidal reference trajectory with 100° magnitude is imposed to the rotational DoF of 3-RRP mechanism to carry out shoulder extension/flexion movement, while volunteer is attached to second prototype of ASSISTON-ARM. Figure 5.7 presents the reference trajectory and the tra-

jectory traced by the subject during a sample trial. RMS error of 4.63°
is calculated for this sample trial. Figure 5.8 presents translational move-
ments of the shoulder measured during the same trial. Here, solid (blue)
encirclements refer to shoulder extension, while dashed (red) encirclements
denote shoulder flexion. One can observe from Figure 5.8 that, as expected,
shoulder follows a distinct closed loop trajectory during extension and flexion
movements. ASSISTON-ARM is capable of measuring shoulder translations
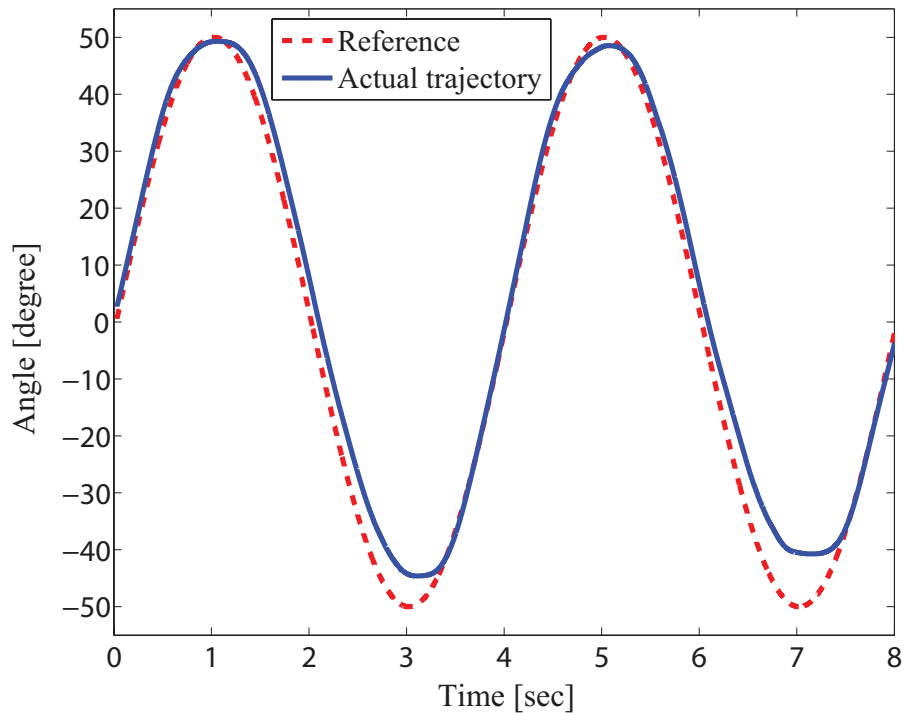in SH rhythm, which may be useful for diagnostic purposes.

Figure 5.7: Reference and actual trajectories of end-effector of the second
prototype 3<u>R</u>RP mechanism during flexion/extension of the shoulder joint

In Figure 5.9 closed-loop impedance control architecture is depicted. Aim
of the impedance control is rendering a desired impedance. In order to ensure
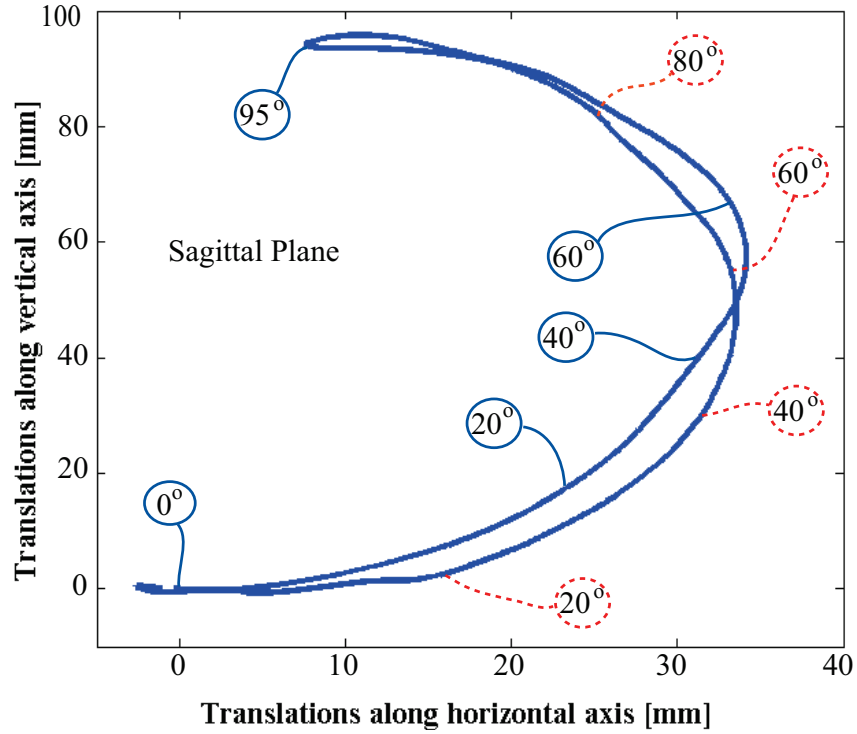that desired impedance is implemented with the system, namely force sens-

Figure 5.8: End-effector translation of 3-R̲RP mechanism in the sagittal plane during flexion/extension of the shoulder joint

ing mechanisms (force/torque sensors) should be included to control loop algorithm of impedance control. In the figure F_s represents force/torque which is acting on system and observed by force/torque sensor. Closed loop impedance control realized with the desired impedance $Z_d(s)$ and inner force controller $F_3(s)$ for the robot.
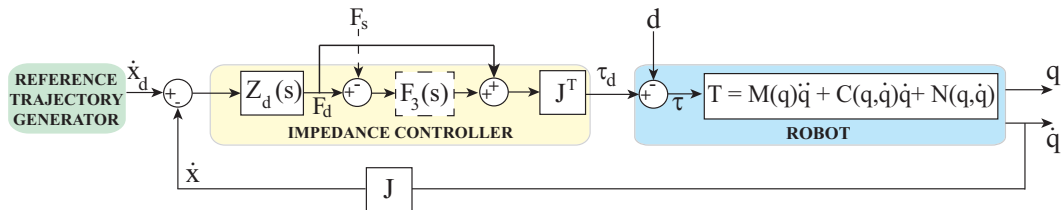

Figure 5.9: Block diagram for closed loop impedance control

During the experiments, like the open-loop impedance control experiments we have fixed the first revolute joint responsible for shoulder abduction/adduction by setting a high stiffness value of 50 Nm/rad. To impose flexion/extension movements to volunteers, we have used a stiffness value of 50 Nm/rad for task space rotations of 3-RRP mechanism, while setting very low stiffness values (10 N/m) for its translations. With setting inner force control gain to 0.5, we have increased impedance rendering performance of ASSISTON-ARM. Like open-loop impedance control with closed-loop impedance control, rotational part of flexion/extension movement can be imposed to the subject, while translations due to SH rhythm are left to the subject.

At the closed-loop control experiment, 0.25 Hz sinusoidal reference trajectory with 100° magnitude is imposed to the rotational DoF of 3-RRP mechanism to carry out shoulder extension/flexion movement, while volunteer is attached to second prototype of ASSISTON-ARM. Figure 5.9 presents the reference trajectory and the trajectory traced by the subject during a sample trial. Introducing a force/torque sensor at the impedance control experiment increases performance of trajectory tracking of shoulder module. As a consequence RMS error of 2.39° is calculated for this experiment.
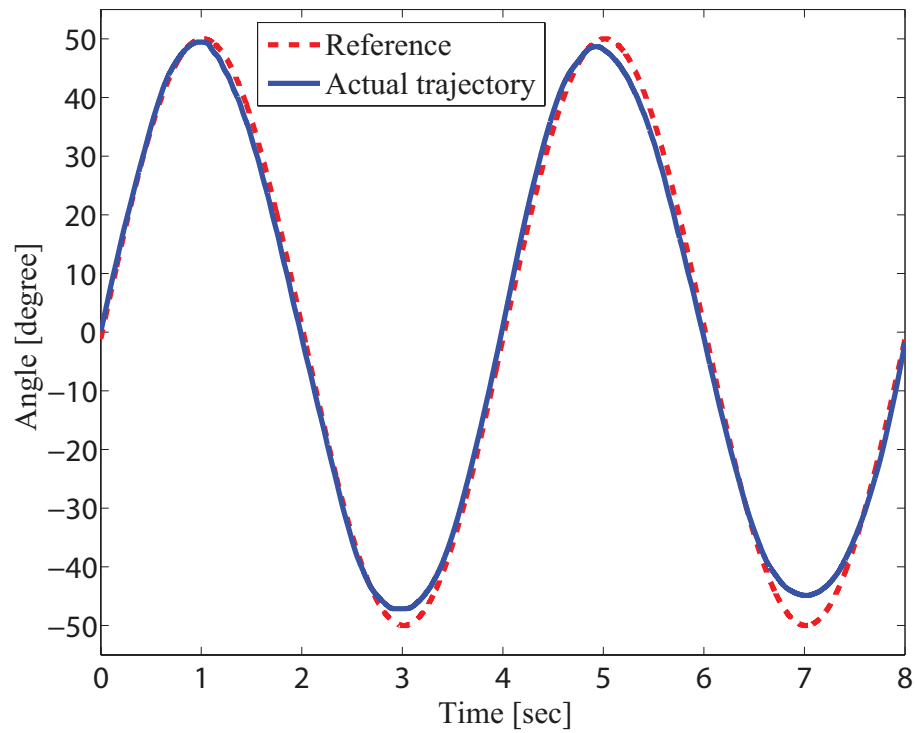
Figure 5.10: Reference and actual trajectories of end-effector of the second prototype 3RRP mechanism during flexion/extension of the shoulder joint under close-loop impedance control

Chapter VI

6 Conclusions and Future Work

We have presented the kinematics, workspace analysis and detailed design of ASSISTON-ARM, a novel arm exoskeleton for robot-assisted rehabilitation that enables mobilization of the shoulder girdle along with all shoulder rotations. While workspace of ASSISTON-ARM covers the whole reachable workspace of human arm, user evaluation analysis with current backdriveable prototype verify that shoulder module of ASSISTON-ARM can permit shoulder mobilization during exercises. Moreover, since elbow module consists of a Schmidt Coupling and the forearm-wrist module features a passive slider, both of these modules possess self-aligning characteristics. ASSISTON-ARM is verified to be passively backdriveable thanks to its capstan based transmission and spring-based passive gravity compensation mechanism. Passive backdriveability is key to passive self-alignment of the mechanism and safety of the device even under power failures.

Our future work includes integration of the forearm-wrist module and Schmidt coupling to the final prototype of the exoskeleton. Currently, ASSISTON-ARM is controlled using laboratory type control modules and amplifiers. Integration of EtherCAT based control hardware with the exoskeleton, implementation and testing of advanced passivity-based control strategies, such as passive velocity field control [76], are other future directions we have planned

for. Also, active compensation of remaining gravity effects will be carried out. In order to actively compensate gravity, dynamic model of AssistOn-Arm will be generated and model of spring based gravity compensation mechanism will subtracted from dynamics of the exoskeleton. Finally, larger scale human subject experiments and case studies with stroke patients constitute parts of our future work.

References

[1] Global burden of stroke. `http://www.who.int/cardiovascular_diseases/en/cvd_atlas_15_burden_stroke.pdf`.

[2] Economic cost of stroke. `http://www.who.int/cardiovascular_diseases/en/cvd_atlas_17_economics.pdf`.

[3] Cathrin Bütefisch, Horst Hummelsheim, Petra Denzler, and Karl-Heinz Mauritz. Repetitive training of isolated movements improves the outcome of motor rehabilitation of the centrally paretic hand. *Journal of the Neurological Sciences*, 130(1):59 – 68, 1995.

[4] Gert Kwakkel, Robert C Wagenaar, Jos WR Twisk, Gustaaf J Lankhorst, and Johan C Koetsier. Intensity of leg and arm training after primary middle-cerebral-artery stroke: a randomised trial. *The Lancet*, 354(9174):191 – 196, 1999.

[5] Nestor A. Bayona, Jamie Bitensky, Katherine Salter, and Robert Teasell. The role of task-specific training in rehabilitation therapies. *Topics in Stroke Rehabilitation*, 12(3):58–65, June 2005.

[6] A Sunderland, D J Tinson, E L Bradley, D Fletcher, R Langton Hewer, and D T Wade. Enhanced physical therapy improves recovery of arm function after stroke. a randomised controlled trial. *Journal of Neurology, Neurosurgery and Psychiatry*, 55(7):530–535, 1992.

[7] Johanna H van der Lee, Ingrid AK Snels, Heleen Beckerman, Gustaaf J Lankhorst, Robert C Wagenaar, and Lex M Bouter. Exercise therapy

for arm function in stroke patients: a systematic review of randomized controlled trials. *Clinical Rehabilitation*, 15(1):20–31, 2001.

[8] T. Platz. Evidence-based arm rehabilitation-a systematic review of the literature. *Nervenarzt*, 74(10):841–9, oct 2003.

[9] G. B. Prange, M. J. Jannink, C. G. Groothuis-Oudshoorn, H. J. Hermens, and M. J. Ijzerman. Systematic review of the effect of robot-aided therapy on recovery of the hemiparetic arm after stroke. *Journal of rehabilitation research and development*, 43(2):171–184, April 2006.

[10] Gert Kwakkel, Boudewijn J. Kollen, and Hermano I. Krebs. Effects of robot-assisted therapy on upper limb recovery after stroke: A systematic review. *Neurorehabilitation and Neural Repair*, 22(2):111–121, March/April 2008.

[11] N. Hogan, H.I. Krebs, J. Charnnarong, P. Srikrishna, and A. Sharon. Mit-manus: a workstation for manual therapy and training. i. In *Robot and Human Communication, 1992. Proceedings., IEEE International Workshop on*, pages 161 –165, September 1992.

[12] Theresa Sukal, Michael Ellis, and Julius Dewald. Shoulder abduction-induced reductions in reaching work area following hemiparetic stroke: Neuroscientific implications. *Experimental Brain Research*, 183(2):215–223, 2007.

[13] A. Frisoli, F. Rocchi, S. Marcheschi, A. Dettori, F. Salsedo, and M. Bergamasco. A new force-feedback arm exoskeleton for haptic interaction in virtual environments. In *Eurohaptics Conference and Sym-*

posium on Haptic Interfaces for Virtual Environment and Teleoperator Systems, World Haptics*, pages 195 – 201, march 2005.

[14] T. Nef, M. Mihelj, G. Kiefer, C. Perndl, R. Muller, and R. Riener. Armin - exoskeleton for arm therapy in stroke patients. In *Rehabilitation Robotics, 2007. ICORR 2007. IEEE 10th International Conference on*, pages 68 –74, 2007.

[15] J.C. Perry, J. Rosen, and S. Burns. Upper-limb powered exoskeleton design. *IEEE/ASME Transactions on Mechatronics*, 12(4):408 –417, 2007.

[16] Mine Sarac, Mehmet Alper Ergin, and Volkan Patoglu. Assiston-mobile: A series elastic holonomic mobile platform for upper extremity rehabilitation. In *World Haptics Conference (WHC), 2013*, pages 283–288, 2013.

[17] A. Schiele and F.C.T. van der Helm. Kinematic design to improve ergonomics in human machine interaction. *Neural Systems and Rehabilitation Engineering, IEEE Transactions on*, 14(4):456 –469, 2006.

[18] A.H.A. Stienen, E.E.G. Hekman, F.C.T. van der Helm, and H. van der Kooij. Self-aligning exoskeleton axes through decoupling of joint rotations and translations. *Robotics, IEEE Transactions on*, 25(3):628 –633, 2009.

[19] P. S. Lum, S. Mulroy, R. L. Amdur, P. Requejo, B. I. Prilutsky, and A. W. Dromerick. Gains in upper extremity function after stroke via recovery or compensation: Potential differential effects on amount of real-world limb use. *Topics in Stroke Rehabilitation*, 16(4):237–253, 2009.

[20] D.P. Romilly, C. Anglin, R.G. Gosine, C. Hershler, and S.U. Raschke. A functional task analysis and motion simulation for the development of a powered upper-limb orthosis. *IEEE Transactions on Rehabilitation Engineering*, 2(3):119 –129, sep 1994.

[21] Ge Wu, HEJ Veeger, Mohsen Makhsous, Peter Roy, Carolyn Anglin, Jochem Nagels, Andrew Karduna, Kevin McQuade, Xuguang Wang, and Frederick Werner. ISB recommendation on definitions of joint coordinate systems of various joints for the reporting of human joint motion–Part II: Shoulder, elbow, wrist and hand. *Journal of Biomechanics*, 2005.

[22] J. Lenarcic and M. Stanisic. A humanoid shoulder complex and the humeral pointing kinematics. *IEEE Transactions on Robotics and Automation*, 19(3):499 – 506, 2003.

[23] H. Moskowitz, CR. Goodman, E. Smith, E. Balthazar, and H.Z. Mellins. Hemiplegic shoulder. *NY State Journal of Medicine*, 69(4):548–550, 1969.

[24] R. D. Zorowitz, M. B. Hughes, D. Idank, T. Ikai, and M. V. Johnston. Shoulder pain and subluxation after stroke: Correlation of coincidence? *American Journal of Occupational Therapy*, 50:194–201, 1996.

[25] H. C. Hanger, P. Whitewood, G. Brown, M. C. Ball, J. Harper, R. Cox, and R. A. Sainbury. A randomized controlled trial of strapping to prevent post-stroke shoulder pain. *Clinical Rehabilitation*, 14:370–380, 2000.

[26] E. Dursun, N. Dursun, C. E. Ural, and A. Cakci. Glenohumeral joint subluxation and reflex symathetic dystrophy in hemiplegic patients. *Archives of Physical Medicine and Rehabilitation*, 81:944–946, 2000.

[27] D.G. Caldwell, C. Favede, and N. Tsagarakis. Dextrous exploration of a virtual world for improved prototyping. In *Robotics and Automation, 1998. Proceedings. 1998 IEEE International Conference on*, volume 1, pages 298 –303 vol.1, may 1998.

[28] A. Schiele and G. Visentin. The ESA human arm exoskeleton for space robotics telepresence. In *International Symposium on Artificial Intelligence, Robotics and Automation in Space, i-SAIRAS*, 2003.

[29] C. Carignan, M. Liszka, and S. Roderick. Design of an arm exoskeleton with scapula motion for shoulder rehabilitation. In *Advanced Robotics, 2005. ICAR '05. Proceedings., 12th International Conference on*, pages 524 –531, 2005.

[30] K. Kiguchi, M.H. Rahman, M. Sasaki, and K. Teramoto. Development of a 3DOF mobile exoskeleton robot for human upper-limb motion assist. *Robotics and Autonomous Systems*, 56(8):678–691, 2008.

[31] R.J.Jr. Sanchez, E. Wolbrecht, R. Smith, J. Liu, S. Rao, S. Cramer, T. Rahman, J.E. Bobrow, and D.J. Reinkensmeyer. A pneumatic robot for re-training arm movement after stroke: Rationale and mechanical design. In *International Conference on Rehabilitation Robotics*, pages 500 – 504, 2005.

[32] T. Nef, M. Guidali, and R. Riener. Armin iii - arm therapy exoskeleton with an ergonomic shoulder actuation. *Applied Bionics and Biomechanics*, 2(6):127–142, 2009.

[33] A.H.A. Stienen, E.E.G. Hekman, F.C.T. Van der Helm, G.B. Prange, M.J.A. Jannink, A.M.M. Aalsma, and H. Van der Kooij. Dampace: dynamic force-coordination trainer for the upper extremities. In *Rehabilitation Robotics, 2007. ICORR 2007. IEEE 10th International Conference on*, pages 820 –826, 2007.

[34] A.H.A. Stienen, E.E.G. Hekman, H. ter Braak, A.M.M. Aalsma, F.C.T. van der Helm, and H. van der Kooij. Design of a rotational hydroelastic actuator for a powered exoskeleton for upper limb rehabilitation. *IEEE Transactions on Biomedical Engineering*, 57(3):728 –735, 2010.

[35] B. Dehez and J. Sapin. ShouldeRO An alignment-free two-dof rehabilitation robot for the shoulder complex. In *IEEE International Conference on Rehabilitation Robotics*, 2011.

[36] Donghan Koo, Pyung Hun Chang, Min Kyun Sohn, and Ji hyeon Shin. Shoulder mechanism design of an exoskeleton robot for stroke patient rehabilitation. In *IEEE International Conference on Rehabilitation Robotics*, 2011.

[37] H.S. Park, Y. Ren, and L.Q. Zhang. IntelliArm: An exoskeleton for diagnosis and treatment of patients with neurological impairments. In *IEEE/RAS-EMBS International Conference on Biomedical Robotics and Biomechatronics*, pages 109–114, 2008.

[38] S. Ball, I. Brown, and S. Scott. MEDARM: A rehabilitation robot with 5DoF at the shoulder complex. In *IEEE/ASME International Conference on Advanced Intelligent Mechatronics*, 2007.

[39] A. Frisoli, M. Bergamasco, M.C. Carboncini, and B. Rossi. Robotic assisted rehabilitation in virtual reality with the l-exos. *Stud Health Technol Inform*, 145:40–54, 2009.

[40] R.J. Sanchez, Jiayin Liu, S. Rao, P. Shah, R. Smith, T. Rahman, S.C. Cramer, J.E. Bobrow, and D.J. Reinkensmeyer. Automating arm movement training following severe stroke: Functional exercises with quantitative feedback in a gravity-reduced environment. *Neural Systems and Rehabilitation Engineering, IEEE Transactions on*, 14(3):378 –389, sept. 2006.

[41] P. Letier, M. Avraam, S. Veillerette, M. Horodinca, M. De Bartolomei, A. Schiele, and A. Preumont. SAM: A 7-DoF portable arm exoskeleton with local joint control. In *IEEE/RSJ International Conference on Intelligent Robots and Systems*, pages 3501 –3506, 2008.

[42] M. Bottlang, S. M. Madey, C. M. Steyers, J. L. Marsh, and T. D. Brown. Assessment of elbow joint kinematics in passive motion by electromagnetic motion tracking. *Journal of Orthopaedic Research*, 18(2):195–202, 2000.

[43] T. Lenzi, N. Vitiello, S. M. De Rossi, S. Roccella, F. Vecchi, and M.C. Carrozza. NEUROExos: A variable impedance powered elbow exoskeleton. In *IEEE Internatinal Conference of Robotics and Automation*, 2011.

[44] Thomas B. Moeslund. Modelling the human arm. Technical report, Aalborg University, 2002.

[45] S. J. Ball. *Novel robotic mechanisms for upper-limb rehabilitation and assessment*. PhD thesis, Queen's University, Ontario, Canada, 2008.

[46] T. B. Moeslund, C. B. Madsen, and E. Granum. Modelling the 3D pose of a human arm and the shoulder complex utilising only two parameters. *Integrated Computer-Aided Engineering*, 12(2):159–175, 2005.

[47] C.C. Norkin and D.J. White. Measurement of joint motion, a guide to goniometry. F. A. Davis Company, 2009.

[48] Ahmetcan Erdogan and Volkan Patoglu. Passive velocity field control of a forearm-wrist rehabilitation robot. In *International Conference on Rehabilitation Robotics (ICORR2011)*, 2011.

[49] Ahmetcan Erdogan and Volkan Patoglu. Kinematics and control of a 3rps-r mechanism using euler parameters. In *ECCOMAS Thematic Conference on Multibody Dynamics*, 2011.

[50] Besir Celebi, Mustafa Yalcin, and Volkan Patoglu. ASSISTON-KNEE: A self-aligning knee exoskeleton. In *International Conference on Rehabilitation Robotics, ICORR*, 2013.

[51] Mehmet Alper Ergin and Volkan Patoglu. A self-adjusting knee exoskeleton for robot-assisted treatment of knee injuries. In *IEEE/RSJ International Conference on Intelligent Robots and Systems*, 2011.

109

[52] Mehmet Alper Ergin and Volkan Patoglu. Assiston-se: A self-aligning shoulder-elbow exoskeleton. In *IEEE International Conference on Robotics and Automation*, 2012.

[53] R. Schmidt. Coupling, 2 1974.

[54] Thomas R. Kane and David A. Levinson. The Use of Kane's Dynamical Equations in Robotics. *The International Journal of Robotics Research*, 2(3):3–21, 1983.

[55] Nicholas P. Chironis, editor. *Spring Mechanisms - Point Balancing and Continous Balancing*. McGraw-Hill, New York, 1961.

[56] R.M. Nathan. Perfect spring equilibrators for rotatable bodies. *ASME Journal of Mechanisms, Transmissions, and Automation in Design*, 107(4):508–512, 1989.

[57] D.A. Streit and E. Shin. Equilibrators for planar linkages. *Journal of Mechanical Design*, 115(3):604–611, 1993.

[58] W.D. Van Dorsser, J.L. Herder, B.M. Wisse, and R. Barents. Balancing device, 06 2008.

[59] D.A. Streit and B.J. Gilmore. Perfect spring equilibrators for rotatable bodies. *Journal of Mechanisms, Transmissions and Automation in Design*, 111(4):451–458, 1989.

[60] T. Rahman, R. Ramanathan, R. Seliktar, and W. Harwin. A simple technique to passively gravity-balance articulated mechnanisms. *ASME Journal of Mechanical Design*, 117(4):655–658, 1995.

[61] A. Agrawal and S.K. Agrawal. Design of gravity balancing leg orthosis using non-zero free length springs. *Mechanism and Machine Theory*, 40(6):693–709, 2005.

[62] S.K. Banala, S.K. Agrawal, A. Fattah, V. Krishnamoorthy, W. Hsu, J. Scholz, and K. Rudolph. Gravity balancing leg orthosis and its performance evaluation. *IEEE Transactions on Robotics*, 22(6):1228–1239, 2006.

[63] C. Baradat, V. Arakelian, S. Briot, and S. Guegan. Design and prototyping of a new balancing mechanism for spatial parallel manipulators. *Journal of Mechanical Design*, 130(7):072305, 2008.

[64] P.Y. Lin, W.B. Shieh, and Chen D.Z. Design of a gravity-balanced general spatial serial-type manipulator. *Journal of Mechanisms and Robotics*, 2(8):031003, 2010.

[65] P. Pratch, P. Minotti, and M. Dohan. Synthesis and balancing of cam modulated linkages. In *ASME Design Technology Conference*, 1987.

[66] A. Agrawal, G. Gardner, and S. Pledgie. Design and fabrication of a gravity balanced planar mechanism using auxiliary parallelograms. *ASME Journal of Mechanical Design*, 123(4):525–528, 2001.

[67] Tozeren Aydin. *Human Body Dynamics Classical Mechanics and Human Movement*, pages 1–3. Springer, New York, 2000.

[68] D. Gentry Steele and Claud A. Bramblett. *The Anatomy and Biology of the Human Skeleton*, pages 153–172. Texas A and M University Press, United States of America, 2007.

[69] M. Sardelli, R.Z. Tashjian, and B.A. MacWilliams. Functional elbow range of motion for contemporary tasks. *The Journal of Bone And Joint Surgery*, 93(5):471–477, 2011.

[70] B. Loverna, L.A. Strouda, N.A. Ferranb, S.L. Evansa, R.O. Evansb, and C.A. Holta. Motion analysis of the glenohumeral joint during activities of daily living. *Computer Methods in Biomechanics and Biomedical Engineering*, 13(6):803–809, 2010.

[71] Andrew Arthur Amis. *Operative Elbow Surgery Expert Consult: Online and Print*, pages 29–44. Churchill Livingstone, China, 2012.

[72] J. Ryu, W. Cooney, and An K. Chao E. Askew, L. and. The journal of hand surgery. *Computer Methods in Biomechanics and Biomedical Engineering*, 16(3):409–419, 1991.

[73] Leo J. Stocco. *Robot Design Optimization with Haptic Interface Applications.* PhD thesis, The University of Bitish Columbia, 1999.

[74] C. Carignan, J. Tang, S. Roderick, and M. Naylor. A configuration-space approach to controlling a rehabilitation arm exoskeleton. In *IEEE International Conference on Rehabilitation Robotics*, pages 179 –187, 2007.

[75] R.F. Beer and J.P.A. Dewald. Abnormal joint torque patterns in the paretic upper limb of subjects with hemiparesis. *Muscle and Nerve*, 24:273–283, 2001.

[76] Ahmetcan Erdogan and Volkan Patoglu. Online generation of velocity fields for passive contour following. In *IEEE World Haptics Conference (WHC2011)*, 2011.

APPENDICES

Jacobian of ASSISTON-ARM

After differentiating (28) and (35), Jacobian matrix of ASSISTON-ARM J_{exo} is calculated as

$$J_{exo} = \begin{bmatrix} J1 & J2 & J3 & J4 & J5 & J6 \end{bmatrix}^T \qquad (53)$$

where Ji $i = 1..6$ are 1 by 11 array and

$J1[1,1] = 0$

$J1[1,2] = -\cos\alpha_2 \cos\theta (y_e - k_8 \sin\alpha_3)$

$J1[1,3] = k_8(\sin\alpha_3 \sin\theta + \sin\alpha_2 \cos\alpha_3 \cos\theta)$

$J1[1,4] = -1$

$J1[1,5] = 0$

$J1[1,6] = y_e \sin\alpha_2 \sin\theta - k_8 \cos\alpha_3 \cos\theta - \cos\theta(k_6 + k_7 + z_e) - k_8 \sin\alpha_2 \sin\alpha_3 \sin\theta$

$J1[1,7] = -\sin\alpha_2 \cos\theta$

$J1[1,8] = -\sin\theta$

$J1[1,9] = 0$

$J1[1,10] = 0$

$J1[1,11] = 0$

$J2[1,1] = y_e \cos\alpha_1 \cos\alpha_2 + \cos\alpha_1(k_5 - k_3 - d1) + y_e \sin\alpha_1 \sin\alpha_2 \sin\theta - k_6 \sin\alpha_1 \cos\theta - \sin\alpha_1(z_s + \cos\theta(k_7 + z_e)) - k_8(\sin\alpha_1 \sin\alpha_2 + \sin\theta \cos\alpha_1 \cos\alpha_2)(\sin\alpha_3 \sin\theta + \sin\alpha_2 \cos\alpha_3 \cos\theta) - k_8 \cos\alpha_2 \cos\theta(\sin\alpha_1 \cos\alpha_2 \cos\alpha_3 + \cos\alpha_1(\sin\alpha_3 \cos\theta -$

$\sin \alpha_2 \sin \theta \cos \alpha_3))$

$J2[1,2] = -(y_e - k_8 \sin \alpha_3)(\sin \alpha_1 \sin \alpha_2 + \sin \theta \cos \alpha_1 \cos \alpha_2)$

$J2[1,3] = -k_8(\sin \alpha_1 \cos \alpha_2 \cos \alpha_3 + \cos \alpha_1(\sin \alpha_3 \cos \theta - \sin \alpha_2 \sin \theta \cos \alpha_3))$

$J2[1,4] = 0$

$J2[1,5] = \cos \alpha_1$

$J2[1,6] = -\cos \alpha_1(k_8 \sin \theta \cos \alpha_3 + y_e \sin \alpha_2 \cos \theta + \sin \theta(k_6 + k_7 + z_e) - k_8 \sin \alpha_2 \sin \alpha_3 \cos \theta)$

$J2[1,7] = \sin \alpha_1 \cos \alpha_2 - \sin \alpha_2 \sin \theta \cos \alpha_1$

$J2[1,8] = \cos \alpha_1 \cos \theta$

$J2[1,9] = 0$

$J2[1,10] = 0$

$J2[1,11] = 0$

$J3[1,1] = k_6 \cos \alpha_1 \cos \theta + y_e \sin \alpha_1 \cos \alpha_2 + \sin \alpha_1(k_5 - k_3 - d1) + \cos \alpha_1(z_s +$

$\cos \theta(k_7 + z_e)) + k_8(\sin \alpha_3 \sin \theta + \sin \alpha_2 \cos \alpha_3 \cos \theta)(\sin \alpha_2 \cos \alpha_1 - \sin \alpha_1 \sin \theta \cos \alpha_2) +$

$k_8 \cos \alpha_2 \cos \theta(\cos \alpha_1 \cos \alpha_2 \cos \alpha_3 - \sin \alpha_1(\sin \alpha_3 \cos \theta - \sin \alpha_2 \sin \theta \cos \alpha_3)) -$

$y_e \sin \alpha_2 \sin \theta \cos \alpha_1$

$J3[1,2] = (y_e - k_8 \sin \alpha_3)(\sin \alpha_2 \cos \alpha_1 - \sin \alpha_1 \sin \theta \cos \alpha_2)$

$J3[1,3] = k_8(\cos \alpha_1 \cos \alpha_2 \cos \alpha_3 - \sin \alpha_1(\sin \alpha_3 \cos \theta - \sin \alpha_2 \sin \theta \cos \alpha_3))$

$J3[1,4] = 0$

$J3[1,5] = \sin \alpha_1$

$J3[1,6] = -\sin \alpha_1(k_8 \sin \theta \cos \alpha_3 + y_e \sin \alpha_2 \cos \theta + \sin \theta(k_6 + k_7 + z_e) - k_8 \sin \alpha_2 \sin \alpha_3 \cos \theta)$

$J3[1,7] = -\cos \alpha_1 \cos \alpha_2 - \sin \alpha_1 \sin \alpha_2 \sin \theta$

$J3[1,8] = \sin \alpha_1 \cos \theta$

$J3[1,9] = 0$

$J3[1,10] = 0$

$J3[1,11] = 0$

$J4[1,1] = (\sin\epsilon_w \sin\varphi_w{}^2 \cos\omega_w{}^2 + \sin\omega_w \cos\varphi_w(\sin\varphi_w \cos\epsilon_w$

$-\sin\epsilon_w \sin\omega_w \cos\varphi_w))((\sin\alpha_1 \sin\alpha_2 + \sin\theta\cos\alpha_1\cos\alpha_2)(\sin\omega\sin\varphi + \sin\epsilon\cos\omega\cos\varphi)$

$+\ \cos\epsilon\cos\varphi(\cos\alpha_1\cos\alpha_3\cos\theta - \sin\alpha_3(\sin\alpha_1\cos\alpha_2 - \sin\alpha_2\sin\theta\cos\alpha_1)) -$

$(\sin\varphi\cos\omega$

$-\ \sin\epsilon\sin\omega\cos\varphi)(\sin\alpha_3\cos\alpha_1\cos\theta + \cos\alpha_3(\sin\alpha_1\cos\alpha_2$

$-\ \sin\alpha_2\sin\theta\cos\alpha_1)))/(\cos\omega_w(\sin\epsilon_w{}^2(\sin\omega_w{}^2\cos\varphi_w{}^2 - \sin\varphi_w{}^2\cos\omega_w{}^2)$

$-\ \sin\omega_w\sin\varphi_w\cos\epsilon_w(2\sin\epsilon_w\cos\varphi_w - \sin\omega_w\sin\varphi_w\cos\epsilon_w)))$

$-\ \sin\omega_w\sin\varphi_w\cos\epsilon_w((\sin\alpha_2\cos\alpha_1 - \sin\alpha_1\sin\theta\cos\alpha_2)(\sin\omega\cos\varphi$

$-\ \sin\epsilon\sin\varphi\cos\omega) + \sin\varphi\cos\epsilon(\sin\alpha_1\cos\alpha_3\cos\theta$

$+\ \sin\alpha_3(\cos\alpha_1\cos\alpha_2 + \sin\alpha_1\sin\alpha_2\sin\theta)) + (\cos\omega\cos\varphi$

$+\ \sin\epsilon\sin\omega\sin\varphi)(\sin\alpha_1\sin\alpha_3\cos\theta - \cos\alpha_3(\cos\alpha_1\cos\alpha_2$

$+\ \sin\alpha_1\sin\alpha_2\sin\theta)))/(\sin\epsilon_w{}^2(\sin\omega_w{}^2\cos\varphi_w{}^2 - \sin\varphi_w{}^2\cos\omega_w{}^2)$

$-\ \sin\omega_w\sin\varphi_w\cos\epsilon_w(2\sin\epsilon_w\cos\varphi_w - \sin\omega_w\sin\varphi_w\cos\epsilon_w))$

$J4[1,2] = \cos\epsilon_w(\cos\theta\tan\omega_w(\sin\varphi_w\cos\epsilon_w - \sin\epsilon_w\sin\omega_w\cos\varphi_w)(\sin\alpha_2\cos\epsilon\cos\omega$

$+\sin\alpha_3\sin\epsilon\cos\alpha_2 + \sin\omega\cos\alpha_2\cos\alpha_3\cos\epsilon) + \sin\omega_w\sin\varphi_w(\sin\alpha_3\sin\varphi\cos\epsilon(\sin\alpha_1\sin\alpha_2$

$+\ \sin\theta\cos\alpha_1\cos\alpha_2) - (\sin\alpha_1\cos\alpha_2 - \sin\alpha_2\sin\theta\cos\alpha_1)(\sin\omega\cos\varphi$

$-\ \sin\epsilon\sin\varphi\cos\omega) - \cos\alpha_3(\sin\alpha_1\sin\alpha_2 + \sin\theta\cos\alpha_1\cos\alpha_2)(\cos\omega\cos\varphi$

$+\ \sin\epsilon\sin\omega\sin\varphi)))/(\sin\epsilon_w{}^2(\sin\omega_w{}^2\cos\varphi_w{}^2 - \sin\varphi_w{}^2\cos\omega_w{}^2)$

$-\ \sin\omega_w\sin\varphi_w\cos\epsilon_w(2\sin\epsilon_w\cos\varphi_w - \sin\omega_w\sin\varphi_w\cos\epsilon_w))$

$-\ (\sin\epsilon_w\sin\varphi_w{}^2\cos\omega_w{}^2 + \sin\omega_w\cos\varphi_w(\sin\varphi_w\cos\epsilon_w$

$-\ \sin\epsilon_w\sin\omega_w\cos\varphi_w))(\sin\alpha_3\cos\epsilon\cos\varphi(\sin\alpha_2\cos\alpha_1 - \sin\alpha_1\sin\theta\cos\alpha_2)$

$+(\sin\omega\sin\varphi + \sin\epsilon\cos\omega\cos\varphi)(\cos\alpha_1\cos\alpha_2 + \sin\alpha_1\sin\alpha_2\sin\theta) + \cos\alpha_3(\sin\alpha_2\cos\alpha_1$

$-\sin\alpha_1\sin\theta\cos\alpha_2)(\sin\varphi\cos\omega - \sin\epsilon\sin\omega\cos\varphi))/(\cos\omega_w(\sin\epsilon_w{}^2(\sin\omega_w{}^2\cos\varphi_w{}^2$

$-\sin\varphi_w{}^2\cos\omega_w{}^2) - \sin\omega_w\sin\varphi_w\cos\epsilon_w(2\sin\epsilon_w\cos\varphi_w - \sin\omega_w\sin\varphi_w\cos\epsilon_w)))$

$J4[1,3] = \cos\epsilon_w(\tan\omega_w(\sin\varphi_w\cos\epsilon_w - \sin\epsilon_w\sin\omega_w\cos\varphi_w)(\sin\epsilon(\sin\alpha_3\sin\theta$

$+\sin\alpha_2\cos\alpha_3\cos\theta)+\sin\omega\cos\epsilon(\sin\theta\cos\alpha_3-\sin\alpha_2\sin\alpha_3\cos\theta))$

$-\sin\omega_w\sin\varphi_w(\sin\varphi\cos\epsilon(\sin\alpha_3\cos\alpha_1\cos\theta+\cos\alpha_3(\sin\alpha_1\cos\alpha_2$

$-\sin\alpha_2\sin\theta\cos\alpha_1))-(\cos\omega\cos\varphi+\sin\epsilon\sin\omega\sin\varphi)(\cos\alpha_1\cos\alpha_3\cos\theta$

$-\sin\alpha_3(\sin\alpha_1\cos\alpha_2-\sin\alpha_2\sin\theta\cos\alpha_1))))/(\sin\epsilon_w{}^2(\sin\omega_w{}^2\cos\varphi_w{}^2$

$-\sin\varphi_w{}^2\cos\omega_w{}^2)-\sin\omega_w\sin\varphi_w\cos\epsilon_w(2\sin\epsilon_w\cos\varphi_w-\sin\omega_w\sin\varphi_w\cos\epsilon_w))$

$-(\sin\epsilon_w\sin\varphi_w{}^2\cos\omega_w{}^2+\sin\omega_w\cos\varphi_w(\sin\varphi_w\cos\epsilon_w$

$-\sin\epsilon_w\sin\omega_w\cos\varphi_w))(\cos\epsilon\cos\varphi(\sin\alpha_1\sin\alpha_3\cos\theta-\cos\alpha_3(\cos\alpha_1\cos\alpha_2$

$+\sin\alpha_1\sin\alpha_2\sin\theta))+(\sin\varphi\cos\omega-\sin\epsilon\sin\omega\cos\varphi)(\sin\alpha_1\cos\alpha_3\cos\theta$

$+\sin\alpha_3(\cos\alpha_1\cos\alpha_2+\sin\alpha_1\sin\alpha_2\sin\theta)))/(\cos\omega_w(\sin\epsilon_w{}^2(\sin\omega_w{}^2\cos\varphi_w{}^2$

$-\sin\varphi_w{}^2\cos\omega_w{}^2)-\sin\omega_w\sin\varphi_w\cos\epsilon_w(2\sin\epsilon_w\cos\varphi_w-\sin\omega_w\sin\varphi_w\cos\epsilon_w)))$

$J4[1,4]=0$

$J4[1,5]=0$

$J4[1,6]=-\sin\alpha_1(\sin\epsilon_w\sin\varphi_w{}^2\cos\omega_w{}^2+\sin\omega_w\cos\varphi_w(\sin\varphi_w\cos\epsilon_w$

$-\sin\epsilon_w\sin\omega_w\cos\varphi_w))(\cos\epsilon\cos\varphi(\sin\theta\cos\alpha_3-\sin\alpha_2\sin\alpha_3\cos\theta)$

$-\cos\alpha_2\cos\theta(\sin\omega\sin\varphi+\sin\epsilon\cos\omega\cos\varphi)-(\sin\alpha_3\sin\theta+\sin\alpha_2\cos\alpha_3\cos\theta)(\sin\varphi\cos\omega$

$-\sin\epsilon\sin\omega\cos\varphi))/(\cos\omega_w(\sin\epsilon_w{}^2(\sin\omega_w{}^2\cos\varphi_w{}^2-\sin\varphi_w{}^2\cos\omega_w{}^2)$

$-\sin\omega_w\sin\varphi_w\cos\epsilon_w(2\sin\epsilon_w\cos\varphi_w-\sin\omega_w\sin\varphi_w\cos\epsilon_w)))$

$-\cos\epsilon_w(\tan\omega_w(\sin\varphi_w\cos\epsilon_w-\sin\epsilon_w\sin\omega_w\cos\varphi_w)(\sin\epsilon(\cos\alpha_3\cos\theta$

$+\sin\alpha_2\sin\alpha_3\sin\theta)-\sin\theta\cos\alpha_2\cos\epsilon\cos\omega-\sin\omega\cos\epsilon(\sin\alpha_3\cos\theta$

$-\sin\alpha_2\sin\theta\cos\alpha_3))+\sin\omega_w\sin\varphi_w\cos\alpha_1(\sin\varphi\cos\epsilon(\sin\theta\cos\alpha_3$

$-\sin\alpha_2\sin\alpha_3\cos\theta)+\cos\alpha_2\cos\theta(\sin\omega\cos\varphi-\sin\epsilon\sin\varphi\cos\omega)$

$+(\sin\alpha_3\sin\theta+\sin\alpha_2\cos\alpha_3\cos\theta)(\cos\omega\cos\varphi+\sin\epsilon\sin\omega\sin\varphi)))/(\sin\epsilon_w{}^2(\sin\omega_w{}^2\cos\varphi_w{}^2$

$-\sin\varphi_w{}^2\cos\omega_w{}^2)-\sin\omega_w\sin\varphi_w\cos\epsilon_w(2\sin\epsilon_w\cos\varphi_w-\sin\omega_w\sin\varphi_w\cos\epsilon_w))$

$J4[1,7]=0$

$J4[1,8]=0$

$J4[1,9]=\cos\epsilon_w(\tan\omega_w(\sin\varphi_w\cos\epsilon_w-\sin\epsilon_w\sin\omega_w\cos\varphi_w)(\sin\epsilon\cos\alpha_2\cos\omega\cos\theta$

$-\cos\epsilon(\sin\theta\cos\alpha_3 - \sin\alpha_2\sin\alpha_3\cos\theta) - \sin\epsilon\sin\omega(\sin\alpha_3\sin\theta$

$+ \sin\alpha_2\cos\alpha_3\cos\theta)) - \sin\omega_w\sin\varphi\sin\varphi_w(\sin\epsilon(\cos\alpha_1\cos\alpha_3\cos\theta$

$- \sin\alpha_3(\sin\alpha_1\cos\alpha_2 - \sin\alpha_2\sin\theta\cos\alpha_1)) - \cos\epsilon\cos\omega(\sin\alpha_1\sin\alpha_2$

$+ \sin\theta\cos\alpha_1\cos\alpha_2) - \sin\omega\cos\epsilon(\sin\alpha_3\cos\alpha_1\cos\theta + \cos\alpha_3(\sin\alpha_1\cos\alpha_2$

$- \sin\alpha_2\sin\theta\cos\alpha_1))))/(\sin\epsilon_w{}^2(\sin\omega_w{}^2\cos\varphi_w{}^2 - \sin\varphi_w{}^2\cos\omega_w{}^2)$

$-\sin\omega_w\sin\varphi_w\cos\epsilon_w(2\sin\epsilon_w\cos\varphi_w - \sin\omega_w\sin\varphi_w\cos\epsilon_w)) - \cos\varphi(\sin\epsilon_w\sin\varphi_w{}^2\cos\omega_w{}^2+$

$\sin\omega_w\cos\varphi_w(\sin\varphi_w\cos\epsilon_w$

$- \sin\epsilon_w\sin\omega_w\cos\varphi_w))(\cos\epsilon\cos\omega(\sin\alpha_2\cos\alpha_1 - \sin\alpha_1\sin\theta\cos\alpha_2)$

$+ \sin\epsilon(\sin\alpha_1\cos\alpha_3\cos\theta + \sin\alpha_3(\cos\alpha_1\cos\alpha_2 + \sin\alpha_1\sin\alpha_2\sin\theta))$

$- \sin\omega\cos\epsilon(\sin\alpha_1\sin\alpha_3\cos\theta - \cos\alpha_3(\cos\alpha_1\cos\alpha_2$

$+ \sin\alpha_1\sin\alpha_2\sin\theta)))/(\cos\omega_w(\sin\epsilon_w{}^2(\sin\omega_w{}^2\cos\varphi_w{}^2 - \sin\varphi_w{}^2\cos\omega_w{}^2)$

$- \sin\omega_w\sin\varphi_w\cos\epsilon_w(2\sin\epsilon_w\cos\varphi_w - \sin\omega_w\sin\varphi_w\cos\epsilon_w)))$

$J4[1,10] = \cos\epsilon_w(\cos\epsilon\tan\omega_w(\sin\varphi_w\cos\epsilon_w - \sin\epsilon_w\sin\omega_w\cos\varphi_w)(\sin\omega\cos\alpha_2\cos\theta$

$+ \cos\omega(\sin\alpha_3\sin\theta + \sin\alpha_2\cos\alpha_3\cos\theta)) - \sin\omega_w\sin\varphi_w((\sin\alpha_1\sin\alpha_2$

$+ \sin\theta\cos\alpha_1\cos\alpha_2)(\cos\omega\cos\varphi + \sin\epsilon\sin\omega\sin\varphi) + (\sin\omega\cos\varphi$

$- \sin\epsilon\sin\varphi\cos\omega)(\sin\alpha_3\cos\alpha_1\cos\theta + \cos\alpha_3(\sin\alpha_1\cos\alpha_2$

$- \sin\alpha_2\sin\theta\cos\alpha_1))))/(\sin\epsilon_w{}^2(\sin\omega_w{}^2\cos\varphi_w{}^2 - \sin\varphi_w{}^2\cos\omega_w{}^2)$

$- \sin\omega_w\sin\varphi_w\cos\epsilon_w(2\sin\epsilon_w\cos\varphi_w - \sin\omega_w\sin\varphi_w\cos\epsilon_w))$

$- (\sin\epsilon_w\sin\varphi_w{}^2\cos\omega_w{}^2 + \sin\omega_w\cos\varphi_w(\sin\varphi_w\cos\epsilon_w$

$- \sin\epsilon_w\sin\omega_w\cos\varphi_w))((\sin\alpha_2\cos\alpha_1 - \sin\alpha_1\sin\theta\cos\alpha_2)(\sin\varphi\cos\omega$

$- \sin\epsilon\sin\omega\cos\varphi) - (\sin\omega\sin\varphi + \sin\epsilon\cos\omega\cos\varphi)(\sin\alpha_1\sin\alpha_3\cos\theta$

$- \cos\alpha_3(\cos\alpha_1\cos\alpha_2 + \sin\alpha_1\sin\alpha_2\sin\theta)))/(\cos\omega_w(\sin\epsilon_w{}^2(\sin\omega_w{}^2\cos\varphi_w{}^2$

$- \sin\varphi_w{}^2\cos\omega_w{}^2) - \sin\omega_w\sin\varphi_w\cos\epsilon_w(2\sin\epsilon_w\cos\varphi_w - \sin\omega_w\sin\varphi_w\cos\epsilon_w)))$

$J4[1,11] = \sin\omega_w\sin\varphi_w\cos\epsilon_w((\sin\alpha_1\sin\alpha_2 + \sin\theta\cos\alpha_1\cos\alpha_2)(\sin\omega\sin\varphi$

$+ \sin\epsilon\cos\omega\cos\varphi) + \cos\epsilon\cos\varphi(\cos\alpha_1\cos\alpha_3\cos\theta - \sin\alpha_3(\sin\alpha_1\cos\alpha_2$

$- \sin\alpha_2\sin\theta\cos\alpha_1)) - (\sin\varphi\cos\omega - \sin\epsilon\sin\omega\cos\varphi)(\sin\alpha_3\cos\alpha_1\cos\theta$

$$+ \cos \alpha_3 (\sin \alpha_1 \cos \alpha_2 - \sin \alpha_2 \sin \theta \cos \alpha_1)))/(\sin \epsilon_w{}^2 (\sin \omega_w{}^2 \cos \varphi_w{}^2$$

$$- \sin \varphi_w{}^2 \cos \omega_w{}^2) - \sin \omega_w \sin \varphi_w \cos \epsilon_w (2 \sin \epsilon_w \cos \varphi_w - \sin \omega_w \sin \varphi_w \cos \epsilon_w))$$

$$- (\sin \epsilon_w \sin \varphi_w{}^2 \cos \omega_w{}^2 + \sin \omega_w \cos \varphi_w (\sin \varphi_w \cos \epsilon_w$$

$$- \sin \epsilon_w \sin \omega_w \cos \varphi_w))((\sin \alpha_2 \cos \alpha_1 - \sin \alpha_1 \sin \theta \cos \alpha_2)(\sin \omega \cos \varphi$$

$$- \sin \epsilon \sin \varphi \cos \omega) + \sin \varphi \cos \epsilon (\sin \alpha_1 \cos \alpha_3 \cos \theta + \sin \alpha_3 (\cos \alpha_1 \cos \alpha_2$$

$$+ \sin \alpha_1 \sin \alpha_2 \sin \theta)) + (\cos \omega \cos \varphi + \sin \epsilon \sin \omega \sin \varphi)(\sin \alpha_1 \sin \alpha_3 \cos \theta$$

$$- \cos \alpha_3 (\cos \alpha_1 \cos \alpha_2 + \sin \alpha_1 \sin \alpha_2 \sin \theta)))/(\cos \omega_w (\sin \epsilon_w{}^2 (\sin \omega_w{}^2 \cos \varphi_w{}^2$$

$$- \sin \varphi_w{}^2 \cos \omega_w{}^2) - \sin \omega_w \sin \varphi_w \cos \epsilon_w (2 \sin \epsilon_w \cos \varphi_w - \sin \omega_w \sin \varphi_w \cos \epsilon_w)))$$

$$J5[1,1] = \sin \varphi_w (\sin \epsilon_w \cos \omega_w ((\sin \alpha_2 \cos \alpha_1 - \sin \alpha_1 \sin \theta \cos \alpha_2)(\sin \omega \cos \varphi$$

$$- \sin \epsilon \sin \varphi \cos \omega) + \sin \varphi \cos \epsilon (\sin \alpha_1 \cos \alpha_3 \cos \theta + \sin \alpha_3 (\cos \alpha_1 \cos \alpha_2$$

$$+ \sin \alpha_1 \sin \alpha_2 \sin \theta)) + (\cos \omega \cos \varphi + \sin \epsilon \sin \omega \sin \varphi)(\sin \alpha_1 \sin \alpha_3 \cos \theta$$

$$- \cos \alpha_3 (\cos \alpha_1 \cos \alpha_2 + \sin \alpha_1 \sin \alpha_2 \sin \theta))) + (\sin \epsilon_w \cos \varphi_w$$

$$- \sin \omega_w \sin \varphi_w \cos \epsilon_w)((\sin \alpha_1 \sin \alpha_2 + \sin \theta \cos \alpha_1 \cos \alpha_2)(\sin \omega \sin \varphi$$

$$+ \sin \epsilon \cos \omega \cos \varphi) + \cos \epsilon \cos \varphi (\cos \alpha_1 \cos \alpha_3 \cos \theta - \sin \alpha_3 (\sin \alpha_1 \cos \alpha_2$$

$$- \sin \alpha_2 \sin \theta \cos \alpha_1)) - (\sin \varphi \cos \omega - \sin \epsilon \sin \omega \cos \varphi)(\sin \alpha_3 \cos \alpha_1 \cos \theta$$

$$+ \cos \alpha_3 (\sin \alpha_1 \cos \alpha_2 - \sin \alpha_2 \sin \theta \cos \alpha_1))))/(\sin \epsilon_w{}^2 (\sin \omega_w{}^2 \cos \varphi_w{}^2$$

$$- \sin \varphi_w{}^2 \cos \omega_w{}^2) - \sin \omega_w \sin \varphi_w \cos \epsilon_w (2 \sin \epsilon_w \cos \varphi_w - \sin \omega_w \sin \varphi_w \cos \epsilon_w))$$

$$J5[1,2] = -(\sin \epsilon_w \cos \theta (\sin \varphi_w \cos \epsilon_w - \sin \epsilon_w \sin \omega_w \cos \varphi_w)(\sin \alpha_2 \cos \epsilon \cos \omega$$

$$+ \sin \alpha_3 \sin \epsilon \cos \alpha_2 + \sin \omega \cos \alpha_2 \cos \alpha_3 \cos \epsilon)$$

$$+ \sin \epsilon_w \sin \varphi_w \cos \omega_w (\sin \alpha_3 \sin \varphi \cos \epsilon (\sin \alpha_1 \sin \alpha_2 + \sin \theta \cos \alpha_1 \cos \alpha_2)$$

$$- (\sin \alpha_1 \cos \alpha_2 - \sin \alpha_2 \sin \theta \cos \alpha_1)(\sin \omega \cos \varphi - \sin \epsilon \sin \varphi \cos \omega)$$

$$- \cos \alpha_3 (\sin \alpha_1 \sin \alpha_2 + \sin \theta \cos \alpha_1 \cos \alpha_2)(\cos \omega \cos \varphi + \sin \epsilon \sin \omega \sin \varphi))$$

$$+ \sin \varphi_w (\sin \epsilon_w \cos \varphi_w - \sin \omega_w \sin \varphi_w \cos \epsilon_w)(\sin \alpha_3 \cos \epsilon \cos \varphi (\sin \alpha_2 \cos \alpha_1$$

$$- \sin \alpha_1 \sin \theta \cos \alpha_2) + (\sin \omega \sin \varphi + \sin \epsilon \cos \omega \cos \varphi)(\cos \alpha_1 \cos \alpha_2$$

$$+ \sin \alpha_1 \sin \alpha_2 \sin \theta) + \cos \alpha_3 (\sin \alpha_2 \cos \alpha_1 - \sin \alpha_1 \sin \theta \cos \alpha_2)(\sin \varphi \cos \omega$$

$$- \sin \epsilon \sin \omega \cos \varphi)))/(\sin \epsilon_w{}^2(\sin \omega_w{}^2 \cos \varphi_w{}^2 - \sin \varphi_w{}^2 \cos \omega_w{}^2)$$

$$- \sin \omega_w \sin \varphi_w \cos \epsilon_w(2 \sin \epsilon_w \cos \varphi_w - \sin \omega_w \sin \varphi_w \cos \epsilon_w))$$

$$J5[1,3] = (\sin \epsilon_w \sin \varphi_w \cos \omega_w(\sin \varphi \cos \epsilon(\sin \alpha_3 \cos \alpha_1 \cos \theta + \cos \alpha_3(\sin \alpha_1 \cos \alpha_2$$

$$- \sin \alpha_2 \sin \theta \cos \alpha_1)) - (\cos \omega \cos \varphi + \sin \epsilon \sin \omega \sin \varphi)(\cos \alpha_1 \cos \alpha_3 \cos \theta$$

$$- \sin \alpha_3(\sin \alpha_1 \cos \alpha_2 - \sin \alpha_2 \sin \theta \cos \alpha_1))) - \sin \epsilon_w(\sin \varphi_w \cos \epsilon_w$$

$$- \sin \epsilon_w \sin \omega_w \cos \varphi_w)(\sin \epsilon(\sin \alpha_3 \sin \theta + \sin \alpha_2 \cos \alpha_3 \cos \theta)$$

$$+ \sin \omega \cos \epsilon(\sin \theta \cos \alpha_3 - \sin \alpha_2 \sin \alpha_3 \cos \theta)) - \sin \varphi_w(\sin \epsilon_w \cos \varphi_w$$

$$- \sin \omega_w \sin \varphi_w \cos \epsilon_w)(\cos \epsilon \cos \varphi(\sin \alpha_1 \sin \alpha_3 \cos \theta - \cos \alpha_3(\cos \alpha_1 \cos \alpha_2$$

$$+ \sin \alpha_1 \sin \alpha_2 \sin \theta)) + (\sin \varphi \cos \omega - \sin \epsilon \sin \omega \cos \varphi)(\sin \alpha_1 \cos \alpha_3 \cos \theta$$

$$+ \sin \alpha_3(\cos \alpha_1 \cos \alpha_2 + \sin \alpha_1 \sin \alpha_2 \sin \theta)))))/(\sin \epsilon_w{}^2(\sin \omega_w{}^2 \cos \varphi_w{}^2$$

$$- \sin \varphi_w{}^2 \cos \omega_w{}^2) - \sin \omega_w \sin \varphi_w \cos \epsilon_w(2 \sin \epsilon_w \cos \varphi_w - \sin \omega_w \sin \varphi_w \cos \epsilon_w))$$

$$J5[1,4] = 0$$

$$J5[1,5] = 0$$

$$J5[1,6] = (\sin \epsilon_w(\sin \varphi_w \cos \epsilon_w - \sin \epsilon_w \sin \omega_w \cos \varphi_w)(\sin \epsilon(\cos \alpha_3 \cos \theta$$

$$+ \sin \alpha_2 \sin \alpha_3 \sin \theta) - \sin \theta \cos \alpha_2 \cos \epsilon \cos \omega - \sin \omega \cos \epsilon(\sin \alpha_3 \cos \theta$$

$$- \sin \alpha_2 \sin \theta \cos \alpha_3)) + \sin \epsilon_w \sin \varphi_w \cos \alpha_1 \cos \omega_w(\sin \varphi \cos \epsilon(\sin \theta \cos \alpha_3$$

$$- \sin \alpha_2 \sin \alpha_3 \cos \theta) + \cos \alpha_2 \cos \theta(\sin \omega \cos \varphi - \sin \epsilon \sin \varphi \cos \omega)$$

$$+ (\sin \alpha_3 \sin \theta + \sin \alpha_2 \cos \alpha_3 \cos \theta)(\cos \omega \cos \varphi + \sin \epsilon \sin \omega \sin \varphi))$$

$$- \sin \alpha_1 \sin \varphi_w(\sin \epsilon_w \cos \varphi_w - \sin \omega_w \sin \varphi_w \cos \epsilon_w)(\cos \epsilon \cos \varphi(\sin \theta \cos \alpha_3$$

$$- \sin \alpha_2 \sin \alpha_3 \cos \theta) - \cos \alpha_2 \cos \theta(\sin \omega \sin \varphi + \sin \epsilon \cos \omega \cos \varphi) - (\sin \alpha_3 \sin \theta$$

$$+ \sin \alpha_2 \cos \alpha_3 \cos \theta)(\sin \varphi \cos \omega - \sin \epsilon \sin \omega \cos \varphi)))/(\sin \epsilon_w{}^2(\sin \omega_w{}^2 \cos \varphi_w{}^2$$

$$- \sin \varphi_w{}^2 \cos \omega_w{}^2) - \sin \omega_w \sin \varphi_w \cos \epsilon_w(2 \sin \epsilon_w \cos \varphi_w - \sin \omega_w \sin \varphi_w \cos \epsilon_w))$$

$$J5[1,7] = 0$$

$$J5[1,8] = 0$$

$$J5[1,9] = (\sin \epsilon_w \sin \varphi \sin \varphi_w \cos \omega_w(\sin \epsilon(\cos \alpha_1 \cos \alpha_3 \cos \theta - \sin \alpha_3(\sin \alpha_1 \cos \alpha_2$$

$$- \sin \alpha_2 \sin \theta \cos \alpha_1)) - \cos \epsilon \cos \omega(\sin \alpha_1 \sin \alpha_2 + \sin \theta \cos \alpha_1 \cos \alpha_2)$$

$$- \sin\omega\cos\epsilon(\sin\alpha_3\cos\alpha_1\cos\theta + \cos\alpha_3(\sin\alpha_1\cos\alpha_2 - \sin\alpha_2\sin\theta\cos\alpha_1)))$$

$$- \sin\epsilon_w(\sin\varphi_w\cos\epsilon_w - \sin\epsilon_w\sin\omega_w\cos\varphi_w)(\sin\epsilon\cos\alpha_2\cos\omega\cos\theta$$

$$- \cos\epsilon(\sin\theta\cos\alpha_3 - \sin\alpha_2\sin\alpha_3\cos\theta) - \sin\epsilon\sin\omega(\sin\alpha_3\sin\theta$$

$$+ \sin\alpha_2\cos\alpha_3\cos\theta)) - \sin\varphi_w\cos\varphi(\sin\epsilon_w\cos\varphi_w$$

$$- \sin\omega_w\sin\varphi_w\cos\epsilon_w)(\cos\epsilon\cos\omega(\sin\alpha_2\cos\alpha_1 - \sin\alpha_1\sin\theta\cos\alpha_2)$$

$$+ \sin\epsilon(\sin\alpha_1\cos\alpha_3\cos\theta + \sin\alpha_3(\cos\alpha_1\cos\alpha_2 + \sin\alpha_1\sin\alpha_2\sin\theta))$$

$$- \sin\omega\cos\epsilon(\sin\alpha_1\sin\alpha_3\cos\theta - \cos\alpha_3(\cos\alpha_1\cos\alpha_2$$

$$+ \sin\alpha_1\sin\alpha_2\sin\theta)))) / (\sin\epsilon_w{}^2(\sin\omega_w{}^2\cos\varphi_w{}^2 - \sin\varphi_w{}^2\cos\omega_w{}^2)$$

$$- \sin\omega_w\sin\varphi_w\cos\epsilon_w(2\sin\epsilon_w\cos\varphi_w - \sin\omega_w\sin\varphi_w\cos\epsilon_w))$$

$$J5[1,10] = (\sin\epsilon_w\sin\varphi_w\cos\omega_w((\sin\alpha_1\sin\alpha_2 + \sin\theta\cos\alpha_1\cos\alpha_2)(\cos\omega\cos\varphi$$

$$+ \sin\epsilon\sin\omega\sin\varphi) + (\sin\omega\cos\varphi - \sin\epsilon\sin\varphi\cos\omega)(\sin\alpha_3\cos\alpha_1\cos\theta$$

$$+ \cos\alpha_3(\sin\alpha_1\cos\alpha_2 - \sin\alpha_2\sin\theta\cos\alpha_1))) - \sin\epsilon_w\cos\epsilon(\sin\varphi_w\cos\epsilon_w$$

$$- \sin\epsilon_w\sin\omega_w\cos\varphi_w)(\sin\omega\cos\alpha_2\cos\theta + \cos\omega(\sin\alpha_3\sin\theta$$

$$+ \sin\alpha_2\cos\alpha_3\cos\theta)) - \sin\varphi_w(\sin\epsilon_w\cos\varphi_w - \sin\omega_w\sin\varphi_w\cos\epsilon_w)((\sin\alpha_2\cos\alpha_1$$

$$- \sin\alpha_1\sin\theta\cos\alpha_2)(\sin\varphi\cos\omega - \sin\epsilon\sin\omega\cos\varphi) - (\sin\omega\sin\varphi$$

$$+ \sin\epsilon\cos\omega\cos\varphi)(\sin\alpha_1\sin\alpha_3\cos\theta - \cos\alpha_3(\cos\alpha_1\cos\alpha_2$$

$$+ \sin\alpha_1\sin\alpha_2\sin\theta)))) / (\sin\epsilon_w{}^2(\sin\omega_w{}^2\cos\varphi_w{}^2 - \sin\varphi_w{}^2\cos\omega_w{}^2)$$

$$- \sin\omega_w\sin\varphi_w\cos\epsilon_w(2\sin\epsilon_w\cos\varphi_w - \sin\omega_w\sin\varphi_w\cos\epsilon_w))$$

$$J5[1,11] = - \sin\varphi_w(\sin\epsilon_w\cos\omega_w((\sin\alpha_1\sin\alpha_2 + \sin\theta\cos\alpha_1\cos\alpha_2)(\sin\omega\sin\varphi$$

$$+ \sin\epsilon\cos\omega\cos\varphi) + \cos\epsilon\cos\varphi(\cos\alpha_1\cos\alpha_3\cos\theta - \sin\alpha_3(\sin\alpha_1\cos\alpha_2$$

$$- \sin\alpha_2\sin\theta\cos\alpha_1)) - (\sin\varphi\cos\omega - \sin\epsilon\sin\omega\cos\varphi)(\sin\alpha_3\cos\alpha_1\cos\theta$$

$$+ \cos\alpha_3(\sin\alpha_1\cos\alpha_2 - \sin\alpha_2\sin\theta\cos\alpha_1))) + (\sin\epsilon_w\cos\varphi_w$$

$$- \sin\omega_w\sin\varphi_w\cos\epsilon_w)((\sin\alpha_2\cos\alpha_1 - \sin\alpha_1\sin\theta\cos\alpha_2)(\sin\omega\cos\varphi$$

$$- \sin\epsilon\sin\varphi\cos\omega) + \sin\varphi\cos\epsilon(\sin\alpha_1\cos\alpha_3\cos\theta + \sin\alpha_3(\cos\alpha_1\cos\alpha_2$$

$$+ \sin\alpha_1\sin\alpha_2\sin\theta)) + (\cos\omega\cos\varphi + \sin\epsilon\sin\omega\sin\varphi)(\sin\alpha_1\sin\alpha_3\cos\theta$$

$$- \cos\alpha_3(\cos\alpha_1\cos\alpha_2 + \sin\alpha_1\sin\alpha_2\sin\theta)))) / (\sin\epsilon_w{}^2(\sin\omega_w{}^2\cos\varphi_w{}^2$$

$$- \sin\varphi_w{}^2 \cos\omega_w{}^2) - \sin\omega_w \sin\varphi_w \cos\epsilon_w(2\sin\epsilon_w \cos\varphi_w - \sin\omega_w \sin\varphi_w \cos\epsilon_w))$$

$$J6[1,1] = -\cos\varphi_w(\sin\epsilon_w \sin\omega_w((\sin\alpha_2 \cos\alpha_1 - \sin\alpha_1 \sin\theta \cos\alpha_2)(\sin\omega \cos\varphi$$

$$-\sin\epsilon \sin\varphi \cos\omega) + \sin\varphi \cos\epsilon(\sin\alpha_1 \cos\alpha_3 \cos\theta + \sin\alpha_3(\cos\alpha_1 \cos\alpha_2$$

$$+\sin\alpha_1 \sin\alpha_2 \sin\theta)) + (\cos\omega \cos\varphi + \sin\epsilon \sin\omega \sin\varphi)(\sin\alpha_1 \sin\alpha_3 \cos\theta$$

$$-\cos\alpha_3(\cos\alpha_1 \cos\alpha_2 + \sin\alpha_1 \sin\alpha_2 \sin\theta))) + \tan\omega_w(\sin\epsilon_w \cos\varphi_w$$

$$-\sin\omega_w \sin\varphi_w \cos\epsilon_w)((\sin\alpha_1 \sin\alpha_2 + \sin\theta \cos\alpha_1 \cos\alpha_2)(\sin\omega \sin\varphi$$

$$+\sin\epsilon \cos\omega \cos\varphi) + \cos\epsilon \cos\varphi(\cos\alpha_1 \cos\alpha_3 \cos\theta - \sin\alpha_3(\sin\alpha_1 \cos\alpha_2$$

$$-\sin\alpha_2 \sin\theta \cos\alpha_1)) - (\sin\varphi \cos\omega - \sin\epsilon \sin\omega \cos\varphi)(\sin\alpha_3 \cos\alpha_1 \cos\theta$$

$$+\cos\alpha_3(\sin\alpha_1 \cos\alpha_2 - \sin\alpha_2 \sin\theta \cos\alpha_1)))))/(\sin\epsilon_w{}^2(\sin\omega_w{}^2 \cos\varphi_w{}^2$$

$$-\sin\varphi_w{}^2 \cos\omega_w{}^2) - \sin\omega_w \sin\varphi_w \cos\epsilon_w(2\sin\epsilon_w \cos\varphi_w - \sin\omega_w \sin\varphi_w \cos\epsilon_w))$$

$$J6[1,2] = \cos\varphi_w(\sin\epsilon_w \sin\omega_w(\sin\alpha_3 \sin\varphi \cos\epsilon(\sin\alpha_1 \sin\alpha_2 + \sin\theta \cos\alpha_1 \cos\alpha_2)$$

$$-(\sin\alpha_1 \cos\alpha_2 - \sin\alpha_2 \sin\theta \cos\alpha_1)(\sin\omega \cos\varphi - \sin\epsilon \sin\varphi \cos\omega)$$

$$-\cos\alpha_3(\sin\alpha_1 \sin\alpha_2 + \sin\theta \cos\alpha_1 \cos\alpha_2)(\cos\omega \cos\varphi + \sin\epsilon \sin\omega \sin\varphi))$$

$$+\tan\omega_w(\sin\epsilon_w \cos\varphi_w - \sin\omega_w \sin\varphi_w \cos\epsilon_w)(\sin\alpha_3 \cos\epsilon \cos\varphi(\sin\alpha_2 \cos\alpha_1$$

$$-\sin\alpha_1 \sin\theta \cos\alpha_2) + (\sin\omega \sin\varphi + \sin\epsilon \cos\omega \cos\varphi)(\cos\alpha_1 \cos\alpha_2$$

$$+\sin\alpha_1 \sin\alpha_2 \sin\theta) + \cos\alpha_3(\sin\alpha_2 \cos\alpha_1 - \sin\alpha_1 \sin\theta \cos\alpha_2)(\sin\varphi \cos\omega$$

$$-\sin\epsilon \sin\omega \cos\varphi)))/(\sin\epsilon_w{}^2(\sin\omega_w{}^2 \cos\varphi_w{}^2 - \sin\varphi_w{}^2 \cos\omega_w{}^2)$$

$$-\sin\omega_w \sin\varphi_w \cos\epsilon_w(2\sin\epsilon_w \cos\varphi_w - \sin\omega_w \sin\varphi_w \cos\epsilon_w))$$

$$-\cos\theta(\sin\alpha_2 \cos\epsilon \cos\omega + \sin\alpha_3 \sin\epsilon \cos\alpha_2$$

$$+\sin\omega \cos\alpha_2 \cos\alpha_3 \cos\epsilon)(\sin\varphi_w \sin\epsilon_w{}^2 \cos\omega_w{}^2 + \sin\omega_w \cos\epsilon_w(\sin\epsilon_w \cos\varphi_w$$

$$-\sin\omega_w \sin\varphi_w \cos\epsilon_w))/(\cos\omega_w(\sin\epsilon_w{}^2(\sin\omega_w{}^2 \cos\varphi_w{}^2 - \sin\varphi_w{}^2 \cos\omega_w{}^2)$$

$$-\sin\omega_w \sin\varphi_w \cos\epsilon_w(2\sin\epsilon_w \cos\varphi_w - \sin\omega_w \sin\varphi_w \cos\epsilon_w)))$$

$$J6[1,3] = -(\sin\varphi_w \sin\epsilon_w{}^2 \cos\omega_w{}^2 + \sin\omega_w \cos\epsilon_w(\sin\epsilon_w \cos\varphi_w$$

$$-\sin\omega_w \sin\varphi_w \cos\epsilon_w))(\sin\epsilon(\sin\alpha_3 \sin\theta + \sin\alpha_2 \cos\alpha_3 \cos\theta)$$

$$+\sin\omega \cos\epsilon(\sin\theta \cos\alpha_3 - \sin\alpha_2 \sin\alpha_3 \cos\theta))/(\cos\omega_w(\sin\epsilon_w{}^2(\sin\omega_w{}^2 \cos\varphi_w{}^2$$

$-\sin\varphi_w{}^2\cos\omega_w{}^2) - \sin\omega_w\sin\varphi_w\cos\epsilon_w(2\sin\epsilon_w\cos\varphi_w - \sin\omega_w\sin\varphi_w\cos\epsilon_w)))$

$-\cos\varphi_w(\sin\epsilon_w\sin\omega_w(\sin\varphi\cos\epsilon(\sin\alpha_3\cos\alpha_1\cos\theta + \cos\alpha_3(\sin\alpha_1\cos\alpha_2$

$-\sin\alpha_2\sin\theta\cos\alpha_1)) - (\cos\omega\cos\varphi + \sin\epsilon\sin\omega\sin\varphi)(\cos\alpha_1\cos\alpha_3\cos\theta$

$-\sin\alpha_3(\sin\alpha_1\cos\alpha_2 - \sin\alpha_2\sin\theta\cos\alpha_1))) - \tan\omega_w(\sin\epsilon_w\cos\varphi_w$

$-\sin\omega_w\sin\varphi_w\cos\epsilon_w)(\cos\epsilon\cos\varphi(\sin\alpha_1\sin\alpha_3\cos\theta - \cos\alpha_3(\cos\alpha_1\cos\alpha_2$

$+\sin\alpha_1\sin\alpha_2\sin\theta)) + (\sin\varphi\cos\omega - \sin\epsilon\sin\omega\cos\varphi)(\sin\alpha_1\cos\alpha_3\cos\theta$

$+\sin\alpha_3(\cos\alpha_1\cos\alpha_2 + \sin\alpha_1\sin\alpha_2\sin\theta)))))/(\sin\epsilon_w{}^2(\sin\omega_w{}^2\cos\varphi_w{}^2$

$-\sin\varphi_w{}^2\cos\omega_w{}^2) - \sin\omega_w\sin\varphi_w\cos\epsilon_w(2\sin\epsilon_w\cos\varphi_w - \sin\omega_w\sin\varphi_w\cos\epsilon_w))$

$J6[1,4] = 0$

$J6[1,5] = 0$

$J6[1,6] = (\sin\varphi_w\sin\epsilon_w{}^2\cos\omega_w{}^2 + \sin\omega_w\cos\epsilon_w(\sin\epsilon_w\cos\varphi_w$

$-\sin\omega_w\sin\varphi_w\cos\epsilon_w))(\sin\epsilon(\cos\alpha_3\cos\theta + \sin\alpha_2\sin\alpha_3\sin\theta)$

$-\sin\theta\cos\alpha_2\cos\epsilon\cos\omega - \sin\omega\cos\epsilon(\sin\alpha_3\cos\theta$

$-\sin\alpha_2\sin\theta\cos\alpha_3))/(\cos\omega_w(\sin\epsilon_w{}^2(\sin\omega_w{}^2\cos\varphi_w{}^2 - \sin\varphi_w{}^2\cos\omega_w{}^2)$

$-\sin\omega_w\sin\varphi_w\cos\epsilon_w(2\sin\epsilon_w\cos\varphi_w - \sin\omega_w\sin\varphi_w\cos\epsilon_w)))$

$-\cos\varphi_w(\sin\epsilon_w\sin\omega_w\cos\alpha_1(\sin\varphi\cos\epsilon(\sin\theta\cos\alpha_3 - \sin\alpha_2\sin\alpha_3\cos\theta)$

$+\cos\alpha_2\cos\theta(\sin\omega\cos\varphi - \sin\epsilon\sin\varphi\cos\omega) + (\sin\alpha_3\sin\theta$

$+\sin\alpha_2\cos\alpha_3\cos\theta)(\cos\omega\cos\varphi + \sin\epsilon\sin\omega\sin\varphi)) - \sin\alpha_1\tan\omega_w(\sin\epsilon_w\cos\varphi_w$

$-\sin\omega_w\sin\varphi_w\cos\epsilon_w)(\cos\epsilon\cos\varphi(\sin\theta\cos\alpha_3 - \sin\alpha_2\sin\alpha_3\cos\theta)$

$-\cos\alpha_2\cos\theta(\sin\omega\sin\varphi + \sin\epsilon\cos\omega\cos\varphi) - (\sin\alpha_3\sin\theta$

$+\sin\alpha_2\cos\alpha_3\cos\theta)(\sin\varphi\cos\omega - \sin\epsilon\sin\omega\cos\varphi)))/(\sin\epsilon_w{}^2(\sin\omega_w{}^2\cos\varphi_w{}^2$

$-\sin\varphi_w{}^2\cos\omega_w{}^2) - \sin\omega_w\sin\varphi_w\cos\epsilon_w(2\sin\epsilon_w\cos\varphi_w - \sin\omega_w\sin\varphi_w\cos\epsilon_w))$

$J6[1,7] = 0$

$J6[1,8] = 0$

$J6[1,9] = -(\sin\varphi_w\sin\epsilon_w{}^2\cos\omega_w{}^2 + \sin\omega_w\cos\epsilon_w(\sin\epsilon_w\cos\varphi_w$

$-\sin\omega_w\sin\varphi_w\cos\epsilon_w))(\sin\epsilon\cos\alpha_2\cos\omega\cos\theta - \cos\epsilon(\sin\theta\cos\alpha_3$

$$- \sin\alpha_2 \sin\alpha_3 \cos\theta) - \sin\epsilon \sin\omega(\sin\alpha_3 \sin\theta$$

$$+ \sin\alpha_2 \cos\alpha_3 \cos\theta))/(\cos\omega_w(\sin\epsilon_w{}^2(\sin\omega_w{}^2 \cos\varphi_w{}^2 - \sin\varphi_w{}^2 \cos\omega_w{}^2)$$

$$- \sin\omega_w \sin\varphi_w \cos\epsilon_w(2\sin\epsilon_w \cos\varphi_w - \sin\omega_w \sin\varphi_w \cos\epsilon_w)))$$

$$- \cos\varphi_w(\sin\epsilon_w \sin\omega_w \sin\varphi(\sin\epsilon(\cos\alpha_1 \cos\alpha_3 \cos\theta - \sin\alpha_3(\sin\alpha_1 \cos\alpha_2$$

$$- \sin\alpha_2 \sin\theta \cos\alpha_1)) - \cos\epsilon \cos\omega(\sin\alpha_1 \sin\alpha_2 + \sin\theta \cos\alpha_1 \cos\alpha_2)$$

$$- \sin\omega \cos\epsilon(\sin\alpha_3 \cos\alpha_1 \cos\theta + \cos\alpha_3(\sin\alpha_1 \cos\alpha_2 - \sin\alpha_2 \sin\theta \cos\alpha_1)))$$

$$- \cos\varphi \tan\omega_w(\sin\epsilon_w \cos\varphi_w - \sin\omega_w \sin\varphi_w \cos\epsilon_w)(\cos\epsilon \cos\omega(\sin\alpha_2 \cos\alpha_1$$

$$- \sin\alpha_1 \sin\theta \cos\alpha_2) + \sin\epsilon(\sin\alpha_1 \cos\alpha_3 \cos\theta + \sin\alpha_3(\cos\alpha_1 \cos\alpha_2$$

$$+ \sin\alpha_1 \sin\alpha_2 \sin\theta)) - \sin\omega \cos\epsilon(\sin\alpha_1 \sin\alpha_3 \cos\theta - \cos\alpha_3(\cos\alpha_1 \cos\alpha_2$$

$$+ \sin\alpha_1 \sin\alpha_2 \sin\theta))))/(\sin\epsilon_w{}^2(\sin\omega_w{}^2 \cos\varphi_w{}^2 - \sin\varphi_w{}^2 \cos\omega_w{}^2)$$

$$- \sin\omega_w \sin\varphi_w \cos\epsilon_w(2\sin\epsilon_w \cos\varphi_w - \sin\omega_w \sin\varphi_w \cos\epsilon_w))$$

$$J6[1, 10] = - \cos\epsilon(\sin\omega \cos\alpha_2 \cos\theta + \cos\omega(\sin\alpha_3 \sin\theta$$

$$+ \sin\alpha_2 \cos\alpha_3 \cos\theta))(\sin\varphi_w \sin\epsilon_w{}^2 \cos\omega_w{}^2 + \sin\omega_w \cos\epsilon_w(\sin\epsilon_w \cos\varphi_w$$

$$- \sin\omega_w \sin\varphi_w \cos\epsilon_w))/(\cos\omega_w(\sin\epsilon_w{}^2(\sin\omega_w{}^2 \cos\varphi_w{}^2 - \sin\varphi_w{}^2 \cos\omega_w{}^2)$$

$$- \sin\omega_w \sin\varphi_w \cos\epsilon_w(2\sin\epsilon_w \cos\varphi_w - \sin\omega_w \sin\varphi_w \cos\epsilon_w)))$$

$$- \cos\varphi_w(\sin\epsilon_w \sin\omega_w((\sin\alpha_1 \sin\alpha_2 + \sin\theta \cos\alpha_1 \cos\alpha_2)(\cos\omega \cos\varphi$$

$$+ \sin\epsilon \sin\omega \sin\varphi) + (\sin\omega \cos\varphi - \sin\epsilon \sin\varphi \cos\omega)(\sin\alpha_3 \cos\alpha_1 \cos\theta$$

$$+ \cos\alpha_3(\sin\alpha_1 \cos\alpha_2 - \sin\alpha_2 \sin\theta \cos\alpha_1))) - \tan\omega_w(\sin\epsilon_w \cos\varphi_w$$

$$- \sin\omega_w \sin\varphi_w \cos\epsilon_w)((\sin\alpha_2 \cos\alpha_1 - \sin\alpha_1 \sin\theta \cos\alpha_2)(\sin\varphi \cos\omega$$

$$- \sin\epsilon \sin\omega \cos\varphi) - (\sin\omega \sin\varphi + \sin\epsilon \cos\omega \cos\varphi)(\sin\alpha_1 \sin\alpha_3 \cos\theta$$

$$- \cos\alpha_3(\cos\alpha_1 \cos\alpha_2 + \sin\alpha_1 \sin\alpha_2 \sin\theta))))/(\sin\epsilon_w{}^2(\sin\omega_w{}^2 \cos\varphi_w{}^2 - \sin\varphi_w{}^2 \cos\omega_w{}^2)$$

$$- \sin\omega_w \sin\varphi_w \cos\epsilon_w(2\sin\epsilon_w \cos\varphi_w - \sin\omega_w \sin\varphi_w \cos\epsilon_w))$$

$$J6[1, 11] = \cos\varphi_w(\sin\epsilon_w \sin\omega_w((\sin\alpha_1 \sin\alpha_2 + \sin\theta \cos\alpha_1 \cos\alpha_2)(\sin\omega \sin\varphi$$

$$+ \sin\epsilon \cos\omega \cos\varphi) + \cos\epsilon \cos\varphi(\cos\alpha_1 \cos\alpha_3 \cos\theta - \sin\alpha_3(\sin\alpha_1 \cos\alpha_2$$

$$- \sin\alpha_2 \sin\theta \cos\alpha_1)) - (\sin\varphi \cos\omega - \sin\epsilon \sin\omega \cos\varphi)(\sin\alpha_3 \cos\alpha_1 \cos\theta$$

$$+ \cos\alpha_3(\sin\alpha_1 \cos\alpha_2 - \sin\alpha_2 \sin\theta \cos\alpha_1))) + \tan\omega_w(\sin\epsilon_w \cos\varphi_w$$

$$-\sin\omega_w\sin\varphi_w\cos\epsilon_w)((\sin\alpha_2\cos\alpha_1-\sin\alpha_1\sin\theta\cos\alpha_2)(\sin\omega\cos\varphi$$

$$-\sin\epsilon\sin\varphi\cos\omega)+\sin\varphi\cos\epsilon(\sin\alpha_1\cos\alpha_3\cos\theta+\sin\alpha_3(\cos\alpha_1\cos\alpha_2$$

$$+\sin\alpha_1\sin\alpha_2\sin\theta))+(\cos\omega\cos\varphi+\sin\epsilon\sin\omega\sin\varphi)(\sin\alpha_1\sin\alpha_3\cos\theta$$

$$-\cos\alpha_3(\cos\alpha_1\cos\alpha_2+\sin\alpha_1\sin\alpha_2\sin\theta))))/(\sin\epsilon_w{}^2(\sin\omega_w{}^2\cos\varphi_w{}^2$$

$$-\sin\varphi_w{}^2\cos\omega_w{}^2)-\sin\omega_w\sin\varphi_w\cos\epsilon_w(2\sin\epsilon_w\cos\varphi_w-\sin\omega_w\sin\varphi_w\cos\epsilon_w))$$